FORMATION AND TECTONIC EVOLUTION OF ZILDAT OPHIOLITIC MÉLANGE, INDUS SUTURE ZONE, NW HIMALAYA, INDIA

By

KOUSHICK SEN

Under the Guidance of

DR. BARUN K MUKHERJEE, SCEINTIST – C

WADIA INSTITUTE OF HIMALAYAN GEOLOGY
DEHRADUN

Submitted

IN PARTIAL FULFILLMENT OF THE REQUIREMENT OF THE DEGREE OF DOCTOR OF PHILOSOPHY

IN

GEOSCIENCE

TO

UNIVERSITY OF PETROLEUM AND ENERGY STUDIES
DEHRADUN

April, 2015

Wadia Institute of Himalayan Geology
(an autonomous institution of Dept. of Science & Technology)
33 GMS Road,Dehra Dun-248 001 (Uttarakhand)

Dr. Barun Kumar Mukherjee, PhD,
JSPS, (Japan)
Scientist-C

Certificate

This is to certify that the thesis entitled "Formation and Tectonic Evolution of Zildat Ophiolitic Mélange, Indus Suture Zone, NW Himalaya, India" is a bonafied work of Mr Koushick Sen, which has been completed under my supervision. Further it is certified that he has fulfilled all the terms and conditions pertaining to PhD ordinances of the University of Petroleum & Energy Studies, Dehra Dun and Wadia Institute of Himalayan Geology, Dehra Dun and that he is entitled to submit this original thesis work for the Ph.D. Degree in University of Petroleum & Energy Studies.

The content of the thesis, in full or parts have not been submitted to any other Institute or University for the award of any other degree or diploma.

Date: *April 2015*

Place: Dehra Dun

FAX: 0135-2625212 Tel (off): 01352525189
E-Mail:baun@wihg.res.in : mukherjeebarun@yahoo.co.in
Web:www.wihg.res.in

<u>Declaration</u>

I hereby declare that this submission is my own work and that, to the best of my knowledge and belief, it contains no material previously published or written by another person nor material which has been accepted for the award of any other degree or diploma of the university or other institute of higher learning, except where due acknowledgment has been made in the text.

April   , 2015   _(Koushick Sen)_

To my parents

&

family members

Contents

Contents

Executive Summery

Mélanges (French – 'mixtures') are the mappable units of chaotic rocks, formed in the accretionary wedge above a subduction zone, commonly found at the convergent plate margins. Mélange preserves signature of complex multi stage tectonic processes. The Zildat Ophiolitic Mélange (ZOM) is one such classical mélange that created mainly by coupling effect of subduction and accretion at the expense of Neo-Tethyan subduction and India-Eurasia collision.

The ZOM is characterised by disrupted multi-layered tectonic slices of composite lithology. It has oceanic lithospheric aggregates arranged in a block-in-matrix fashion which are highly disrupted in nature. The ZOM is a multilayer tectonic slices composed of ophiolite fragments, metabasic volcaniclastics, oceanic sediments and reworked clasts of various oceanic components.

The overall mélange package is heterogeneously deformed with a gradation of shearing intensity moving across the ZOM. A wide range of mineralogical assemblages found within the melange suggests a clock wise P-T evolution from a high-pressure (blueschist) condition to lower greenschist facies via epidote-amphibolite condition. The obtained P-T condition from the melange matrix cannot be correlated with the metamorphism of individual clasts present within ZOM. Merging the various components present within the ZOM, it suggests a poly-metamorphic evolution of the melange.

Executive Summery

A prominent fluid rock interaction is observed within the melange which caused by large scale mass movement, evaluated from geochemical studies. Stable Isotope study of ZOM carbonates show a bimodal distribution pattern of isotope values suggesting considerable amount of fluid infiltration prevailed at the last stage of mélange evolution. The restricted silica rich fluid was derived from the adjacent continental rock of Tso-Morari Crystalline at the latest stages of melange emplacement. The emplacement of ZOM is not uniform. It is squeezed up during continued continental convergence with the presence of two oppositely dipping thrust boundaries, where the rigid Nidar Ophiolitic Complex (NOC) acted as a fixed boundary back-stop. The presence of serpentine and talc can be acted as lubricator to assist the emplacement.

The bulk geochemical analyses of the basic (basalt) rocks of ZOM suggests their alkaline OIB affinity, formed in within plate tectonic setting. They hint a pre-subduction volcanism event, prior to the melange formation.

List of Figures

Chapter 4

Chapter 5

Chapter 6

hydrocarbon signature. Please gone through the text for details.

Chapter 7

CHAPTER 1

Introduction

INTRODUCTION

1.1. STATEMENT OF THE THESIS

Ophiolitic mélange is a store house of the incoherent lithologies, it decodes the closure of an oceanic realm during the convergence of continental plates. Present study encompasses the evidences of polyphase deformation & metamorphism, high strain fabrics and complete evolutionary history of an ophiolitic mélange. The study of mineralogy, geochemistry and isotopic traces, unravelling the mélange geometry, its formation and complete emplacement history.

1.2. DEFINITION OF THE PROBLEM

After the pioneering work by Gansser in 1974, the origin and geometry of the ophiolitic mélange, whether is a sedimentary package or tectonic slice; this debate has always been at the central part of discussion related to subduction zone mélanges. Significant effort have put into these subduction zone mélange rocks found in paleo suture zones as they are potential to understand a complete story of an orogenic belt, from pre-subduction architecture to syn-subduction and collision induced tectonic processes. The Indus Suture Zone mélange demarcates the boundary between oceanic and continental domain. It has incoherent and undefined lithologies which mimics variety of geodynamic processes and architectural configuration of orogenic belt. There are various aspects of studying mélange which are consider to be

the major problem to the earth science community. This thesis focuses on some of the basic problems of mélange understanding in Indus Suture Zone. They are: 1. Nature of the mélange; 2. Geometry and lithology of mélange unit; 3. Behaviour of oceanic sediments; 4. Pattern of emplacement history; 5. Protolith of subducted rocks. In the present thesis the ophiolitic mélange rocks are studied thoroughly by applying several methods: field study, macro to micro scale mineralogical analyses and bulk rock geochemical study.

1.3.   MOTIVATION

Convergent plate margins are the most tectonically dynamic and seismically active areas on Earth. Due to the inaccessibility of subduction zones for direct investigations, the study of fossil subduction zones and associated mélange rocks provide an opportunity to study subduction zone processes. In other words, the study of mélange in convergent plate tectonics, has always been a prime importance to unravel the tectonic evolution of a collisional orogen. In examining the geological aspects, the mélanges and mélange-forming processes are supposedly interlinked with major geological events. These events are significant to understand the crustal evolution of the Earth.

1.4.   DEFINITION OF MÉLANGES & OPHIOLITIC MÉLANGES

The word 'mélange' is of French origin and it means a mixture of incongruous units. In geological sense, mélange means a disordered assemblage of different lihto-units that may or may not have temporal and

spatial inter-relations. Mélanges are common features in orogenic belts and are distributed widely around the world (Raymond, 1984). Mélanges occur extensively in accretionary and collisional zone, represents disrupted and chaotic units including sedimentary, magmatic and metamorphic rocks (commonly as exotic blocks) mixed by stratal disruption and formed by tectonic, diapiric and/or sedimentary processes (Cowan, 1985; Festa et al., 2010; Horton and Rast, 1989; Hsü, 1968; Raymond, 1984; Silver and Beutner, 1980). In spite of many recent studies have been done on mélange rocks, the only consensus is achieved on the definition of melange represents large-scale masses of chaotically fragmented and mixed strata. They are characterized by blocks of all sizes embedded in a sheared matrix of finer-grained nature, show incoherent behaviour and lack of internal continuity.

Gansser (1974) defined the ophiolitic mélange as an olistostromal and tectonic mixture of ophiolitic material and sediments of oceanic origin with exotic blocks. With time the definition has been modified and as per the present understanding the ophiolitic mélanges are spatially and temporally associated with ophiolite nappes in orogenic belts (Dilek and Furnes, 2011; Gansser,1974; Altunkaynak and Dilek, 2006), and may display a complex record of the rift-drift, seafloor spreading and tectonic evolution of ophiolites in a subduction zone setting (Dilek et al., 1999, 2005, 2007; Dilek and Robinson, 2003; Dilek and Furnes, 2009). They may occur as sub-ophiolitic or supra-ophiolitic (overlying the ophioltes) in origin and their matrix may range in composition from serpentinite, serpentinite mud, greywacke, turbiditic rocks, and mud-shale (Dilekand Thy, 2006; Furnes et al., 2012; Phipps, 1984;

Saleeby, 1984; Shervais et al., 2011). The final configuration and development of the structural architecture of ophiolitic mélanges are strongly controlled by ophiolite emplacement and collisional (arc–continent, continent–continent) processes (Dilek, 2006; Dilek and Furnes, 2011; Flower and Dilek, 2003; Furnes et al., 2012; Robertson et al., 2009).

1.5. GLOBAL DISTRIBUTION OF OPHIOLITIC MÉLANGES

Mélanges, usually termed as broken formation occur in many collisional orogenic belts around the world related to subduction/obduction and/or to post-collisional accretionary processes. Collisional orogens display a record of various, long-lived geological events accompanied by complex system during which mélanges and such broken formations may form. These include subduction of oceanic material and emplacement of ophiolites during pre-collisional stages, thickening of crust involving the lithospheric mantle during collisional stages and gravitational instability as a consequence of continued plate indentation during post-collisional stages (Dilek 2006). Formation of mélanges have reported in various tectonic setup. Characteristics differences are notices as variation in clasts and matrix content with their relative proportion. They have been studied extensively around the globe leading to different hypotheses regarding their formation and tectonic evolution. The locations of few important and widely studied mélanges around the globe are shown in Figure 1, and are discussed in brief with their characteristic features.
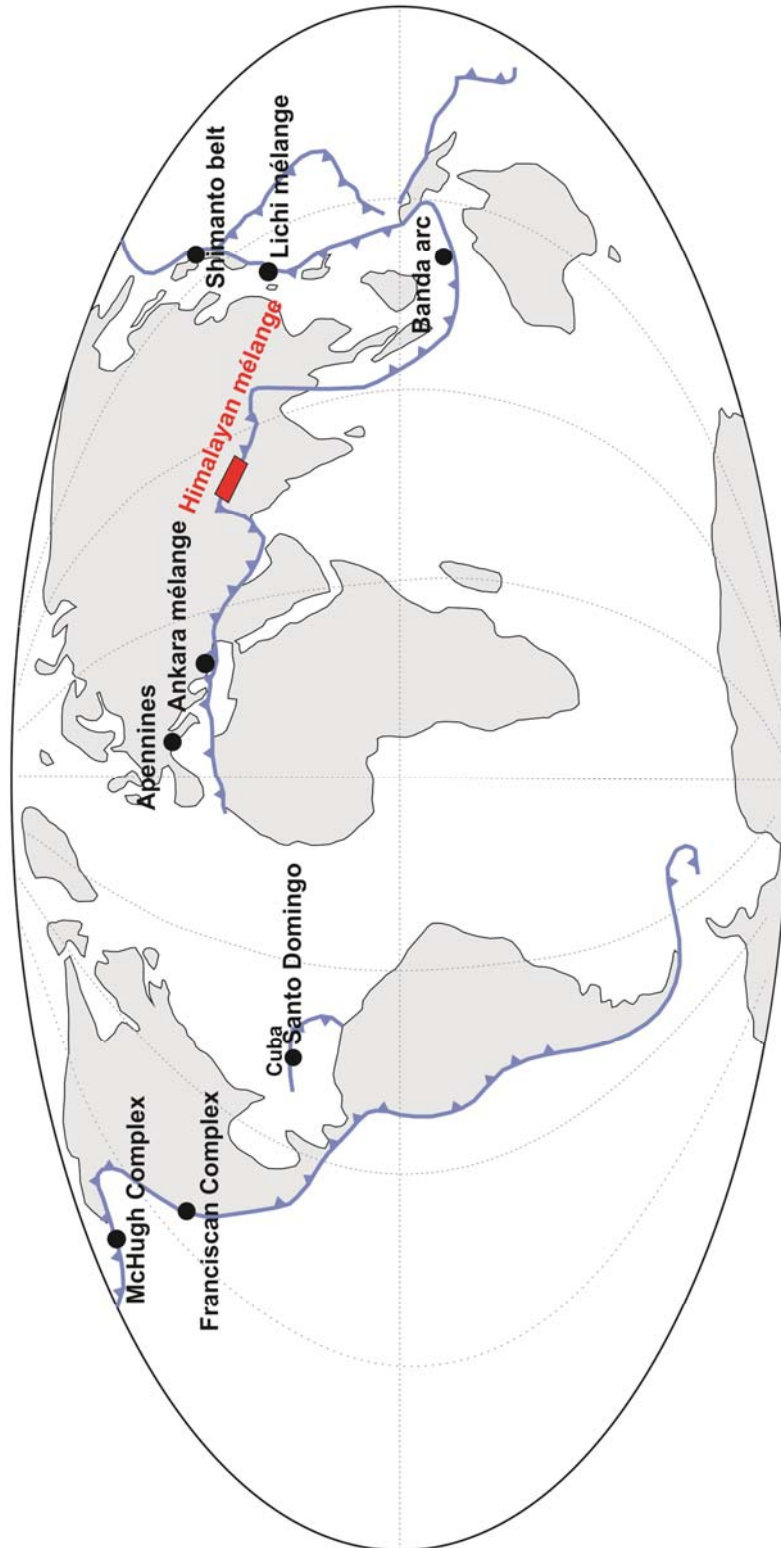
Figure 1: *World map showing the modern and ancient convergent margins, subduction zones and associated mélanges around the world. The present study area of Zildat Ophiolitic Mélanges is part of Indus Suture Zone and is shown as Himalayan Mélanges (marked by red box)*

In eastern Cuba, the mélanges are dominantly of serpentine rich matrix

and represent fragments of subduction channel (García-Casco et al., 2006,

2008b; Lázaro et al., 2009; Blanco- Quintero et al., 2010a, 2010b). These mélanges contain blocks of subducted high-grade garnet-amphibolite and blueschist surrounded by sheared and massive antigoritite interpreted as the matrix of the subduction channel (Blanco- Quintero et al., 2011). The Cretaceous–Miocene Shimanto accretionary complex in SW and Central Japan suggests subsequent peeling off and underplating of the downgoing oceanic basement making a pile of thrust sheets that produced a tectonic mélange (Hara and Kimura, 2008). Mélanges containing high-pressure (and in some cases ultra high pressure) rocks and occurring in accretionary complexes provide significant information about the geodynamic evolution of a subduction channel in terms of pressure, temperature and time (P-T-t) (Cloos, 1982; Federico et al., 2007; Gerya et al., 2002; Hermann et al., 2000). The Franciscan Complex of California is an archetype accretionary complex, show unmetamorphosed sedimentary mélange developed in a nascent forearc basin setting in the San Francisco of coastal California (Hitz & Wakabyashi, 2012). It has blocks of high-pressure metamorphic rocks derived from the Franciscan subduction complex as well as blocks of the Great Valley Group forearc basin strata and the Coast Range Ophiolite in a matrix composed of foliated shale and serpentinite. Malatesta et al. (2012) reported that the Voltri Massif in the Ligurian– Piemontese Units of the Western Alps, Italy, contains serpentinites and metasedimentary rocks enclosing variably deformed lenses of metagabbro, metabasite and peridotite rocks. They show polymetamorphism, including wide range of mineral assemblages ranging from eclogite to blueschist facies formed as a consequences of Alpine subduction. Mixed

tectono-stratigraphic units in some orogenic wedges contain blocks of various size, origin, age, and lithology commonly embedded in a sedimentary matrix by sedimentary and/or diapiric processes. These deposits undergo continuous deformation during the wedge growth and hence keep an intact structural record of the dynamic evolution of a wedge. Codegone et al. (2012) report on the occurrence of small-scale polygenetic mélanges in the Ligurian accretionary complex in the Northern Apennines of Italy, and emphasizes the role of shale diapirism in superposed mélange evolution in orogenic belts. Permian to Cretaceous mélange of the McHugh Complex in Alaska includes blocks and belts of graywacke, argillite, limestone, chert, basalt, gabbro, and ultramafic rocks, intruded by a variety of igneous rocks (Kousy & Bradley, 1999). The Ankara Ophiolitic Mélange in Turkey show rock masses of tectono-sedimentary mixture. It comprises blocks of ultramafic rocks, pillow basalts, radiolarites, limestones and sediments from basinal sequence. The detached and dismembered blocks lie within a highly sheared and brecciated ophiolitic detrital matrix or a block-on-block to sheared sedimentary matrix that varied along the mélange belt (Bora Rojay 2012). The Lichi Mélange of the Coastal Range of Taiwan is composed of exotic ophiolite and sedimentary blocks, metric to kilometric in size and coherent turbidite beds, all embedded in a sheared scaly argillaceous matrix. The Lichi Mélange is controversial in origin, being interpreted either as a subduction complex, or as an olistostrome (Chang et al. 2000). In Indonesia, the Banda orogeny mélange show clay rich litho-tectonic unit of strata and structural discontinuity which formed an extensive suture zone between Asian and Australian plate (Harris et al 1998).

Detail description of Himalayan ophiolitic mélange and the studied Zildat Ophiolitic Mélange is discussed in Chapter 2.

1.6.   FORMATION OF MÉLANGE IN A SUBDUCTION SETUP

Before the advancement of plate tectonics in the early 1970s, it was difficult to explain mélanges in terms of known geological mechanisms. When the theory of plate tectonics was first proposed, mélange was thought to represent the fossil Benioff zone of a plate boundary in a subduction zone (Hamilton, 1969, Hsü, 1971 and Ernst, 1970). However, the mix pattern of mélange rocks led to debate (e.g., Raymond, 1984 and Festa et al., 2010) regarding its origin as fault rocks formed by tectonic, sedimentary or diapiric processes in subduction zones (e.g., Cowan, 1982). Mélanges are not unique to subduction zones: they also formed at various active plate boundary settings such as collision zones, transform boundaries, rifted margins, and even gravitationally unstable passive margins (Raymond, 1984 and Festa, 2010). Although mélanges may characterize diverse geodynamic environments of formation, they are commonly associated with subduction of oceanic lithosphere, collisional events (arc-continent and continent-continent), and intra-continental deformation including rifting and passive margin evolution (Alonso et al., 2008; Dilek, 2006; Festa et al., 2010). Hence, mélanges are co-genetic with emplacement of ophiolites, advancement of thrust and nappe sheets, evolution of foreland basins, formation of submarine landslides (olistostromes) and seismic events (Festa et al., 2010). Mélanges represent a significant component of collisional and accretionary orogenic belts and are

considered as the products of either tangential tectonics, sedimentary processes, diapirism or the interplay of these processes (Festa et al., 2010a,b). Past studies have ascribed the formation of mélanges to various mechanisms ranging from sedimentary processes (Cowan, 1982) to tectonic deformation, by imbricate thrusting within accretionary wedge (Hsu, 1968) or through a combination of all these processes (Raymond, 1984). Mélanges may also form in many tectonic settings: in subduction zones (Aalto, 1982; Federico et al., 2007), fore arc and back arc basins (Huang et al., 2008; Page and Suppe, 1981; Schroetter et al., 2006), transform faults and overthrust belts (Jacobi, 1984), continental interior sedimentary wedges (Krieger, 1977) and passive margins.

1.7.   BROAD OBJECTIVES

Mélange being an assemblage of various rock masses in a subduction setup, it is important to delineate tectonic mixing, mass movement along convergent plate margin and emplacement history of meta-sedimentary rocks while studying mélanges. Considering the complexities of mélange rocks, a multi-proxy approach is adopted to delineate the formational and emplacement pattern of Zildat Ophiolitic Mélange; vis-a-vis, its role in Himalayan evolution. The following broad objectives are focused in the current thesis with the help of mesoscopic, microscopic, petrological, isotopic and geochemical study.

➢   Formation of mélange in a convergent setup

➢   Tectonic context and mélange emplacement pattern

➢   Role of mélange during evolution of the Indus Suture Zone

1.8.   OUTLINE OF THE THESIS AND METHODOLOGY DEPLOYED

Over the past few decades considerable research has been done on "Mélanges and broken formations" and still it is considered to be one of the most dynamic rock mass in geotectonics which are found in suture zones associated with ophiolitic rocks amalgamated as a response of subduction and collisional processes. The melange is an incoherent rock masses are the key constituent of collisional zones (such as ISZ) , such type of melange usually described as being dominated by ophiolite fragment along with pervasive mixing of oceanic sediments and recycled volatile components. The melange is an incoherent rock masses are the key constituent of collisional zones (such as ISZ) , such type of melange usually described as being dominated by ophiolite fragment along with pervasive mixing of oceanic sediments and recycled volatile components. The present thesis is based on such an integrated approach adopted to analyse the role of Zildat Ophiolitic mélange in the evolution of Indus Suture Zone, NW Himalaya, India.

As per the above set objectives, the present thesis work has spread over in the form of seven chapters. Chapter 1 focuses on the introduction of the research problem and its background. It describes the global distribution of mélange and their historical overview has been stated with emphasize the modern status of mélange formational hypotheses. Chapter 2 covers introduction of Himalaya and distribution of Himalayan mélange rocks along Indus Suture Zone. The Zildat Ophiolitic Mélange is highlighted in this chapter with its associated lithologies, also containing the geological map and cross-section of the study area. A multi-dimensional approach is chosen to achieve the goal of understanding the mélange rocks. Chapter 3 describes the

methods and analytical techniques. It contains the details about analytical procedures, instrumentation uses and protocol followed during the analyses. Many state of art instrument were employed to gather minute scale information regarding the rocks. Starting from detailed field work, laboratory analyses and instrumentation includes optical microscopy, fluid inclusion petrography, SEM-EDX, EPMA, IRMS, Raman Spectrometry, XRF, ICP-MS. Chapter 4 deals with mineralogical and structural evolution of Zildat Ophiolitic Mélange. It has detail discussions on field, lithological and structural relationship along with overall mineralogy and petrographic description with in-situ mineralogical analysis. As fluid played a critical role in evolution of mélange rocks and fluid flux is common is such a dynamic set-up, the fluid evolution pattern is documented in Chapter 5. This chapter added new prospect to understand an ophiolitic mélange using fluid inclusion and stable isotope studies. Chapter 6 elaborate bulk geochemical study of mélange rocks to understand the nature of the mélange prior to its formation and emplacement by studying major, trace and rare earth geochemistry of a particular basic unit within the Zildat Ophiolitic Mélange. Finally, the whole research work is summarized in chapter 7 as model reconstruction. A synoptic view of the research is drawn hare with broad implications and future prospects of the present work.

CHAPTER 2

Overview Of The Himalayan Ophiolitic Mélange: Geology & Distribution

OVERVIEW OF THE HIMALAYAN OPHIOLITIC

MÉLANGE: GEOLOGY & DISTRIBUTION

2.1.   GEOLOGICAL FRAMEWORK OF THE HIMALAYA

The Himalaya considered as the youngest and active mountain chain in the world formed due to continent–continent collision between the Indian and the Eurasian plates at around 55 Ma (Argand, 1924; Gansser, 1964; Dewey and Bird, 1970; Dewey and Burke, 1973; Patriat and Achache, 1984; Searle et al., 1987; Molnar, 1988; Dewey et al., 1989; Le Pichon et al., 1992; Brookfield, 1998; Rowley, 1998; Hallet and Molnar, 2001; Clark et al., 2004). By the 1970's, researchers demonstrated that the Himalayan collision resulted from the closure of the Tethyan Ocean through the subduction of the oceanic lithosphere (Desio, 1977; Sengör, 1979). Subsequently N-S crustal shortening of at least 1400 km took place that led to uplift of the Himalaya and the Tibetan Plateau (Molnar and Tapponnier, 1977; Patriat and Achache, 1984; Searle et al., 1987; Dewey et al*.,* 1989; Hodges, 2000; Yin and Harrison, 2000;). The Himalayas, stretches over 2400 km between the Namche Barwa syntaxis to the east and the Nanga Parbat syntaxis to west. The mountain range is arc-shaped, convexs southwards and has two syntaxial bends at its western and eastern ends (Wadia 1931; Valdiya 1980). The northern boundary of the Himalayan range is the east flowing Tsangpo (Tsangpo- big river in Tibetan language) and west flowing Indus River whereas the southern boundary,

known as the Himalayan Frontal Thust (HFT), marks the northern limit of the Indo Gangetic Plain.

Geologically the whole mountain belt is divided into five major domains from south to north on the basis of litho-stratigraphy and structural pattern: **a.** Sub - Himalaya (Lower Tertiary and Siwalik), **b.** Lower Himalaya (Lesser Himalaya), **c.** Higher Himalaya (Central Crystalline), **d.** Tethyan Himalaya and **e.** Trans Himalaya (Gansser, 1964; Le fort, 1975). The north dipping Main Himalayan Thrust (MHT) is considered to be the main basal detachment fault (Zhao et al., 1993; Sharma, 1998). It is proposed that entire sequences from N-S are marked by thrusts that are progressively young towards south. The Tethyan Thrust (TT) separates Tethyan Himalaya from Trans Himalaya. The South Tibetan Detachment (STD) is a low angle normal fault or detachment, considered as syn-orogenic extensional shear zone located at the top of the High Himalayan Crystalline Sequences, which separates Higher Himalayan and Tethyn Himalayan rocks. The Main Central Thrust (MCT, northernmost) separates the crystalline rocks of Higher Himalaya from the meta-sedimentary packages of the Lesser Himalaya. The Main Boundary Thrust (MBT) separates the Lesser Himalayan domain from the Sub Himalayan Lower Tertiary and the foreland sedimentary rocks known as the Siwaliks. The Siwaliks thrust over Ganga alluvium along the Himalayan Frontal Thrust (HFT). The rising of the Himalaya has led to flexural down warping of the under-thrusting Indian plate that lodged the sediments derived from the Himalayas, forming the world's largest terrestrial foreland basin

named as Himalayan Foreland Basin (HFB). The MCT, MBT and HFT are considered to be the imbrications of MHT.

TECTONIC DIVISIONS OF THE HIMALAYA

_____

e. Trans Himalaya - Ophiolitic mélange, ophiolite and volcano-sedimentary rocks (Cretaceous to Miocene)

----------------------------------**ITSZ**--------------------------------------

d. Tethyan Himalayan Sequence (THS) (1840 Ma–40 Ma; Paleoproterozoic to Eocene) metasedimentary sequence

----------------------------------**STD**--------------------------------------

c. Great or High Himalayan Crystalline (HHC) (1200-850 Ma; Late Mesoproterozoic to Early Neoproterozoic) high-grade metamorphic rocks

----------------------------------**Vaikrita Thrust (MCT-II)** -----------------------

(2500-1600 Ma; Paleoproterozoic–Ordovician) Proterozoic granitic gneiss and mica-schist

--------------------------------- **Munsiari Thrust (MCT-I)** -------------------------

b. Lesser Himalayan Sequence (LHS) (1870–520 Ma; Proterozoic–Cambrian) Metasedimentary and meta-volcanic strata

----------------------------------**MBT**---------------------------------

a. Sub – Himalaya: Siwalik Neogene- Quaternary molassic sediments (~20 - 2 Ma)

----------------------------------**MFT**---------------------------------

 Indo-Gangetic plain

Table 2.1: *Tectonic divisions of the Himalaya (Wadia, 1931, Entire Himalaya-Yin, 2006; Nepal - Arita, 1983, Arita et al., 1997; Western Himalaya - Thakur, 1992; Garhwal and Kumaun - Valdiya, 1980).*

a. Sub - Himalaya: The Sub-Himalaya (also called as the Himalayan Foreland Basin) constitutes the foothills of low elevation of the outer Himalayan Range. This zone is essentially composed of Lower Tertiary

(Paleocene to Lower Miocene) marine to brackish water sediments and Upper Tertiary (Middle Miocene to Middle Pleistocene) fresh water molasse deposits, aprt from the the late orogenic intermontane deposits and alluvium. These Tertiary sequences, lying between MBT to the north and the 'active' thrust front (HFT) of the orogen to the south (Meigs *et al.*, 1995; Nakata, 1972; Nakata, 1989; Yeats *et al.*, 1992), suggests a combination of flexural bending of the Indian plate margin and thrust faulting (Beaumont, 1981; Lyon-Caen and Molnar, 1985; Najman et al., 1993; Burbank et al., 1994; Singh, 1999; Meigs, 1997; Störti et al., 1997).
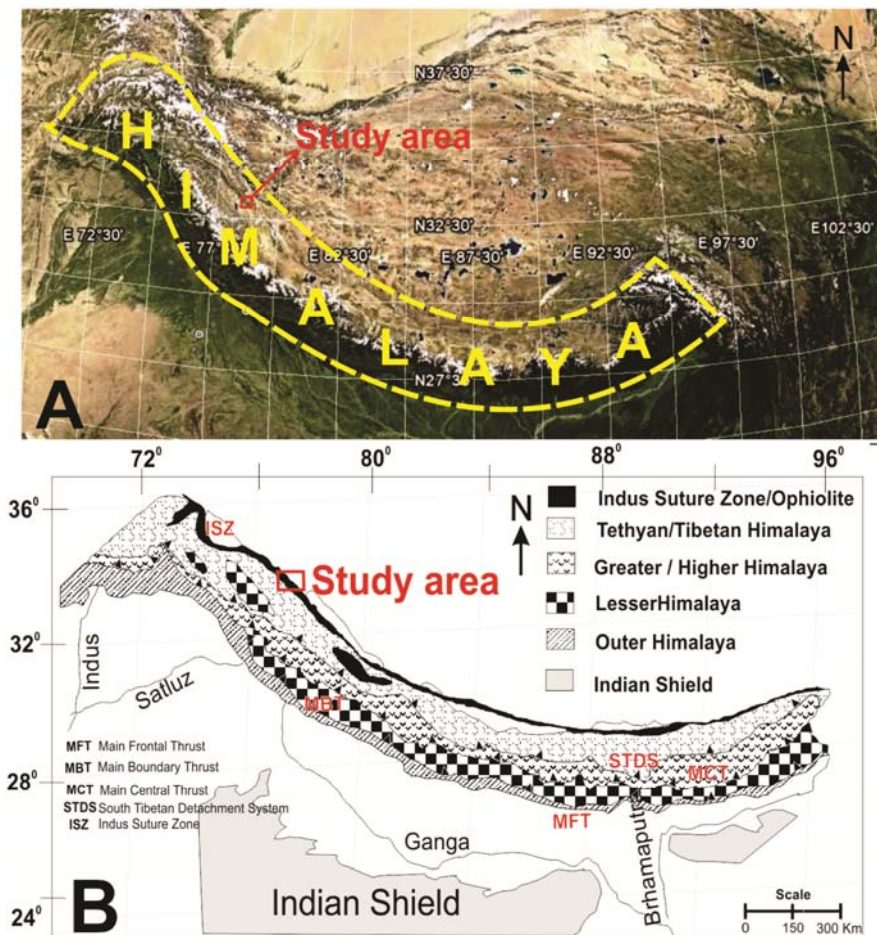
Figure 2.1: (A) *The entire Himalayan range is marked in a google Earth image.* **(B)** *Generalized geological map of Himalaya with its major subdivisions. In both the figure study area has been marked. (After Gansser 1964)*

b. Lesser Himalaya: The Lesser Himalaya mainly consists of Early Proterozoic to Lower Cenozoic detrital sediments from the passive Indian margin intercalated with some granites and acid volcanics (Frank, *et al*., 1977; Valdiya, 1980a; Srikantia and Bhargava, 1982). The predominant rock types are impure quartzites and psammitic phyllites and schists, with subordinate impure marbles, metamorphosed mafic rocks, and augen orthogneisses (Gansser, 1964; Valdiya, 1980a). These low-grade (lower -greenschist to lower-amphibolite facies) clastic metasediments of the Lesser Himalayan zone are confined between MCT to the north and MBT to the South. The Lesser Himalaya (LH) is mainly formed by Upper Proterozoic to lower Cambrian detrital sediments from the passive Indian margin intercalated with some granites and acid volcanics (1840 ±70 Ma [Frank et al 1977]). These sediments thrust over the Sub-Himalaya along the Main Boundary Thrust (MBT).

c. Higher Himalaya (Central Crystalline): The Higher Himalayan rocks usually known as High Himalayan Crystalline Sequence (HHCS) is a 30-20-km thick, medium- to high-grade metamorphic sequence of metasedimentary rocks which are intruded in many places by granites of Ordovician (c. 500 Ma) and early Miocene (c. 22 Ma) age. Although most of the metasediments forming the HHCS are of late Proterozoic to early Cambrian age, much younger metasediments can also be found in several areas. It is now generally accepted that the metasediments of the HHCS represent the metamorphic equivalents of the sedimentary series forming the

base of the overlying Tethys Himalaya. The HHCS forms a major nappe which thrusts over the Lesser Himalaya along the Main Central Thrust (MCT). As a whole the HHC rocks are found in between MCT and STD with varying metamorphic grade. It first increases upward in its lower part and then decreases from the middle to the upper part towards the STD (e.g., Hubbard, 1989; LeFort, 1996). In Himachal Pradesh along the Sutlej River in NW India, inverted metamorphism appears to span the whole HHC from MCT zone to the STD (Vannay and Grasemann, 1998). Deformed and undeformed early to middle Miocene leucogranites are widespread in the HHC, but they are mostly concentrated in the very top part of the GHC (e.g., Gansser, 1964, 1983; LeFort, 1975, 1996; Scaillet et al., 1990, 1995; Guillot et al., 1993, 1995; Parrish and Hodges, 1996; Searle et al., 1997, 1999a,b; Murphy and Harrison, 1999; De`zes et al., 1999; Grujic et al., 2002).

d. Tethyan Himalaya: The Tethys Himalaya is nearly 40 to 50 Km wide and 3 to 5 km high separated from the Trans-Himalayan range on the Tibetan block in the north by the Indus-Tsangpo Suture Zone (ITSZ) (Gansser, 1977). The Tethyan Himalayan Sequence consists of Proterozoic to Eocene siliciclastic and carbonate sedimentary rocks interbedded with Paleozoic and Mesozoic volcanic rocks (Baud et al., 1984; Garzanti et al., 1986, 1987; Gaetani and Garzanti, 1991; Thakur, 1992; Garzanti, 1993, 1999; Brookfield, 1993; Steck et al., 1993; Critelli and Garzanti, 1994; Liu and Einsele, 1994, 1999; Srikantia and Bhargava, 1998). The THS can be divided into four subsequences: (1) Proterozoic to Devonian pre-rift sequence characterized by

laterally persistent lithologic units deposited in an epicratonal setting; (2) Carboniferous–Lower Jurassic rift and post-rift sequence that show dramatic northward changes in thickness and lithofacies; (3) Jurassic–Cretaceous passive continental margin sequence; and (4) uppermost Cretaceous–Eocene syn-collision sequence (Liu and Einsele, 1994; Garzanti, 1999). Stratigraphic analysis of these sediments yields important indications on the geological history of the northern continental margin of the Indian continent from its Gondwanian evolution to its continental collision with Eurasia.

   e. **Trans Himalaya:** Trans- Himalaya, situated at the extreme end of Indian continental margin is considered to be most dynamic region of Himalayan Orogeny, bounded by the Karakoram batholiths to the north and the Zanskar and Tso Morari crystallines to the south, it provides an excellent opportunity to study the passive margin sediments to syn-subduction accretion and magmatism to collisional and post collisional processes. The Indus Suture Zone, ISZ (or Indus-Yarlung-Tsangpo Suture Zone) is considered as the principle unit of Trans-Himalaya which experienced collisional and post collisional activities. The Indus Suture Zone extends north of Himalaya from east to west for about 2500 km and is characterised by ophiolites and ophiolitic mélanges, plutonic-volcanic rock associations of a magmatic arc and flysch and molasse sediments (Thakur & Mishra 1984). The main litho-tectonic units of the area are: (1) the **Ladakh batholith** which has been developed between 110 – 50 Ma (Honegger et al., 1982; Schärer et al. 1984) on the Asian continental margin during northward subduction of Neo Tethys.

(2) the **Indus Molasse**, which is a continental clastic sequence comprising of alluvial fan and fluvio-lacustrine sediments derived mainly from the Ladakh batholith but also from the suture zone itself and the Tethyan Himalaya. These molasses are post-collisional and thus Eocene to post-Eocene. (3) the **Ophiolite & Ophiolitic Mélanges**, which are composed of an intercalation of platform sediments, mafic and ultramafic rocks from the Neotethys oceanic crust. (4) the **Dras Volcanics**, which are relicts of a Late Cretaceous to Late Jurassic volcanic island arc and consist of basalts, dacites, volcanoclastites, pillow lavas and minor radiolarian cherts.

2.2.   HISTORICAL ACCOUNT OF HIMALAYAN OPHIOLITIC MÉLANGE

It was not until the early seventies when continental collision between India-Eurasia was confirmed by the plate tectonic model (Dewev & Burke, 1973; Mohar et al., 1975). During the transition from oceanic to continental subduction, accretionary prisms are obducted in front of the arc and fore-arc area. Later, during continental convergence, accretionary prisms incorporate slices of mixed oceanic crustal rocks from the subducting oceanic slab, which gets metamorphosed and deformed before being juxtaposed over the continental margin. In orogenic domains, these deformed paleo-accretionary prisms delineate suture zones and are included in the ophiolitic mélange zone (Gansser, 1974).
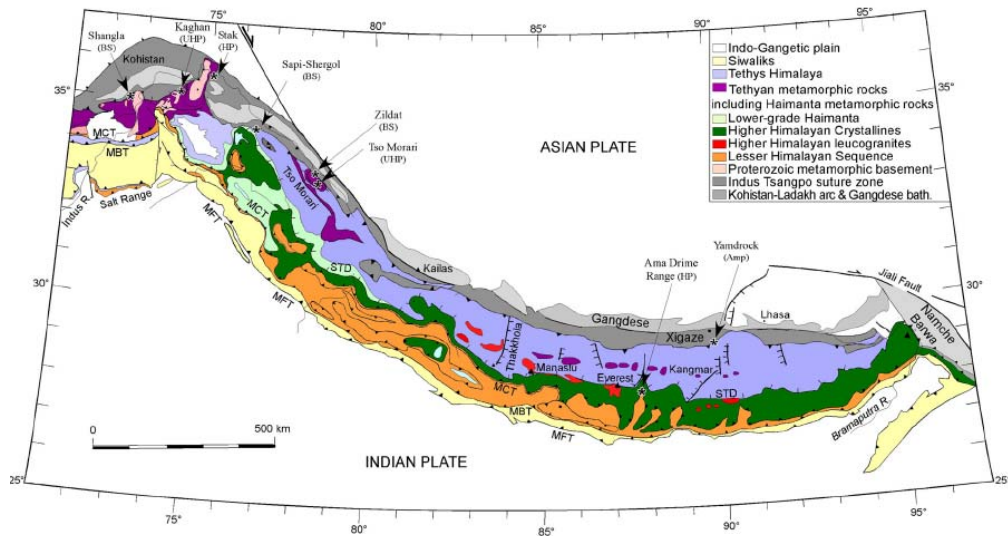
***Figure 2.2:** Geological map of Himalaya showing HP and UHP rock distribution along with ophiolitic mélange along Indus Suture Zone, ISZ (or Indus-Yarlung-Tsangpo Suture Zone) (after Gansser et al 1964., Ding et al., 2001; Guillot et al., 2003; Di Pietro and Pogue, 2004).*

Ophiolite and ophiolitic mélanges are intermittently traceable along the Indus Suture Zone, ISZ (or Indus-Yarlung-Tsangpo Suture Zone) (Gansser 1974; Nicolas et al. 1981; Burg and Chen 1984; Wang et al. 1987). The Indus Suture Zone (ISZ) is a major tectonic unit, north of the main Himalayan Range, extending discontinuously for nearly 2500 Km from Pakistan (locally known as the Main Mantle Thrust:MMT: Tahirkheli et al., 1979) through Ladakh to the Lhasa block in southern Tibet (LeFort, 1975; Molnar & Tapponnier, 1975; Gansser, 1977; Thakur, 1992). Brookfield & Raynolds 1981, suggests a late Cretaceous age for emplacement of the ophiolitic mélanges which occurred during collision of the Indian plate with a southward - facing middle Cretaceous island arc.

Towards the western part in Pakistan, the Indus suture zone is characterized by a thick pile of mélanges that reach maximum extent near Shangla Pass. The rocks are dismembered masses of metavolcanics, phyllites

with smaller lens-shaped bodies of serpentinites, metadolerites, metagreywackes, cherts and marbles metamorphosed under greenschist and blueschist facies (Kazmi et al., 1984). These lithologies were grouped into three mélange units separated by thrust contacts: the Mingora Ophiolitic Mélange, the Charbagh Greenschist Mélange and the Shangla Blueschist Mélange (Kazmi et al., 1984). Guiraud (1982) reported two types of blueschists: (1) schistose, associated with meta- greywackes and metatuffs and (2) associated with tholeitic metabasites. Late Cretaceous age of blueschist metamorphism is suggested by Anczkiewicz et al, (2000). Because the Shangla blueschists occur together with ophiolites, the 80 Ma event was correlated with the ''Cretaceous obduction of ophiolites in the Indus Suture Zone, in southern Tibet'' (Maluski and Matte, 1984; Anczkiewicz et al, 2000).

Towards the extreme East of Indus Suture Zone in Southern Tibet, the suture zone is called as the Yarlung Zangbo Suture Zone (YZSZ) and marks the location where the Neo-Tethyan oceanic domains have been consumed by northward subduction under the Lhasa terrane during the Cretaceous. This mélange consists of an imbricate thrust zone containing numerous south-verging thrust slices, which preserves an ocean floor stratigraphy (Aitchison et al., 2000). Structural and tectonostratigraphic features of the mélange are reminiscent of a remote intra-oceanic subduction complex (Mercier et al., 1984; Searle et al., 1987; Aitchison et al., 2000), and the unit has been interpreted to consist mostly of material off-scraped from the down-going Tethyan slab (Chang, 1984; Ziabrev et al., 2001). Fossil evidences suggest a mid Jurassic to late Cretaceous age of the mélange (Chang, 1984; Mercier et

al., 1984; Wu, 1993; Matsuoka et al., 2001, 2002). Oceanic fragments along the suture have been recently reinterpreted in a supra-subduction zone context (Hebert et al., 2000, 2001, 2003; Aitchison et al., 2000; Huot et al., 2000, 2003; Dubois-Coteˊ et al., 2003). Based on the chemistry data of pyroxene, from YZSZ ophiolitic mélange, Dupis et al., (2005) suggests the nature of the clinopyroxenes are boninites to island-arc tholeiites. The magma compositions suggest supra-subduction-zone setting, particularly from back-arc regions (Hawkins and Melchior, 1985; Hawkins and Allan, 1994).

The central-western part of Indus Suture Zone is characterised by patchy & dismembered rocks of ophiolite and ophiolitic mélange which are found in north western and south eastern part of Ladakh. These rocks are associated with relicts of two paleo-accretionary prisms (Cannat & Mascle, 1990; Corfield et al., 1999; Robertson, 2000): (1) the Sapi-Shergol mélange, which is associated with the Dras arc, and (2) the south Ladakh ophiolitic mélange named Zildat Ophiolitic Mélange, which is associated with the Nidar Ophiolitic complex. Relicts of these paleo-accretionary prisms consist of oceanic crust units including blocks of platform sediments showing low grade metamorphism, as well as, remnant of an early blueschist facies conditions (Frank et al., 1977; Honegger et al., 1982, 1989; Jan, 1987; Reuber et al., 1987; Sutre, 1990; Ahmad et al., 1996; Robertson, 2000). In the Sapi-Shergol mélange, the rock slices are intercalated with ophiolitic units (Honegger et al., 1982, 1989; Robertson, 2000) and are generally considered to be relicts of the oceanic basement of the Dras arc (Robertson, 2000). The blueschists are

22

imbricated with mélange formation of probably upper Cretaceous age, indicating temperature of 350 to 420°C and pressure around 9–11 kbar. Primary alkaline character of the blueschist suggests an oceanic island or a transitional MORB type primary geotectonic setting (Honneger et al., 1989). In south-eastern Ladakh the ISZ preserves **Zildat Ophiolitic Mélange** (ZOM) as the southernmost unit, which is followed in the north by the Nidar Ophiolite Complex. The two units are separated by a thrust contact (Thakur and Misra, 1984; Thakur, 1990). Tectonic interpretation of the Zildat Ophiolitic Mélange and associated Nidar ophiolitic complex has been controversial. Previous workers considered these rocks to represent mixed oceanic crust comprised of ultramafics, gabbros, volcanic rocks and associated sediments (Thakur and Virdi, 1979; Thakur, 1990). However, recent studies of the ultramafic rocks based on mineral chemical data indicate that the Nidar ophiolitic rocks characterised the remnant intra-oceanic island arc and supra-subduction setting rather than an oceanic floor sequence (Mahéo et al., 2000; Sachan, 2001; Ravikant et al., 2004; Ahmad et al., 2008). The Zildat Ophiolitic Mélange is the focus of the present study and the detail geology of the area is mentioned in the following part.

2.3.   GEOLOGICAL CONTEXT OF THE STUDY AREA: ZILDAT OPHIOLITIC MÉLANGE

The Zildat Ophiolitic Mélange (ZOM) is a part of the Indus Suture Zone, which marks the closure of the Tethyan ocean that subsequently lead to the collision between the Indian and the Eurasian continents that gave rise to the present day Himalayan mountain belt. Patchy exposures of ophiolitic

mélange are confined to the ISZ of NW Himalaya (Gansser 1974). It (Thakur and Mishra 1984) is exposed with a NW–SE trend (Fig. 2.3). The ZOM is bounded by the Nidar ophiolite to the north and Tso-Morari Crystalline (TMC) gneisses with ultrahigh-pressure eclogite (Mukherjee and Sachan 2001) to the south. The ZOM consists of clast and matrix of varying litho-units of different ages, called as Sumdo complex (Steck et al. 1998), and is further subdivided into Ribil and Drakkarpo units (de Sigoyer et al. 2004). Mélange blocks appear as grayish-green patchy masses containing eye-shaped thick exotic limestone bodies of 100 s of meters to a few centimetres in size. These exotics are Permian in age and represent the distal part of the Indian continent (Colchen et al. 1994; Corfield et al. 1999). De Sigyoer et al. (2004) inferred this mélange as remnant of seamounts accreted to the Indian margin. The ZOM, as a part of Indus Suture Zone, is separated from the TMC by north easterly dipping Zildat detachment fault. This fault is located between ZOM metasediments and TMC gneisses and has been linked to obduction processes (Thakur and Virdi 1979) and the melange rocks are juxtaposed over TMC along this fault zone (Ravikant 2003). The exhumation of TMC dome is also believed to have taken place along the Zildat detachment fault (Steck et al. 1998, Epard & Steck, 2008), which explains the overprinting of late-stage brittle deformation on the fault zone rocks (de Sigoyer et al. 2004; Mukherjee and Mulchrone 2012). Evidences of decompression melting at places in TMC rocks have also been observed (Guillot et al. 1997; de Sigoyer et al. 1997). In ZOM, relict pieces of blue schist mineral assemblages have also been noticed (Virdi et al. 1977), which, however, is related to its early metamorphic history.

24
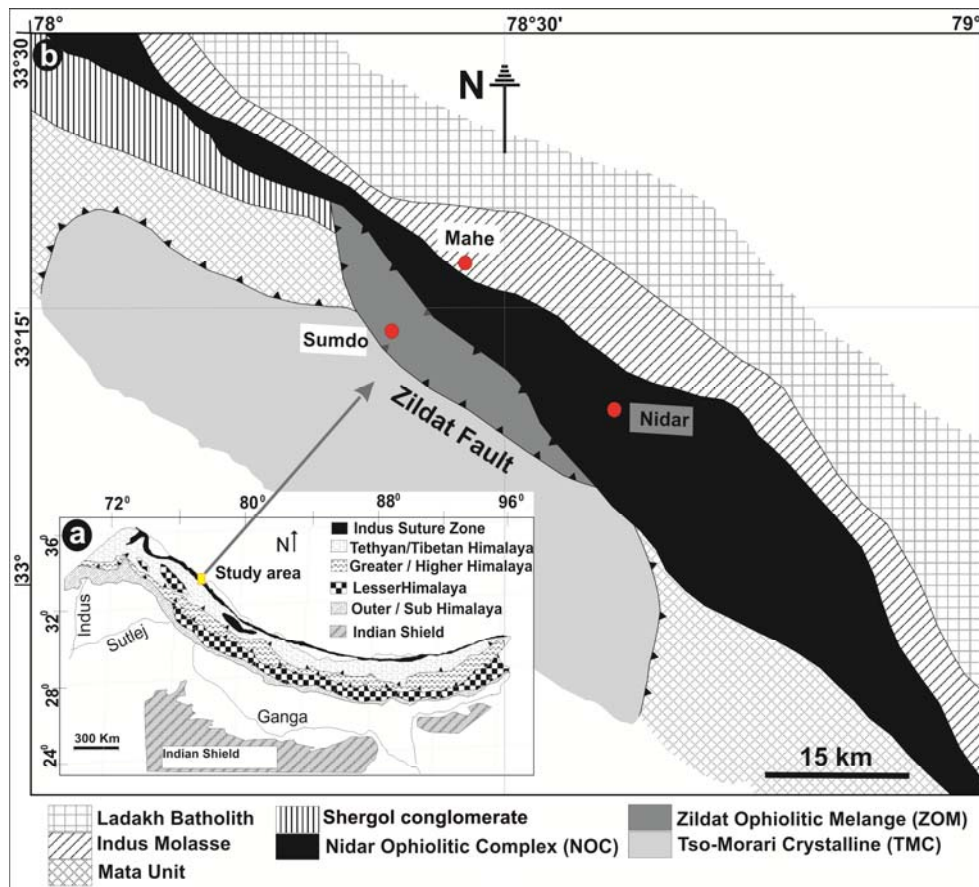
Figure 2.3: *generalize geological map of the Himalaya (after Gansser 1964) b. Detail geological map of the Zildat Ophiolitic Mélange and associated units of the Indus Suture Zone (ISZ);*

The principal lithounits of the study area from north to south transect are; Ladakh Batholith, Indus Molasses, Nidar Ophiolite Complex (NOC), Zildat Ophiolitic Mélange (ZOM) and Tso Morari Crystalline (TMC). The ZOM is bounded by NOC and TMC from northern and southern end. Around 70 samples were collected in two field seasons (years 2010 and 2012) for laboratory study from different litho-units of ZOM and its adjacent units. The details of these three units are discussed below;

Nidar Ophiolite Complex (NOC): Nidar ophiolite is bounded by calc alkaline batholith and Indus molasse to the north. The Nidar ophiolite appears as regional scale "eye" shaped in plain view following the trend of ISZ (Fig.

2.3). The NOC is exposed in two different sections (Mahe-Sumdo valley &

Nidar valley, eastern Ladakh) of the study area. In studied Mahe-Sumdo

section, mainly the crustal part of the NOC is well preserved which is in

thrusted contact with ZOM. These include well-preserved pillow lava and

basalt. Pillow lavas are fine grained and bear vesicles of 1 – 4 mm diameter

(Fig 2.4a).
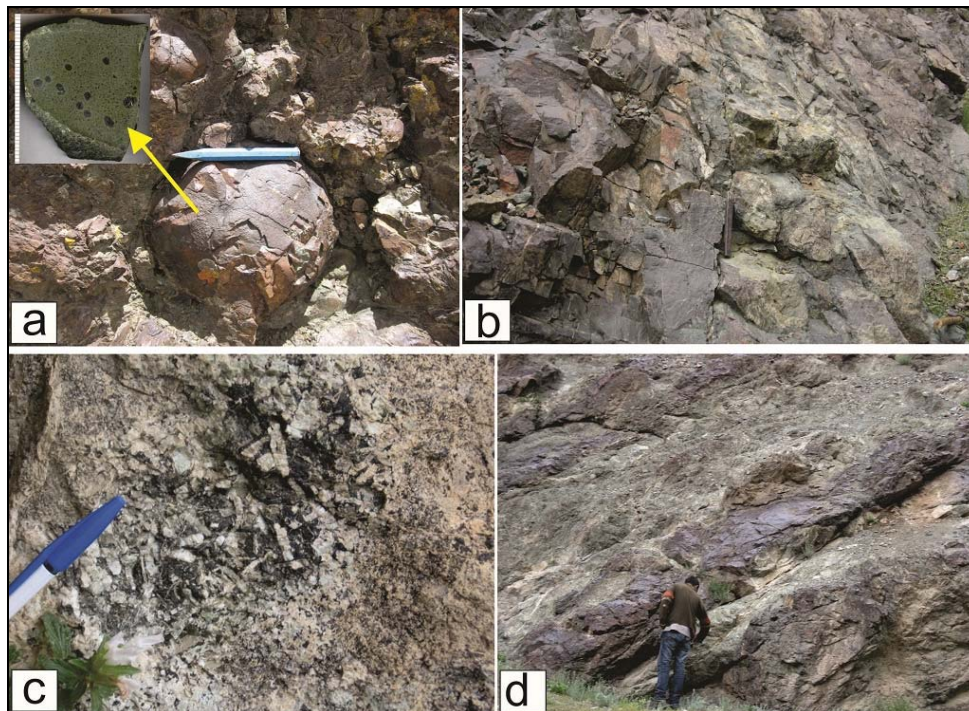
Figure 2.4: *Field characteristics of NOC, situated at the northern boundary of ZOM.* *a)* *fine grained pillow lava and basalt showing vesicles.* *b) sheeted dyke complex.* *c)* *large crystals of plagioclases in gabbro.* *d) intercalation of gabbro and serpentinites*

Next part is sheeted dyke complex which is connected to the pillow lava suite

(Fig 2.4b). The basic dykes are intruded into earlier dykes and create a sheeted

dyke complex (thickness 300 – 500 m). Beneath the sheeted dyke part 1 – 1.5

Km thick mafic cumulates are present. The mafic cumulate part is composed

of layered gabbro, dolerite and basalt. In gabbro large crystals of plagioclases

are observed. Sometimes the sizes of plagioclase crystals are up to ~ 3 cm (Fig

2.4c). In Mahe valley the gabbroic crustal part of the ophiolites has a contact with serpentinized peridotites which is the upper most part of mantle ultramafics of the ophiolite. The contact is identified as petrologic Moho within the NOC. It occurs as a zone which is about 500 m thick having repeated intercalation of gabbro and serpentinites (Fig. 2.4d). The crustal part of the ophiolite in Mahe valley is undeformed, as exemplified by circular vesicles in pillow lavas and random orientation of plagioclase laths in cumulate gabbros. It does not show any penetrative tectonic fabric and there is no similarity between the fabric present within the ophiolite and that in its adjacent mélange or TMC rocks. In the adjacent Nidar valley (Fig. 2.3) the mélange is completely absent. The TMC has a north dipping contact with the mantle section of the ophiolite suite (Fig. 2.3).

Tso Morari Crystalline (TMC): The Tso Morari Crystalline (TMC) represents Paleozoic Indian continental margin, which subducted down below 120 kms below Asian plate (Mukherjee et al, 2003). TMC is a domal structure and consists of both ortho- and para-gneiss and metabasic enclaves. These enclaves are garnet amphibolite to eclogite in nature. Some of these enclaves also contain signature of UHP metamorphism in the form of coesite (Mukherjee & Sachan, 2001). Eclogitization of TMC took place at 20±2 Kbar or ~45 km depth (Guillot et al., 1997). This unit later recognized as UHP terrain, shows metamorphism at 750°C and 4 GPa (Mukherjee et al, 2003). Metamorphic ages obtained by de Sigoyer et al. (2000) suggest ~55 Ma age for eclogitization of TMC, followed by amphibolite facies metamorphism at ~47 Ma. According to these workers, TMC reached upper crustal level at ~30

Ma. However in a recent study by Donaldson et al. (2013) suggests that TMC experienced peak metamorphism at ~47-43 Ma. Evidence of UHP metamorphism of Indian continental crust during the Himalayan Orogeny was first provided by O'Brien et al. (2001) from Kaghan valley of Pakistan. They inferred a pressure condition of >27 Kbar on the basis of the presence of coesite and garnet-omphacite-phengite barometry. Later on, Mukherjee & Sachan (2001) reported inclusion of coesite within garnet from the eclogites of the TMC. These studies inferred a subduction depth of 90-100 km for the leading edge of the Indian continent. These were followed by more petrologic studies from the TMC to constrain the P-T-t path of the TMC eclogites (de Sigoyer et al., 2000, 2004; Donaldson et al., 2013; St. Onge et al., 2013). For example, St. Onge et al. (2013) has used the garnet rim-omphacite-rutile-phengite-lawsonite-talc-quartz (coesite) assemblage to infer a temperature of 630-645°C and 25.5-27.5 Kbar pressure for peak metamorphism of the TMC eclogites. Direct evidence of UHP metamorphism in the TMC eclogites has only been documented in the form of coesite (Mukherjee & Sachan, 2001) and microdiamond (Mukherjee & Sachan, 2004). TMC has a northerly dipping contact with ZOM known as Zildat fault.

Zildat Ophiolitic Mélange (ZOM): ZOM contains clasts of gabbro, serpentine, radiolarian chert, which derived from the adjacent ophiolites and also clasts of blueschists. Sm-Nd whole rock dating of gabbro from NOC gives an age of ~140 Ma (Ahmed et al., 2008). Kojima et al. (2001) inferred an age of ~134 Ma to 113 Ma for the radiolarian cherts of the NOC. Honegger et al. (1989) carried out K-Ar dating on the blueschist clasts present within the

Indus Suture Zone and obtained an age of ~98 Ma for blueschist

metamorphism.

Figure 2.5: *Mesoscopic features within the Zildat ophiolitic Mélange* ***a)*** *Mylonitized quartz vein within metabasics reveals dextral (top-to-the-north) sense of shear.* ***b)*** *Quartz veins within the same metabasics fractured and imbricated (black arrows) due to compression.* ***c)*** *Foliation concordant with attitude of the contact between TMC and ZOM. It has been further warped.* ***d)*** *Clasts of chert and calcite within ZOM showing imbrications and 'top-to-the-south' sense of movement.* ***e)*** *Clast of gabbro present within metagreywacke of ZOM.* ***f)*** *Clast of serpentine within ZOM.* ***g)*** *North verging fault-propagation fold near the contact between ZOM and NOC.* ***h)*** *Exotic carbonate block of ZOM thrusts over NOC. Thrust plane dipping due south.*

The electrons interact with atoms in the sample, producing various signals that can be detected and that contain information about the sample's surface topography and composition. The types of signals produced by a SEM include secondary electrons (SE), back-scattered electrons (BSE), characteristic X-rays, light (cathodoluminescence) (CL), specimen current and transmitted electrons. Only secondary electron detectors are standard equipment in all SEMs which produces three-dimensional images of the object selected for study. All samples must also be of an appropriate size to fit in the specimen chamber and are generally mounted rigidly on a specimen holder called a specimen stub. All the high resolution surface topographic images are-

Figure 3.4: *SEM with EDS attachment in SEM Lab, WIHG, Dehradun, India*

captured in WIHG, Dehradun using ZEISS EVO 40 instrument (Fig. 3.4). The specimen for study is inserted to the high vacuum sample chamber and the surface of the sample must be electrically conductive to prevent the accumulation of electrostatic charge at the surface. Conductive materials in

current use for specimen coating include gold & carbon coating. Carbon coating and carbon tape is used in case of polished rock specimen mounted on glass slide. Where as gold coating is used while studying the rock chip specimen. Instrument conditions are adjusted with due time of analysis depending upon the type of sample and image quality. In all the cases 20 kV accelerating voltage is used but probe current, probe diameter and working distance is tuned in different cases for better image quality.

3.3. MINERAL CHEMISTRY

Mineral chemistry is an essential proxy used in geological science for mineralogical and petrological aspect. In-situ non destructive mode is chosen for such analysis because they give the elemental concentration without destroying the rocks original texture. To generate mineral chemical data SEM-EDS and EPMA was carried out. Details of them are discussed here.

3.3.1. SEM WITH ENERGY DISPERSIVE X-RAY (SEM/EDS) SPECTROSCOPY

Scanning electron microscopy coupled with energy dispersive X-ray spectroscopy (SEM/EDX) is the best known and most widely-used method for surface analytical techniques. High resolution images of surface topography, with excellent depth of field, are produced using a highly-focused, scanning (primary) electron beam. SEM/EDS allow identifying what are the particular elements present in a rock/mineral sample with their relative proportions (Atomic % for example). It has the ability to produce images of polished

sections showing differences in mean atomic number which is very useful in mineralogy & petrology. In addition to low energy secondary electrons (in case of SEM), backscattered electrons and X-rays are generated by primary electron bombardment. The intensity of backscattered electrons can be correlated to the atomic number of the element within the sampling volume. Hence, some qualitative elemental information can be obtained. SEM, accompanied by X-ray analysis, is considered a relatively rapid, inexpensive, and basically non-destructive approach to surface analysis. It is often used to survey surface analytical problems before proceeding to techniques that are more surface-sensitive and specialized.

In the present research SEM/EDX is used for rapid first hand chemical composition of mineral phases. Carbon coated polished rock slides are prepared before chemical analysis of minerals through SEM/EDS. The main objective was to capture backscatter images of rock and minerals which gives a contrasting grey scale image of a mineral phase depending upon its chemical and atomic variability. Along with backscatter images, chemical concentration is gathered by various spot analysis, area scan and line scan. These give a better picture in terms of elemental presence and concentration in terms of atomic percentage. All the backscatter images captured and analysis done at WIHG, Dehradun using ZEISS EVO 40 with Energy Dispersive X-ray Microanalyser - Bruker LN2 free X-Flash 4010 detector. 20 kV accelerating voltage is used with varying probe current, probe diameter working distance.

3.3.2. ELECTRON PROBE MICRO-ANALYSER (EPMA)

Electron probe microanalysis is an analytical technique that is used to know the composition of small areas on specimens. EMPA works on bombardment of accelerated electron beam to the surface of the sample. The electron beam is focused on the surface of a specimen using a series of electromagnetic lenses and these energetic electrons produce characteristic X-rays. The characteristic X-rays are detected at particular wavelengths and their intensities are measured to determine concentrations (efficiently up to 400 ppm), as each atomic element emits specific and identical wavelength of X-rays. EPMA is used for qualitative analysis by which it is possible to detect the presence of elements in the portions of the target sample. Semi - quantitative analysis through EPMA also can be done which involves the measuring of the intensity of X-ray generated form an unknown sample and compare with suitable standard using identical instrumental condition. EPMA is also capable for capturing SE and BSE imaging.

The in-situ mineral chemistry in this research was determined using a CAMECA SX-100 electron microprobe at Wadia Institute (Fig. 3.5). The instrument is provided with a gun chamber with tungsten filament for the generation of electrons, a column with condenser and probe lens to de-magnify the electron beam. It is provided with 4 spectrometers (three vertical and one inclined with diffracting crystals like PET, TAP, LIF and some pseudo-crystals for the generation of good resolution X-rays, and a gas proportional counter to measure the intensities. The instrument is operated using "Peak-Sight Software", which also helps to carry out its various

applications. The instrument is also provided with two rotary pumps, one diffusion pump and an ion pump to maintain good vacuum all along the path of electron beam.
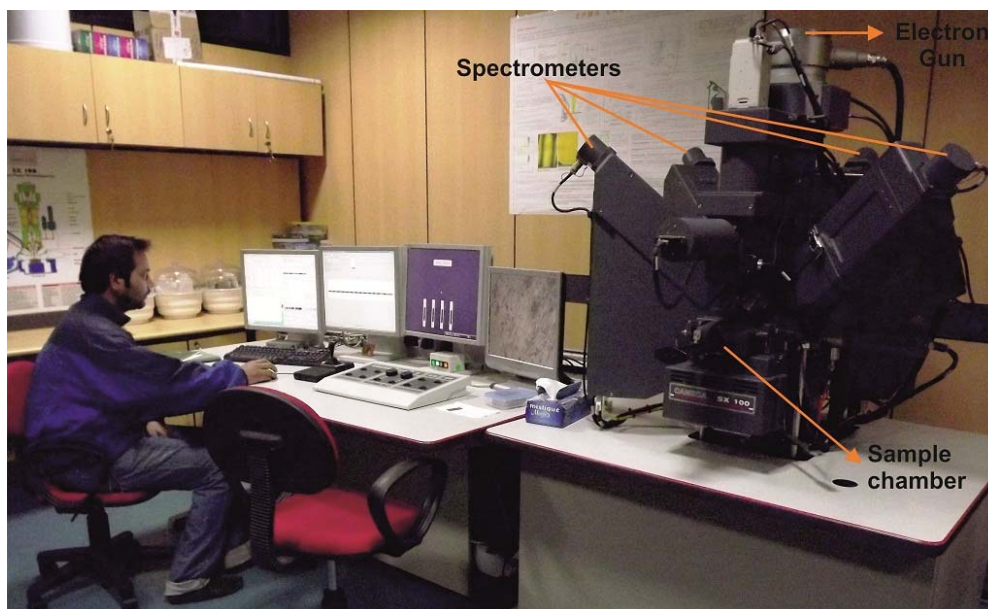
Figure 3.5: *CAMECA SX 100 EPMA instrument in EPMA Lab, WIHG, Dehradun, India*

More than 160 spot analyses are done in four thin sections during the research on various minerals with varying their growth domain. Analytical conditions were 15 kV accelerating voltage and 20 nA probe current. Calibration standards used were generally simple oxides (GEO Standard samples). The diameters of beam at the time of analyses were ~ 3 - 5 μm. The raw data were corrected using the ZAF method. Detection limits were ~ 0.1% and accuracy deviation was less than 5%.

3.4. GEOCHEMICAL STUDY

Rock samples were collected from the ZOM for bulk rock geochemical analysis. From exotic carbonate blocks, 19 carbonate samples were chosen for stable isotope study using Isotope Ratio Mass Spectrometer (IRMS). Bulk rock geochemistry is done by using XRF & ICPMS. All the analysis for stable isotope, major oxides, trace elements and REEs are performed at Wadia Institute of Himalayan Geology, Dehradun.

3.4.1. STABLE ISOTOPE GEOCHEMISTRY USING IRMS

Stable isotope analysis of carbon and oxygen was performed to address the fluid responsible processes during deformation and exhumation of exotic limestone blocks. Applying such stable isotope systematics, valuable information regarding initial fluid behaviour and its modification are recovered.

Isotope-ratio mass spectrometry (IRMS) is a specialization of mass spectrometry, in which mass spectrometric methods are used to measure the relative abundance of isotopes in a given sample. Measurement of natural variations in the abundances of stable isotopes of the same element is normally referred to as 'stable isotope' analysis. This field is of interest because the differences in mass between different isotopes lead to isotope fractionation, causing measurable effects on the isotopic composition of samples. By comparing the detected isotopic ratios to a measured standard, an accurate determination of the isotopic make up of the sample is obtained. For example, carbon isotope ratios are measured relative to the international standard for C.

The C standard is produced from a fossil belemnite found in the Pee Dee formation, which is a limestone formed in the Cretaceous period in South Carolina, U.S.A. The fossil is referred to as VPDB (Vienna Pee Dee Belemnite) and has 13C:12C ratio of 0.0112372. Oxygen isotope ratios are measured relative the standard, V-SMOW (Vienna Standard Mean Ocean Water).

Variations in stable isotope ratios are typically in the parts per thousand (‰) ranges and hence are generally reported as *permil variations*, δ, from some standard. Oxygen isotope fractionations are generally reported in permil deviations from SMOW (standard mean ocean water):

$$\delta^{18}O = \left[\frac{(^{18}O/^{16}O)_{sam} - (^{18}O/^{16}O)_{SMOW}}{(^{18}O/^{16}O)_{SMOW}} \right] \times 10^3$$

The same formula is used to report other stable isotope ratios.
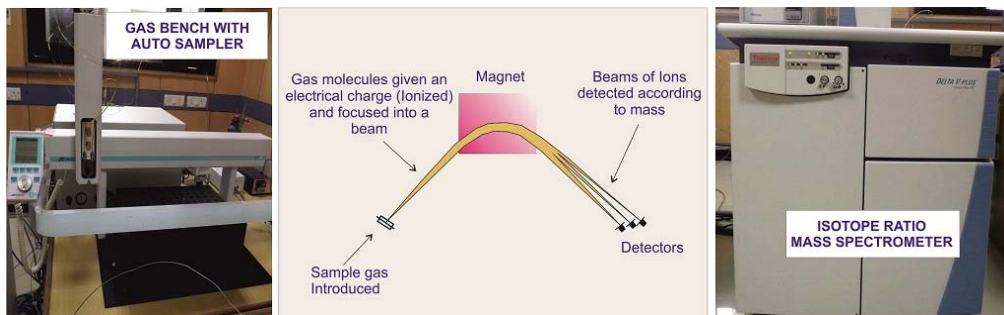
Figure 3.6: *Sample inlet unit and working principle of Stable Isotope Mass Spectrometer at WIHG, Dehradun*

Approximately ~200 µg of powdered samples from each whole rock specimen was weighed for analysis. CO_2 was extracted from calcite by dissolving in 100 % H_3PO_4 at 72º C for 1–2 hours. The extracted gases were analyzed as CO_2 on Thermo Delta V Plus Isotope Ratio Mass Spectrometers

(Fig. 3.6), and the results are expressed relative to V-PDB (Pee Dee belemnite; carbon) and V-SMOW (standard mean ocean water; oxygen). Reference CO2 gas was calibrated against international standards before analysing the unknown samples. Those standards were also run simultaneously with the samples, and the generally yielded values are within the range of ±0.1 ‰.

3.4.2. BULK ROCK GEOCHEMISTRY USING XRF & ICPMS

This study focuses on the geochemistry of the meta-basalts from the terminal part of the mélange. These particular samples were chosen for geochemical studies because they appeared as uniform layered unit rather than mixed disrupted rock unit. The rock samples were powdered using Retsch 2000 ball mill ultra-fine grinder at Wadia Institute. The samples were prepared with care to avoid contamination. Whole-rock compositions were obtained by X-ray fluorescence spectrometry (XRF) for major elements and few trace elements; REEs and some trace elements were determined by ICP mass spectrometry (ICP-MS).

X-ray fluorescence (XRF) spectrometer is an x-ray instrument used for routine chemical analyses of rocks, minerals & sediments. It works on wavelength-dispersive spectroscopic principles that are similar to an electron microprobe (EPMA). The analysis of major and trace elements in geological materials by XRF is made possible by the behaviour of atoms when they interact with X-radiation. For XRF analysis, firstly the basic samples are heated at 1000ºC for LOI calculation. Homogenized sample weighing 6g have been taken and mixed thoroughly with polyvinyl alcohol and made pressed

pellets of 40 mm diameter and 2 mm thick, for the X-Ray Fluorescence
Spectrometry analysis. Major oxides (SiO_2, Al_2O_3, Fe_2O_3, Na_2O, MgO, CaO,
K_2O, MnO, P_2O_5, and TiO_2) and Trace element (Ba, Cr, V, Sc, Co, Ni, Cu, Zn,
Ga, Pb, Th, Rb, U, Sr, Y, Zr and Nb) were analyzed by X-ray Fluorescence
spectrophotometer using BRUKER S8 TIGER at WIHG, Dehradun. Elements
were analyzed against WIHG in-house basic standards (BR, GSP 1) and the
analytical error is within ±5 %.

Figure 3.7: *X-ray fluorescence spectrometry (XRF) & Inductively coupled plasma mass spectrometry (ICP-MS) laboratory, WIHG, Dehradun, India*

Inductively coupled plasma mass spectrometry (ICP-MS) (Fig. 3.7) is
a type of mass spectrometry which is capable of detecting metals and several
non-metals at concentrations as low as part per billion. This is achieved by
ionizing the sample with inductively coupled plasma and then using a mass
spectrometer to separate and quantify those ions. ICPMS works on solution
mode and the hard rock samples are digested through various acid treatments
before inserted for analysis. For ICPMS sample preparation requires utmost
attention as the amount of sample being dissolved is very small (100 mg).
Powdered rock samples (~ 200 meshes) are digested with about 10 ml of HF-
HNO_3 mixture (2:1) in open teflon crucibles on a hot plate. Process is repeated

3- 4 times with evaporation to incipient dryness to ensure complete digestion. It is followed by treatment of $HClO_4$ and contents are evaporated to complete dryness. Finally the dried mass is dissolved in 10 ml of 10% nitric acid and final volume is made up to 100 ml with the help of distilled water. The prepared solution then analysed for trace and REEs using PerkinElmer SCIEX quadrupole type ICP Mass Spectrometer ELAN DRC-e, performed at WIHG, Dehradun. Along with unknown rock samples, blank and reference (standards) samples are also prepared and analysed at same time. JB-1a and JB-2 are used as references which are international standards for basaltic rocks. The analysed data accuracy is well within the accepted error limit (±10%).

3.5. INCIPIENT MINERAL / VOLATILE PHASE CHARACTERISATION

Mélange rocks often show complex mixing of heterogeneous fluid and volatile masses which alter and effect the overall rock unit in various aspect. The fluid inclusion petrography and laser Raman Spectroscopy is executed for this purpose to characterize the incipient mineral & volatile phases.

3.5.1. FLUID INCLUSION PETROGRAPHY

Fluid inclusion petrography is implemented on Zildat Ophiolitic Mélange zone carbonates to categorize their mode of occurrences and generation of fluid influx. To establish various type and generation of fluid with respect to the mineral texture, the tiny fluid inclusions are observed under normal petrological microscope (Nikon ECLIPSE LV100POL at WIHG, Dehra Dun) using high magnification objective lens (50x – 100x).

3.5.2. LASER RAMAN SPECTROSCOPY

Raman spectroscopy is a spectroscopic technique based on inelastic scattering of monochromatic light, usually from a laser source. It is a light scattering technique, and can be thought of in its simplest form as a process where a photon of light interacts with a sample to produce scattered radiation of different wavelengths. Raman spectroscopy is extremely high sensitive instrument which is used for mineral/volatile phase identification.
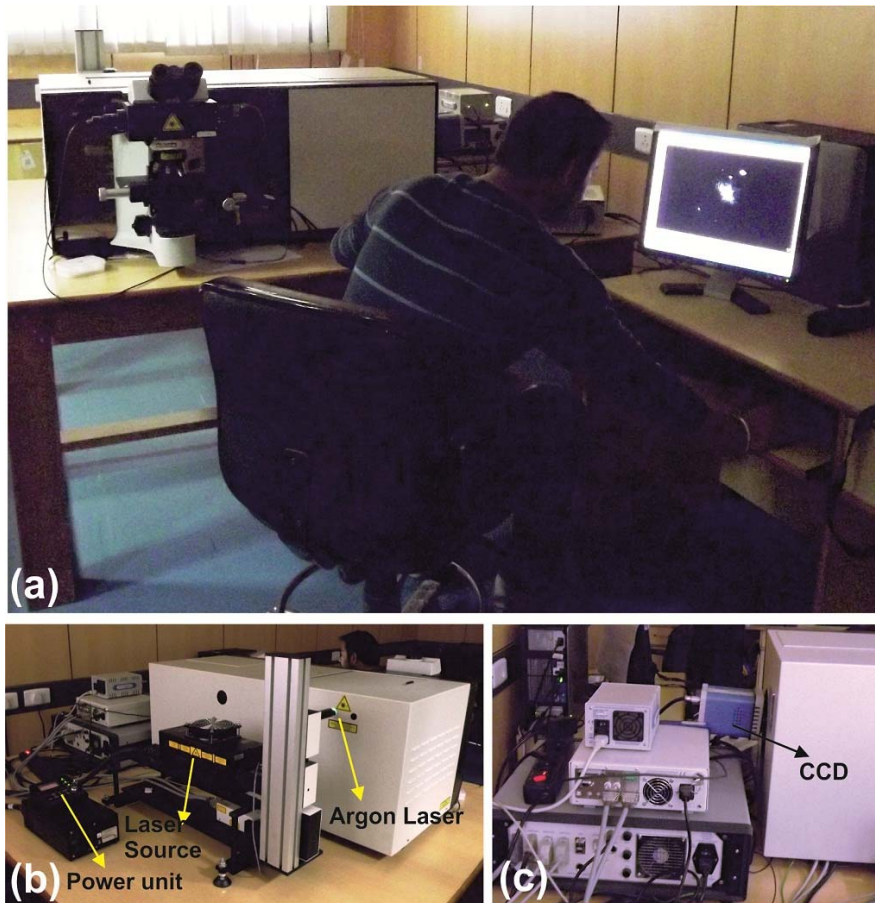
Figure 3.8: *(a) Raman Spectroscope Lab, WIHG, Dehradun, India. (b) The interlock system which control the laser power unit, laser source (c) The Charge Couple Device (CCD) is shown here which produces digital image of spectrum.*

A Raman spectroscope system typically consists of four major components: 1. Excitation source (Laser), 2. Sample illumination system and light collection

optics, 3. Wavelength selector (Filter or Spectrophotometer), 4. Detector (Photodiode array, CCD or PMT)

All the Laser Raman spectroscopy was performed using a LabRAM HR - Horiba Jovin Yuvon Instrument (Fig. 3.8) at the Wadia Institute of Himalayan Geology, Dehra Dun (India). The analyses were done on thin section. Spectra were excited at room temperature with the 514.5 nm line of a green Argon Laser and detected by a Charged Couple Device (CCD) detector. At the time of analysis at least -70^0C temperature was maintained for CCD. OLYMPUS® 50X and 100X objective were used to locate the spot for laser incidence. The laser spot size on the surface had a diameter of approximately 1 - 4 μm and a power of ∼ 4 – 6 amp and 15 – 30 mW. Light was dispersed by a holographic grating with 1800 grooves/mm. RTD exposure times for minor mineral phases were selected between 1- 30 s. Spectra are recorded from 0 - 4000 cm $^{-1}$. In special cases the spectral resolution is increased by narrowing its window. The Raman was calibrated with synthetic silica standard at 520.5 cm^{-1}. The estimated spectral shift at the time of analyses was 1 – 2 cm^{-1}. Acquired data are plotted to reveal unknown mineral/volatile phases between Raman Shift and arbitrary unit.

CHAPTER 4

Mineralogical and Structural Evolution of Zildat Ophiolitic Mélange

MINERALOGICAL AND STRUCTURAL EVOLUTION OF THE

ZILDAT OPHIOLITIC MÉLANGE (ZOM)

4.1. INTRODUCTION

Mélanges represent a significant component of subduction-collision related accretionary orogenic unit that found throughout the world along modern and ancient plate margins. Mélanges at the collisional zone are considered as most dynamic in character and are best candidate to document geological records. Complexities in mélange developed due to the rock masses experience various tectonic processes during subduction-accretion and collision that can lead to intensive deformation and metamorphism with time.

The continued collision between India and Eurasia and northward under thrusting of the Indian plate beneath the Tibetan plateau is the primary driving force for the creation of the Himalayan mountain belt (Dewey & Bird, 1970; McKenzie &Sclater, 1971). This collision zone is marked by NW-SE trending suture zones formed due to the subduction-accretion of oceanic plates and the collisional process of India and Eurasia (Fig 4.1a). The Indus Suture Zone (ISZ) is one such suture zone formed at ~55 Ma (Searle et al., 1984), where the Tethyan oceanic plate was consumed as the Indian plate approached northward and finally collided with Eurasia. The ISZ is characterized by an interesting collisional setting, where an ophiolitic mélange, called as the Zildat Ophiolitic Mélange (ZOM) is sandwiched between UHP crystalline known as

the Tso Morari Crystallines (TMC) and an ophiolite suite called the Nidar

Ophiolitic Complex (NOC) (Thakur & Mishra, 1984) (Fig. 4.1b).
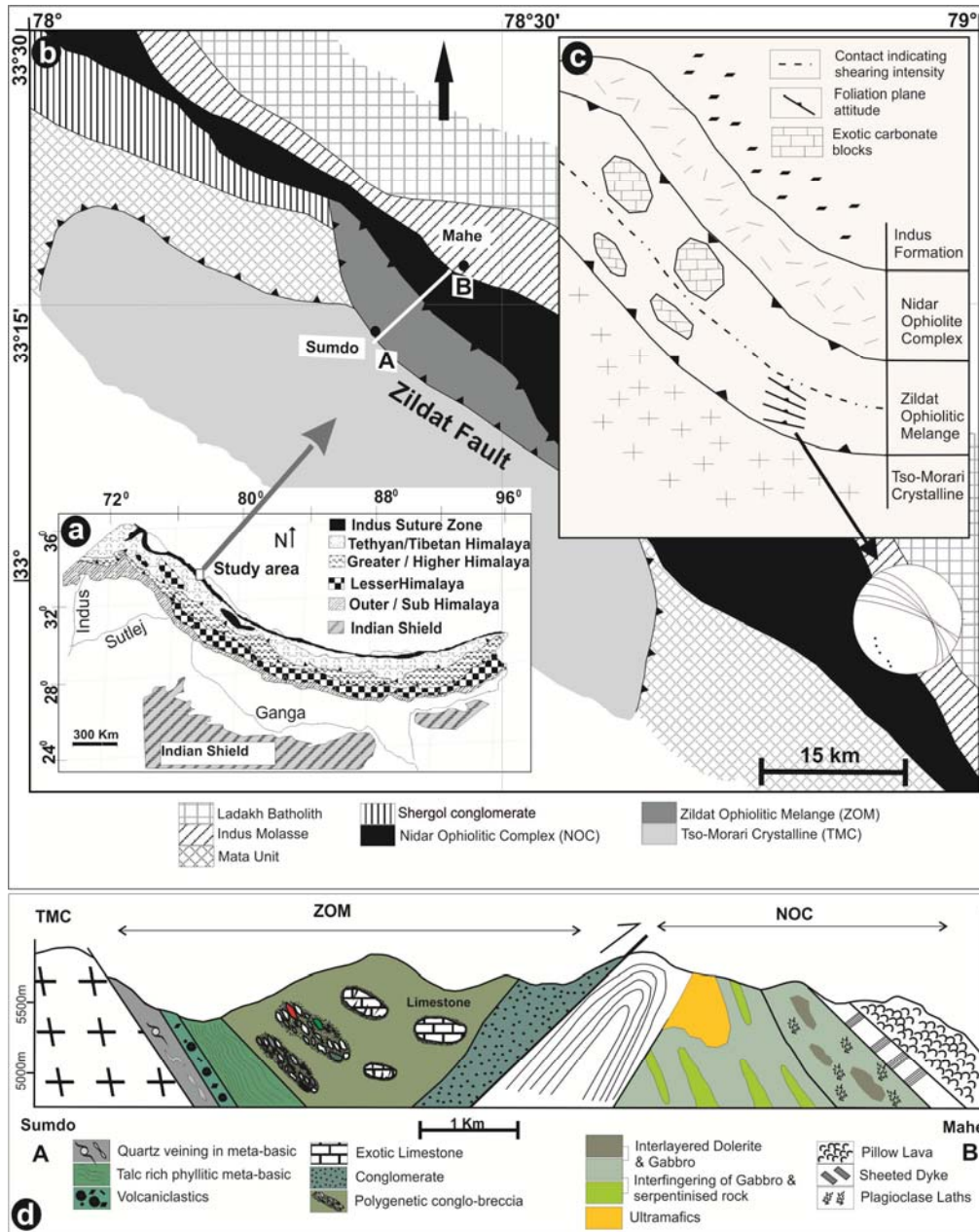
Figure 4.1: a) *Study area marked in the generalized geological map of Himalaya (after Gansser 1964).* *b)* *Simplified geological map of studied part of Indus Suture Zone, NW Himalaya (modified after Thakur and Misra 1984; Steck et al. 1998; Mahéo et al. 2006).* *c)* *lithological contacts & structural features of ZOM rocks with its surrounding lithounits.* *d)* *Cross section (as marked as A-B in Fig. b across the Indus Suture Zone showing various litho-units of the Zildat Ophiolitic Mélange and the Nidar Ophiolitic Complex.*

By definition, Zildat Ophiolitic Mélange is an incoherent undefined rock pieces which are heterogeneously deformed and chaotically distributed. In this chapter, mineralogy and structure of the heterogeneous mélange is studied in detail. This worth studying due to their occurrences at collisional set-up along Indus Suture Zone. Through metamorphic and structural proxies, various questions can be answered in context of overall evolution ZOM and associated rocks. 1. Whether all the separate units of mélange formed or mixed up uniformly; 2. Does the deformation behaviour incoherent across the whole mélange; 3. Can metamorphism any way related to the formation of mélange; 4. Whether metamorphic evolution is continuous and progressive in nature or it is randomly associated; 5. Did internal structure of mélange is incongruous with metamorphism of mélange; 6. Whether ZOM and surrounding rocks collectively played any role in the evolution of the Indus Suture Zone.

4.2. FIELD OBSERVATIONS AND GEOLOGICAL CROSS SECTION

The ZOM rocks are well exposed in a ~8 km stretch from Sumdho to Mahe village along a narrow valley (Fig. 4.1b). The ZOM rocks are bounded by the Nidar Ophiolitic Complex to the north and the Tso-Morari Crystalline to the south separated by the Zildat fault (Fig. 4.1b-c). The ZOM shows systematic lithological variation from southern to northern margin of the mélange (Figure 4.1d). It arranged as a block-in-matrix mixture of different clasts and matrix. Lithologically the ZOM is characterised by 3-4 km thick incoherent heterogeneous rock mass. It appeared as multi-coloured lithological cluster as a whole with variable thickness; consists of 10s of meter thick

blueish green volcaniclastic layer, 500 m thick light green coloured phyllitic metabasic, 3 km thick greyish meta-greywacke or conglo-brecciated unit with large disoriented exotic limestone blocks, 2-3 km thick greenish ultramafic patches with serpentinised groundmass alternatively enriched in talc and asbestos. It has sporadic occurrences of green coloured immature conglomerate with basaltic-gabbro clast. The ZOM out crop has highly disordered lithology which are intensely deformed. The deformation pattern across the whole ZOM unit is not uniform and intensely sheared towards the contact of Zildat fault. Generally, the rocks of the matrix are characterized by a slaty cleavage and incipient to prominent schistosity throughout the mélange. The foliation planes strike roughly in most of the places in a NW-SE direction, but near its contact with the TMC, the strike gradually rotates in a WNW-ESE direction with a steeper dip (Fig. 4.1c). The matrix rocks show folding, crenulation, pencil cleavage, shearing and cataclasis (Fig. 4.2a-d). The matrix fragments are unsorted, sub-angular to sub-rounded grains of lithic fragments. The matrix is fine-grained and made up of quartz, calcite, chlorite, sericite, biotite, serpentine and iron oxides.

The exotic fragments are mainly oceanic lithospheric rocks and pelagic sediments. They are well preserved within a highly sheared basic volcaniclastic matrix. It shows variable sizes and shapes and include marbles, serpentinite and metamorphosed ultramafic rocks, metagabbro, massive metabasalts, and minor chert bodies. The rocks are sporadic and occur both as mappable and un-mappable bodies contain blocks and pebbles of various sizes. Among the exotics, the metamorphosed limestones are notable ranging

from 100s of meter to few centimetres in size. The exotic blocks occur as lensoidal bodies, sheets, slabs, and slices, generally trending NW-SE with the regional trend of the host matrix. At places these exotics are sub-rounded to sub-angular and poorly shorted. The distribution pattern of exotics within ZOM show several sub-units across the whole package (Fig. 4.1d). At the terminal part of ZOM, near the Zildat fault, a pale green coloured mylonitised metabasic layer is observed. It has several generation of quartz veins along with notable distribution of pyrite and goethite (?) (Fig. 4.2e). This unit is intensely foliated, dips toward north. The quartz veins are mylonitized and shows 'down-to-the north' sense of shear indicating normal sense of movement along the Zildat fault (Fig. 4.2f). However, these same veins also show late imbrications, which suggest subsequent thrusting movement along the Zildat fault (Fig 4.2g). Further north, volcaniclasts are present containing clasts of pyroxene, quartz veins and vesicles filled by secondary quartz and calcite (Fig 4.2h). A fine grained meta-basic unit is present at extreme southern part of the mélange, near its contact with the TMC, display intensely shearing also fine grained and foliated. This unit shows multiple generation of greenish-blue patches which are thinly foliated and show enclose wrapping structure which is chloritic in nature (Fig 4.3a). Adjacent to this unit, a meta-basic slice is present that is rich in talc and phyllite. The foliation of this unit is axial planer to tight isoclinals folds, concordant to the attitude of Zildat fault, i.e. northerly dipping. These folds are further gently warped. Further north of these meta-basics lies a unit of polygenic meta-greywacke (Fig 4.3b).
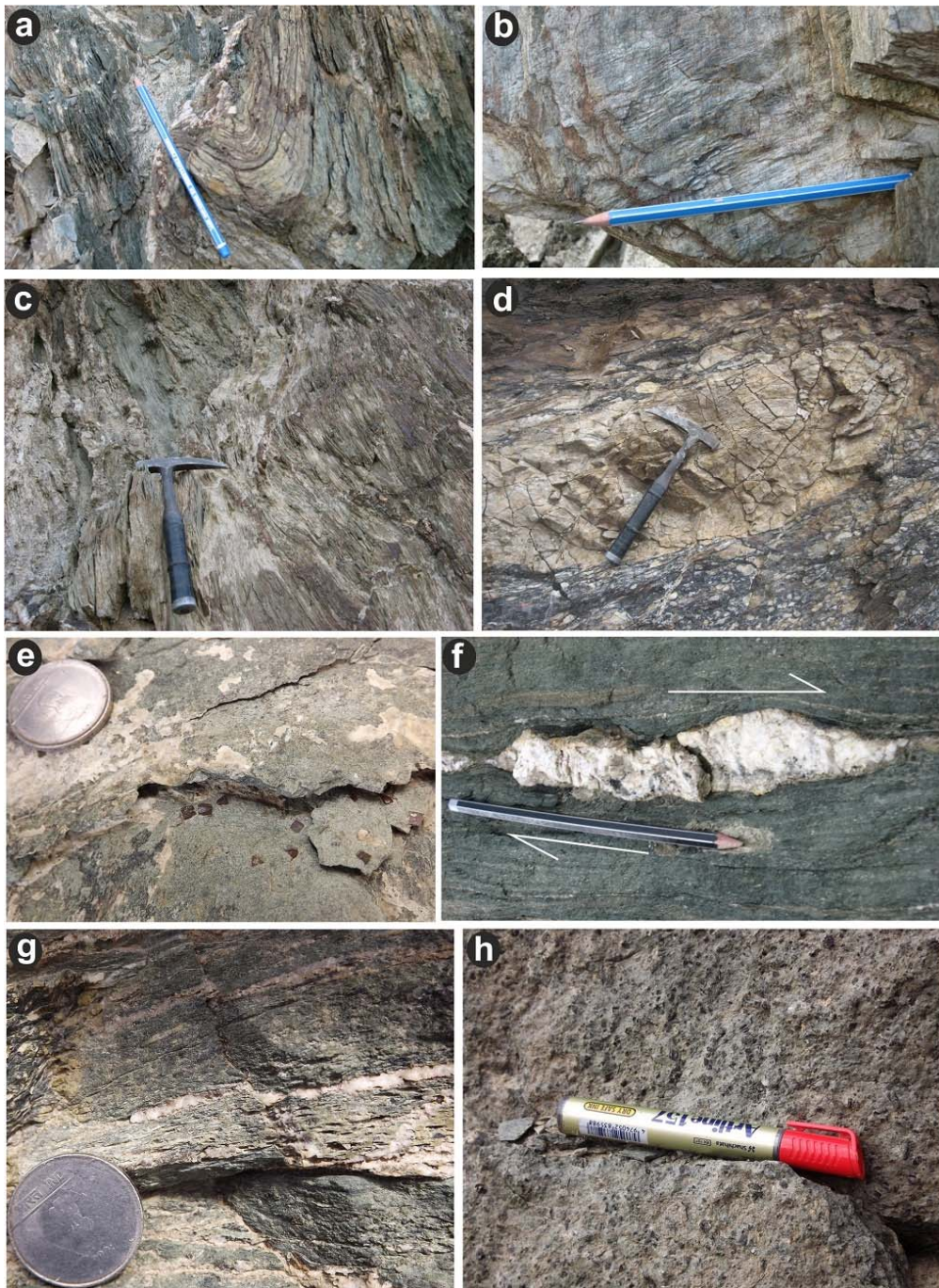
Figure 4.2: *Mega to micro-scale features observed in outcrop of ZOM. **a)** minor fold within ZOM towards the TMC contact part. **b)** plunging crenulation at the marginal part of mélange. **c)** pencil cleavage formed along the foliation plane of basic rocks. **d)** sheared and cataclastic limestone. **e)** pyrite crystals withing the basic rocks. **f)** quartz vein at the marginal part of the mélange showing shearing indication. **g)** displaced quartz vein due to presence of minor faulting. **h)** field photo of volcaniclastic rock unit.*

These meta-greywackes contain clasts of carbonates, chert showing imbrications that suggest 'top-to-the-south' or thrusting movement (Fig 4.3c).

This particular unit also have basic clasts and remnents of serpentine and talc. (Fig. 2.2).
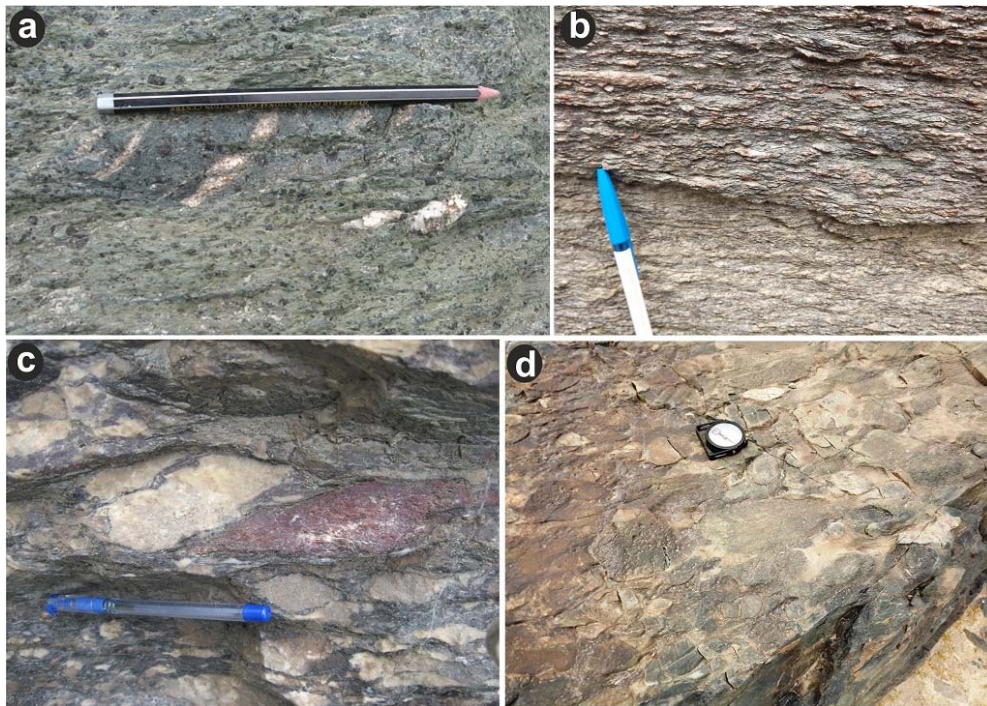
Figure 4.3: *Photograph show distribution of various clasts within ZOM.* **a)** *clast of high-grade metamorphic remnant surrounded by low grade metabasics.* **b)** *meta-greywacke unit with heterogenous clasts.* **c)** *sheared chert and limestone clasts within mélange.* **d)** *conglomerate unit containg clasts of gabbro, ultramafic etc.*

A notable conglomerate body is observed as seperate unit found at the northern most part of the mélange (Fig 4.3d). It consists of various clasts belong to ophiolite, melange and gneisses. This conglomerate is first describe as a post-collisional conglomerate (de Sigoyer et al., 2004) and is the only unit within the ISZ which contains clasts from TMC. However, this type of clast from TMC is not observed within any-sub units of ZOM. At the contact between ZOM and NOC, large isoclinal folds, devoid of any penetrative axial planer fabric, have formed that dips towards south. At this contact the carbonate blocks of ZOM are thrusted over the crustal part of NOC.

4.3. MICROSCOPIC OBSERVATIONS

ZOM is a mixture of various lithologies among which the principal componets are oceanic sediments, ophiolite remnents, exotic catbonates, chert and volcaniclastics. Each components have been thoroughly categorised by detailed petrographic study carried out using high resolution optical microscope and each of these mineral phases are further characterised by quantitative and semi-quantitative analyses. For the study of different mineralogical aspect many state of art instruments (SEM-EDS, EPMA, Raman Spectroscopy) were deployed extensively. The detail methodology and analytical procedures can be found in Chapter 3.

4.3.1. MINERALOGICAL ASSEMBLAGES AND TEXTURAL RELATIONSHIP

The ZOM is divided into various principal sub-units which reflects distinct lithology and wide range of mineralogical assemblages.

a. The volcaniclastic unit present in the ZOM consists of pyroclastic mass (?), angular fragments predominantly of augite, calcite filled vesicles, pyrite, opaque iron oxide, titanite (Fig. 4.4a). The pyroxenes are euhedral in shape surrounded by fine grained matrix, often shows optical zoning and ranging in size from millimetres to few centimetres (Fig. 4.4b). The pyroxene grains are fractured showing alteration at the marginal part and along the margins of micro-fractures. In places, calcite and quartz veins have intruded along the fractures (Fig. 4.4c). Calcite shows two types of mode of occurrences. They are characterised by secondary vesicle fills, which is elongated and stretched

parallel to the schistosity of the rock. The type of calcite formed as vein, are

secondary in origin. Pyrite, goethite and other iron oxides are usually noticed.

Majority of these iron oxides are rhombic to cubic in shape.
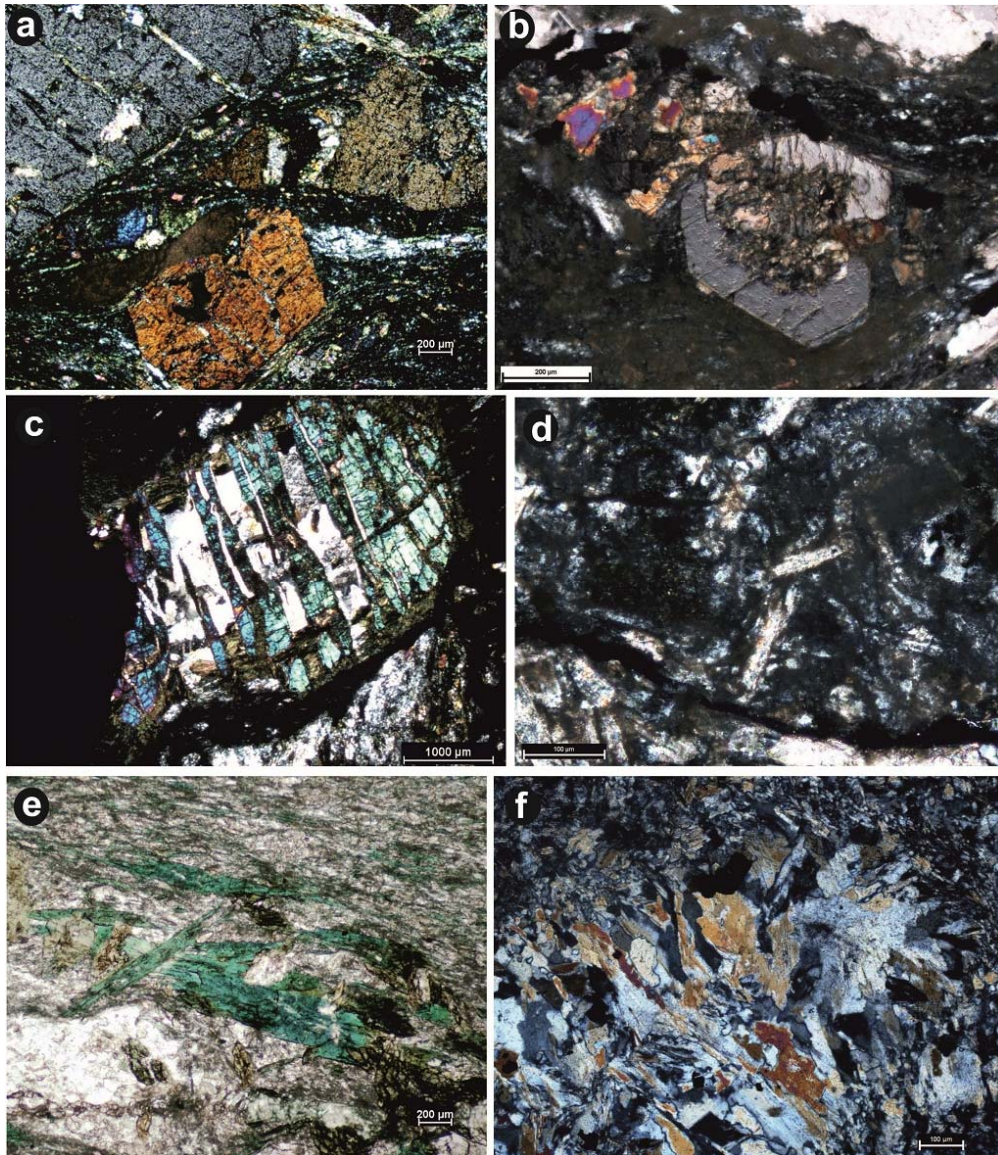
Figure 4.4: Petrography of various lithounits. a) pyroxene and titanite phenocrysts surrounded by greenschist matrix. b) euhedral pyroxene crystal showing optical zoning in cross nicol. c) quartz and calcite veining in fractured pyroxene. d) metabasic matrix showing laths of plagioclase. e) bluish green coloured amphibole present in matrix. f) presence of serpentine in mélange matrix.

b. The meta-greywacke and meta-sedimentary component consists of quartz

and plagioclase lath (albite) with minor amount of epidote, set in an altered

fine-grained chlorite-sericite rich matrix (Fig. 4.4d). This particular unit is

mentioned as conglo-brecciated unit composed of different clasts set in a fine grained altered matrix. Out crop scale exotic limestone blocks are usually noticed in this unit. Due to variable sizes, a detail microstructural study of these exotic carbonates is attempted which is discussed in the following section 4.3.2.

c. The sheared basic unit is observed adjacent to the volcaniclastics. It has abundant of blue - green minerals following the regional schistosity (Fig. 4.4e). These blue-green minerals are dominated by Na-Ca amphiboles. This unit is characterised by different metamorphic histories between clasts and matrix.

d. The talc and serpentinised unit is represented in Fig. 4.4f which is present as minor amount within ZOM. The hydrated ultramafic rocks are also seen as clast within the mélange. The majority of mélange matrix characterised by chlorite-albite-epidote-quartz-calcite-talc-titanite. These assemblages indicate dominance of low grade metamorphism. This unit also showing coupling effect of metasomatism and late hydrothermal alteration may possibly drive through serpentinization and near surface silica rich fluid.

4.3.2. MICROSTRUCTURAL OBSERVATIONS

The dismembered exotic limestone within the mélange zone shows crystalline heterogeneity in mesoscopic scale (Fig 4.5) and also shows varied deformation signatures in microscopic scale (Fig 4.6) ranging from high temperature to low temperature deformation twining. A progressive

deformational history is inferred through microstructural study of calcite described in the next paragraph.
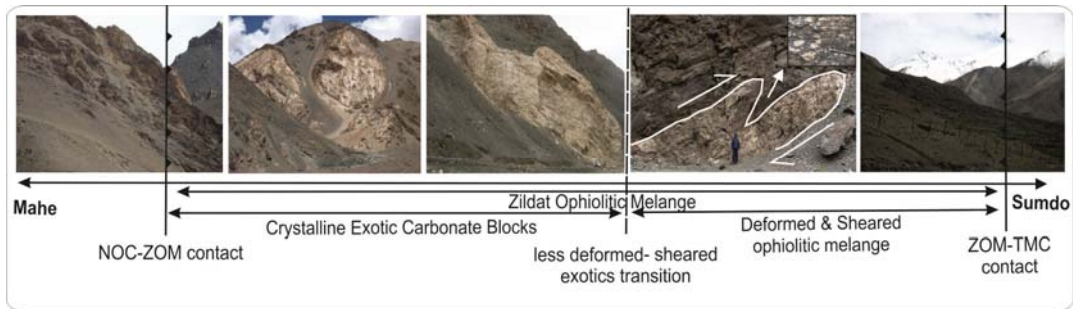
Figure 4.5: panoramic view of exotic limestone blocks within ZOM showing crystalline heterogeneity and intense shearing towards the TMC margin.

Microstructural observations from the carbonates lying away from the Zildat fault zone are characterized by coarse grained calcites having 1–3 mm grain sizes with high mean axial ratios (Fig. 4.6a). Moving towards the Zildat fault zone, they grain size decreases (Fig. 4.6b). Near the Zildat fault zone, the carbonates are sheared and characterized by much smaller grain size in comparison with their counterparts away from the Zildat fault zone. The reduction in grain size is considered to be caused by dynamic recrystallization (Bestmann et al. 2000). These fine-grained carbonates show complete recrystallization, which suggests localization of strain toward the marginal parts of the mélange close to the Zildat fault zone. Exotic carbonates show systematic variation in twin pattern from the interior to the marginal parts of the ZOM. In the core part, the calcites have their boundaries bulged along with sub-grain development (Fig. 4.6c). Sutured (bulged) grain boundaries are formed due to strain-induced grain boundary migration (Schmid et al. 1980). Thick patchy twins (Fig. 4.6d) are recrystallized, and the aggregates of small calcite grains are elongated and oriented along the length of the thick calcite

twins (Fig. 4.6e). These features are caused by dynamic recrystallization of calcite that occurs at post-peak metamorphic temperature ranges of 250–350°C (Burkhard 1993). Sutured grain boundaries are inferred to be a result of grain boundary migration at 250°C (Burkhard 1993). In the marginal part of ZOM, the calcite twins are bent and tapered (Fig. 6f, 6g). These suggest deformation at a relatively lower temperature. To establish relative chronology of different deformation events, crosscutting or offset relationship among twin lamellae are used. A set of 20 m thick twins are crosscut and displaced by relatively thin twins (Fig. 6h). Thick twins (1st generation) indicate relatively higher temperature episode (amphibolites facies conditions) (Burkhard 1993), and these are crosscut by later stage thin twins (2nd generation) during post-metamorphic deformation at a relatively lower temperature (lower greenschistfacies conditions). In the marginal part of the mélange, calcite clasts are stretched and elongated with micro fracturing. Elongated calcite clasts are surrounded by small calcite grains at the margin with a preferred orientation. Such features suggest a late low-temperature deformation episode (lower greenschist) that occurred during the latest stage of mélange exhumation near the Zildat fault zone. The carbonate blocks show increasing intensity of deformation from the interior parts to the contact between the ZOM and TMC. In high-resolution SEM image (using ZEISS EVO40 in WIHG, Dehra Dun), the calcite shows micro scale deformation feature of twinned calcite crystal (Fig. 4.7a). Preservation of pseudo-aragonite phase is also observed in SEM image characterized by its platy–flaky habit (Fig. 4.7b).
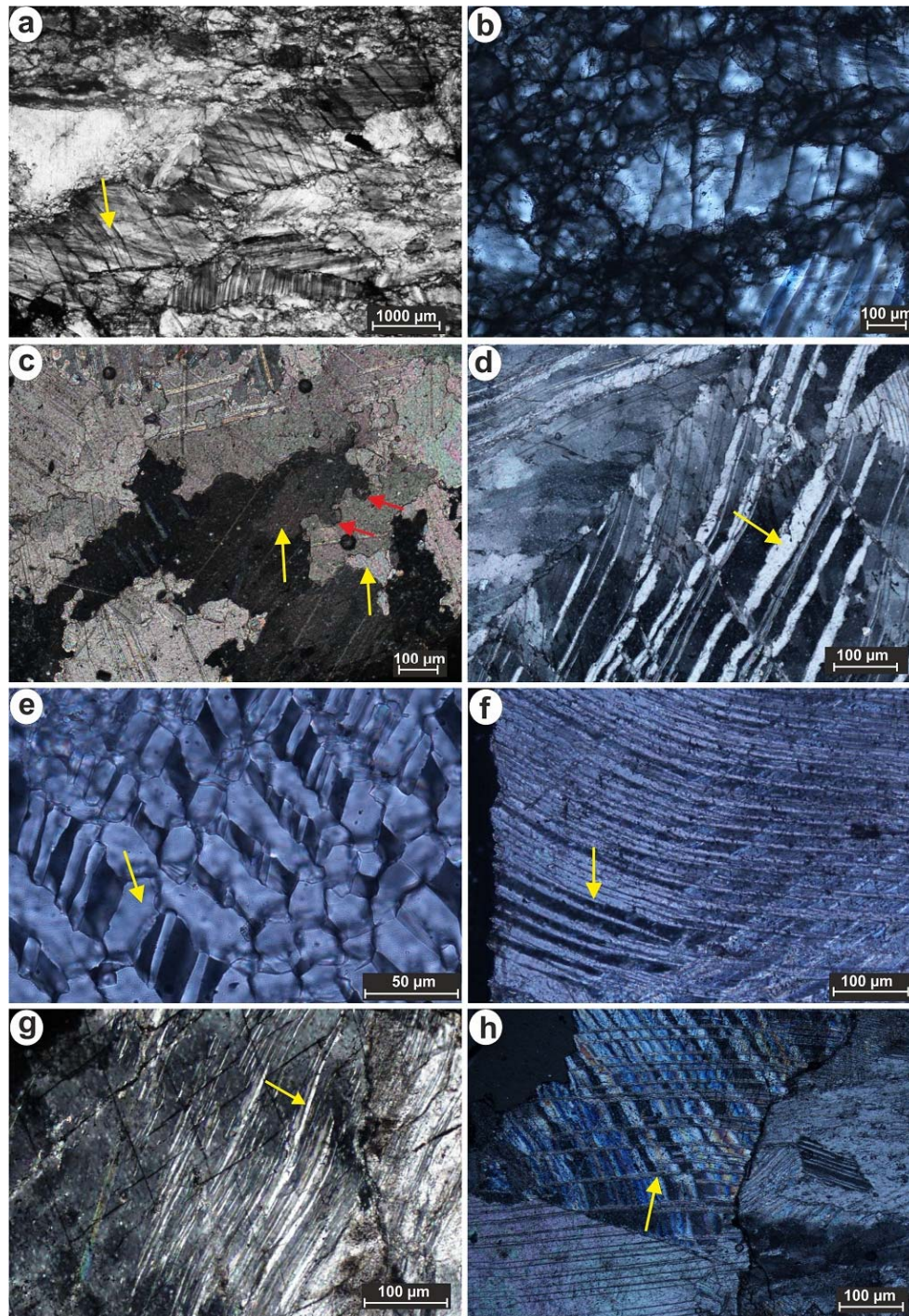
Figure 4.6: *Photomicrographs showing different types of microstructures from exotic carbonates. **(a)** Large calcite grains away from the Zildat fault zone, coarse-grained with high mean axial ratio (marked by yellow arrow). **(b)** 'core and mantle structure' consisting of fractured calcite grain surrounded by recrystallized aggregates of smaller calcite grains. **(c)** calcite grain showing sub-grain formation (yellow arrow) and grain boundary migration (red arrow). **(d)** Thick patchy twinning in calcite (yellow arrow). **(e)** Preferred orientation of recrystallized calcite grains (yellow arrow) along former thicker twin. **(f)** Curved thick calcite twin (yellow arrow) indicating deformation as result of dynamic recrystallization. **(g)** Lens shaped deformation twins (yellow arrow) in calcite. **(h)** Different types of calcite twins crosscut each other. Small offsets (yellow arrow) in earlier thick twins are caused by late deformation.*
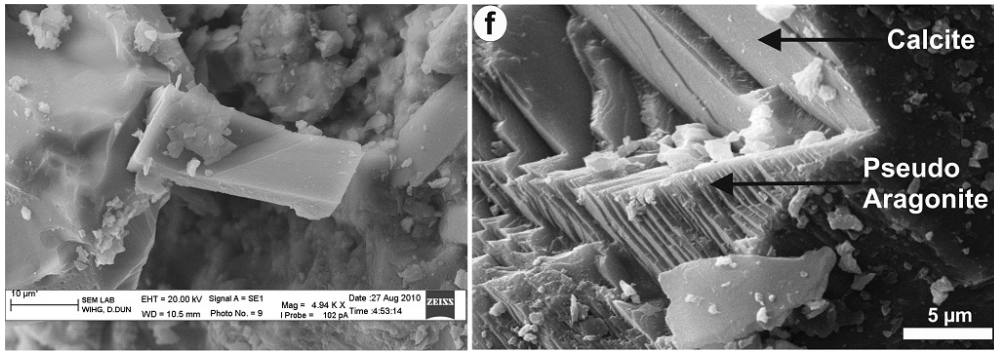
Figure 4.7: a) *deformed and twinned calcite crystal in high resolution SEM image.* **b)** *SEM image of calcite showing preservation of pseudo-aragonite phase, indicating high-pressure metamorphism.*

The presence of pseudo-aragonite indicates an earlier high-pressure $CaCO_3$ phase. The detail petrographic information is compiled in Table 4.1 & 4.2, which is done on representative rock samples from ZOM.

4.4. MINERAL DATA GENERATION AND ANALYSES

All the mineral analyses are listed at the end of this chapter (Table 4.3, 4.4, 4.5)

4.4.1. EPMA & SEM-EDX ANALYSES

The mineral chemical data were analysed using a CAMECA SX-100 electron microprobe and ZEISS EVO 40 scanning electron microscope with Energy Dispersive X-ray Microanalyser - Bruker LN2 free X-Flash 4010 detector at Wadia Institute of Himalayan Geology, Dehradun. The detail instrumentation and analytical conditions are described in chapter 3.

Gross chemical analyses of mineral were done using SEM-EDS. Out of which important mineral were further characterised using EPMA. Two important minerals are chosen for extensive analyses (pyroxene and amphibole). Beside these, feldspar, epidote and opeques are also analysed.

Pyroxene are euhedral to subhedral in shape, ranging from 200-300 µm in size, colorless to light brown in colour and are moderately pleochroic. Optical zoning is prominent in few pyroxene grains along with few twined crystals (Fig. 4.4b). In pyroxene, carbonate and quartz veins are also observed (Fig 4.4c). Microprobe analyses suggests that the pyroxenes are Ca-pyroxene with ~21-23% CaO. Whereas MgO and FeO content varies grossly from ~12-16% and ~4.5-7.5% respectively. $Mg^{\#}$ reflects a variation from 0.74 to 0.85. Augite showing relatively higher TiO_2 (~1-3.5%) and Al_2O_3 (~5-9%) concentration. Such high concentrations of Ti and Al is well significant for titan-augite. Titan-augites show chemical zoning caused by variation in TiO_2 and Al_2O_3 from core to the rim of the crystal. Whereas, the smaller grains of pyroxenes present in the matrix have higher TiO_2 and Al_2O_3 ratio but they do not show any chemical zoning across the grain. The zoning is characterized by an increase in Al_2O_3, TiO_2 and FeO concentration towards the rim in contrast to SiO_2 and MgO. The detail of pyroxene analyses are tabulated in Table: 4.3, and the corresponding analysis spots are shown in figure 4.8. **Titanite** or sphene is dusty brownish in colour which are present in the volcaniclastic unit of the mélange. The grains are mostly smooth and showing a well-defined rim. They are distributed as clasts which are surrounded by the schistose matrix. Chemically they are homogenous in nature. It has ~30% SiO2, ~25-29% CaO and ~30-34% TiO_2 with small amount of FeO and Al_2O_3. The microprobe analysis are shown in Table 4.5. The matrix show wide range of mineralogy, they are strictly fall in the range of 1-50 µm in size. Matrix mineral

characterised by complex mineralogy and show foliation fabric. The matrix is composed of mainly amphibole, albite, iron oxide, epidote etc.
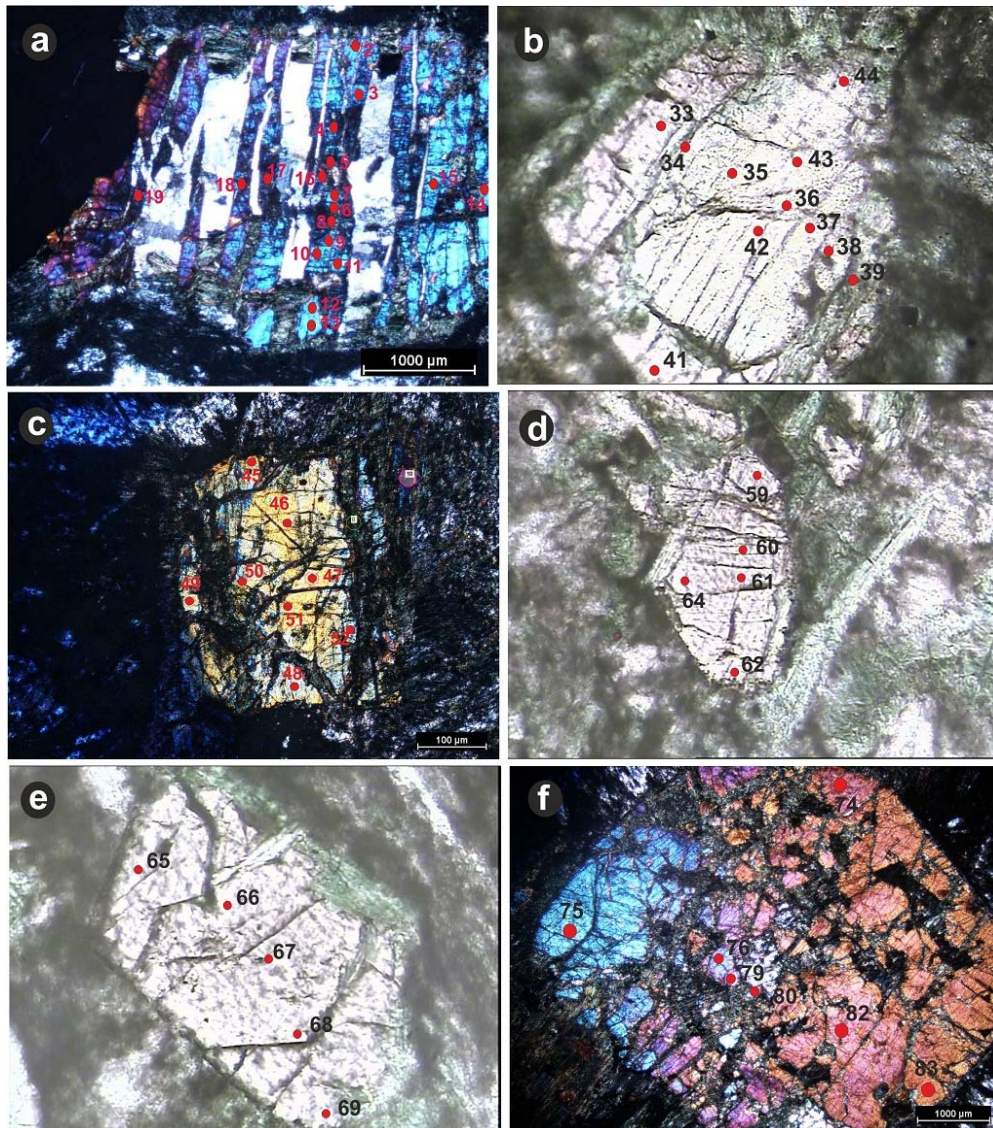
Figure 4.8: *figure showing the textural behaviour of pyroxenes chosen for EPMA spot analysis, the analysis spots are shown in red dot with corresponding analysis number. The results are shown in table 4.3*

Amphibole present in the matrix often show variation in Ca/Na ratio. They also reflect chemical zoning characterised by high concentration of Ca as we move towards the rim part of the grain. They show pleochroism from bluish green to yellowish green. Glucophene and actinolite are common. The Na_2O concentration varies from ~4-6% whereas the CaO varies within a range of 7-

13% (table 4.4). **Feldspars** are present as laths in the matrix rangin from 10-50 µm in length. The feldspars are albitic in nature, with 10-12% Na_2O and 18-20% Al_2O_3 (table 4.6). Opaque **iron oxides** are dominated by FeO with minor concentration of Cr_2O_3 in some places. **Epidotes** are euhedral shape. The composition of most epidotes show little variation within the grain. A small grain of isotropic garnet is also observed in optically and SEM-EDX study reflects Mg/Al/Si present in higher concentration (Fig. 4.9).
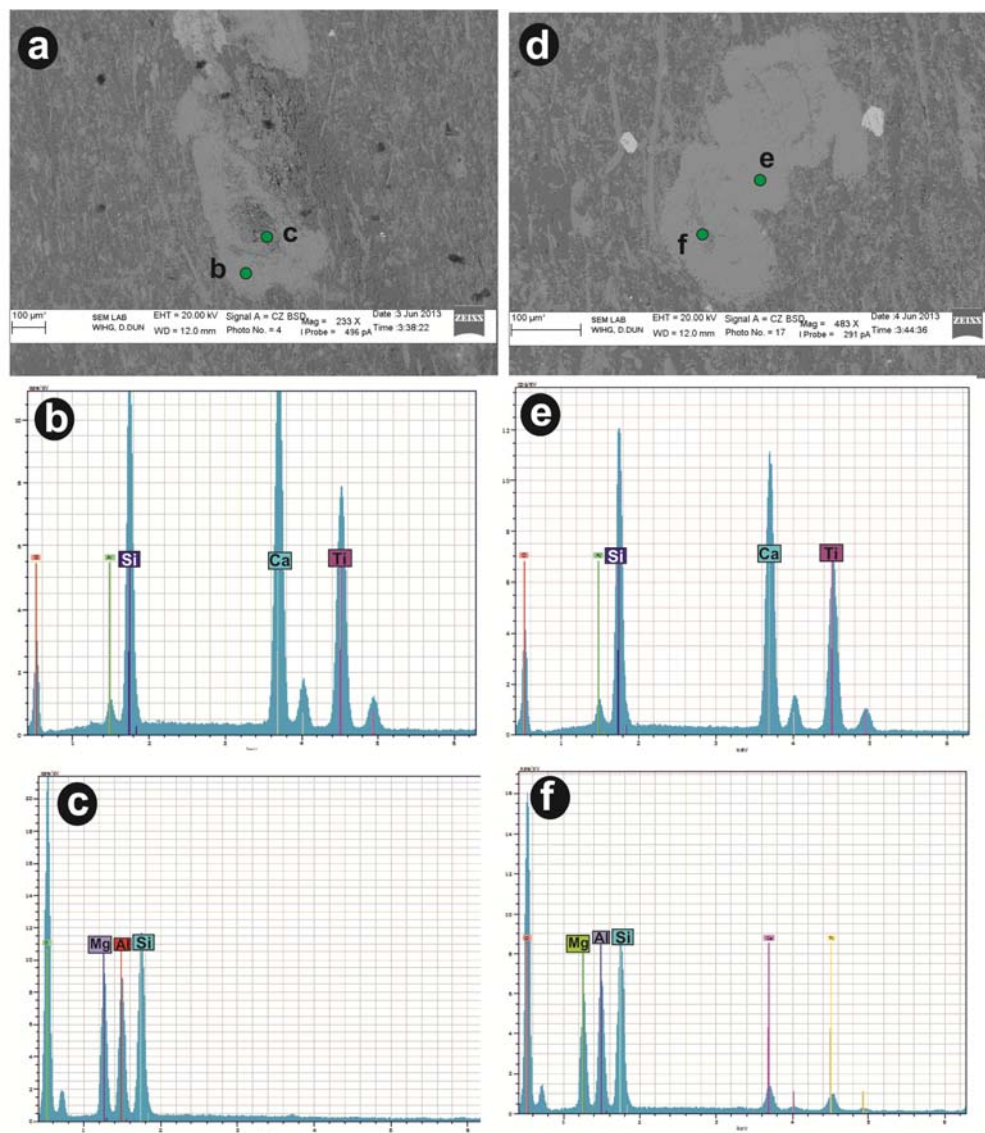
Figure 4.9: *EDS analysis indicating garnet phase within titanite. **a)** & **d)** back scattered image of titanite, green circles indicate the analysis spots. **b)** & **e)** EDS spectra of titanite showing Si, Ca and Ti peaks. **c)** & **f)** EDS spectra of relict garnet (?) phase showing Mg, Al and Si peaks.*

4.4.2. RAMAN SPECTROSCOPIC STUDY

The Laser Raman spectroscopy was performed using a LabRAM HR - Horiba Jovin Yuvon Instrument using 514.5 nm Argon Laser at the Wadia Institute of Himalayan Geology, Dehra Dun. The instrument specification and detailed analytical conditions are described in Chapter 3.
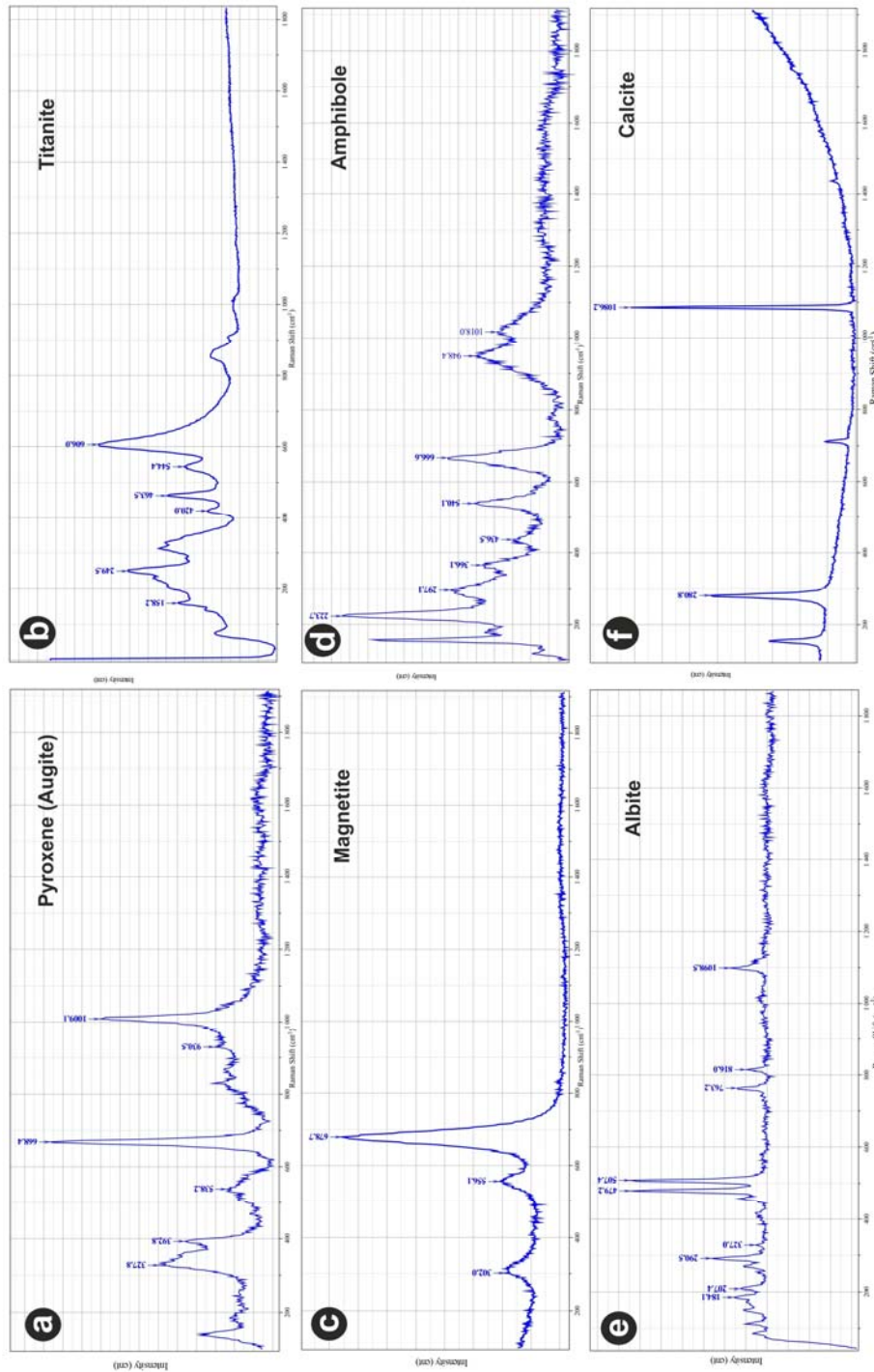
Figure 4.10: *Raman spectra of pyroxene (a), titanite (b), magnetite (c), amphibole (d), albite (e) and calcite (f) from ZOM rocks*

The Raman spectrometry confirms the presence of augite and titanite mineral phases as clasts whereas magnetite, amphibole, albite and calcite constitute the main matrix. In the Raman peaks of **augite** (fig. 4.10a), the stretching modes of $Si-O_{nbr}$ are observed to have higher intensity at 1009 cm^{-1} and weaker peak at 930.5 cm^{-1}. The band assigned to the stretching of the $Si-O_{br}$ bond is located at 668.4 cm^{-1}. The 538.2 cm^{-1} band attributed to the bending of O-Si-O bond. The cation-oxygen vibrations appear at lower frequencies, below 400 cm^{-1} and they are at 392.8 cm^{-1} & 327.8 cm^{-1} (Fig. 4.10a). **Titanite** is characterised on the basis of its diagonastic Raman peak at 606 cm^{-1} along with peaks at 544.4 cm^{-1}, 463.5 cm^{-1}, 420 cm^{-1}, 249.5 cm^{-1} & 158.2 cm^{-1} (Fig. 4.10b). The iron oxide present in the matrix are characterised as **magnetite** from Raman spectrometry as their peak shape and values at 678.7 cm^{-1}, 556.1 cm^{-1} & 320 cm^{-1} (Fig. 4.10c). As the green coloured matrix is retrogressed and expected to give a maxed mineralogical character, the presence of **amphibole** is characterised by peaks at 666.6 cm^{-1}, 540.1 cm^{-1}, 463.5 cm^{-1}, 366.1 cm^{-1}, 297.1 cm^{-1} & 223.7 cm^{-1} (Fig. 4.10d). **Plagioclase** present in matrix are characterised as albite suggested by its doublet nature peak at 479.2 cm^{-1} & 507.4 cm^{-1}. Which is also confirmed by the presence of peaks at 816 cm^{-1}, 763.2 cm^{-1} & 290.5 cm^{-1} (Fig. 4.10e). **C**alcite is observed within the matrix as well as in the form of inclusions within the pyroxene and is characterised by its diagnostic Raman peaks at 1086.2 cm^{-1} & 280.8 cm^{-1} (Fig. 4.10f).

4.5. DISCUSSION

Most of the units of ZOM show signature of recrystallization and polymetamorphism. To establish the various stages of metamorphism in the mélange rock, it is essential to know the nature of the each mélange unit. The mineral assemblases of many sub-units of melange seems near completely altered, so it is difficult to assign complete mineral assemblages and primary metamorphic history. The later modification and crustal metamorphism have been overlay the original signature of the rock. However a line of evidences, particularly metamorphic evolution can be recovered from many units which are less altered. This shows ZOM is broadly classified into three metamorphic episodes.

M1: Mafic-Blueschist facies (units- mafic host with carbonate, volcaniclastisc). The basic mineral assemblages of mafic/volcaniclastic unit show metamorphism under blueschist facies condition. It comprises Na-amphibole; fine grained Ca-amphibole, glaucophene- ribeckite series (upto ~5.74 % Na_2O) (Table 4.3). Greenish chlorite resemblance to paragonite with high FeO, titanite, albite, relict zoisite, clino-pyroxene with high TiO_2 and Al_2O_3 and mica (phengite?). Excess of titanite possibly derived from break down of rutile. As shown in photograph Fig. 4.1, the composite unit of mafic blueschist and volcaniclast of ZOM show resemblance to subduction zone mélange. In matrix remnant of blueschist facies metamorphism over relict phases of eclogites (?). This inference is drown from the high Al_2O_3 content of pyroxene might have replaced the SiO_2 in higher P-T condition. This also supports the occurance of relict garnet composition in titanite (Fig. 4.9). The

limestone blocks surrounded by mafic and volcaniclastic unit preserves pseudo-aragonite phase (Fig. 4.7) which is high pressure polymorph of calcite, indicate aragonite transformation at pressure metamorphism.

M2: The metasedimentaries of ZOM preserves assembleges of (epidote-) amphibolite facies condition. This unit possibly suffered isothermal decompression to attain lower metamorphic condition. It has variable mineral paragenesis and texture to show granoblastic amphibole, plagioclase, epidote and accessories including sphene and apatite. Amphiboles are Na-Ca rich which may derived from high pressure pyroxene (eclogite). This unit also represents mafic hydration and pelitic dehydration which inferred as amphibolite metamorphic condition.

M3: Wide low temperature crustal metamorphism is usually observed across the whole ZOM. Chlorite, actinolite and albite are the most common mineralogy with minor constituents of serpentine, talc and tremolite. This thick meta-sedimentary unit with various clasts were metamorphosed under greenschist (phyllite) metamorphic condition.

In present day ZOM rocks are dominantly a low grade metamorphic condition was prevailed at M3. Although it contains clasts of high grade metamorphic rocks as well as glaucophane in the matrix and garnet composition within titanite belong to M1. At the contact between TMC and ZOM, along the Zildat fault, the quartz veins and their deformation characters support a higher grade metamorphism, was prevailed at M2. Variation in calcite microstructure suggests that the intensity of deformation within the ZOM increases from interior to outer part of the mélange which is more

intense at TMC contact. Clast-matrix relationship aided by major element analysis and relict phase identification from the ZOM suggests its polymetamorphic evolution. This study shows that the mélange matrix represents overprinting of various events of metamorphisms from blueschist to amphibolite to greenschist facies. Moreover, relics of Na- amphibole indicate an even older blueschist metamorphic event. The metamorphic history of ZOM reveals two generations of blueschist metamorphic events: the first in the form of clasts within the matrix (Fig. 4.3a) and the second in the matrix itself which show formation of blueschists along the foliation (Fig. 4.4e). In contrast, increase in TiO_2 content from core to rim of the euhedral titan-augite possibly indicates an early overprint of high temperature metamorphic event on a pristine igneous pyroxene. The chemical analysis of few of the clasts show relict signature of high pressure and high temperature metamorphic condition. Perhaps, this metamorphism may happened prior to the ZOM formation. As the matrix of the ZOM shows presence of high-P amphibole, it can be interpreted that at least part of ZOM, especially which lies in vicinity of the TMC along the Zildat fault, experienced blueschist facies metamorphism. However, it is difficult to ascertain whether this event was older or coeval with high grade metamorphic events of the TMC, which was related to subduction of the Indian continental margin. We further interpret that the amphibolite to greenschist facies metamorphic events retained in the matrix of the foliated metabasics of the ZOM are related to final stages of emplacement of the mélange with respect to exhumation of the TMC. The mélange material from different depths of eclogite-blueschist transition zone

possibly returned through fossil subduction channel which was lubricated by serpentinised matrix.
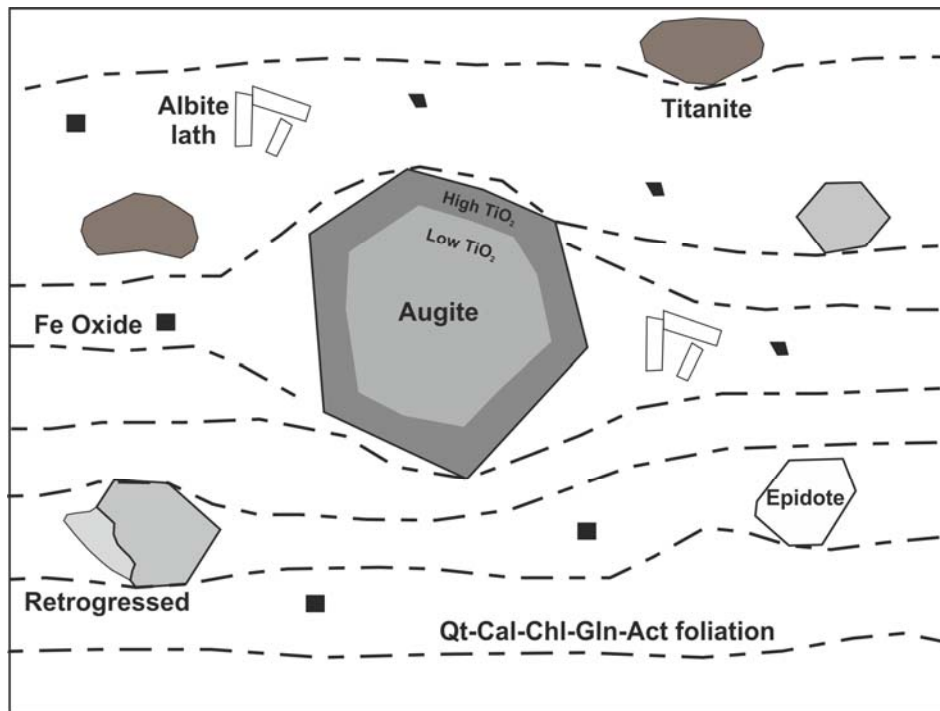
Figure 4.11: *Schematic diagram of volcaniclastic unit of ZOM showing the presence of Ti zoned augite, titanite, epidote and albite lathas which are set in a quartz-calcite-chlorite-glaucophene-actinolite composed matrix.*

In the same line of interpretation de Sigoyer et al. (2004) also suggested three stages of deformation events that caused the exhumation of TMC and these workers have also assessed the evolution of ZOM and NOC during these deformation events. According to them, exhumation of TMC began from ~90 km depth by formation of early upright folds (D1 folds), at this time both ZOM and obducted NOC formed SW verging folds. This event was followed by doming of TMC during D2 deformation, when TMC exhumed up to a depth of ~35 km by folding and shearing. At this time, the part of ZOM adjacent to TMC ('Ribil unit' of de Sigoyer et al., 2004) developed extensional structures and the interior of ZOM ('Drakkarpo unit' of de Sigoyer

et al., 2004) formed double thrusting structure. Finally, the flanks of TMC dome developed normal shear structures, as TMC underwent gravitational collapse (D3) and exhumed to near-surface depth at ~30 Ma. According to their study, during D3 event NOC also developed NE verging backthrusts. However, our field observations suggest three key features that contradict the inferences of de Sigoyer et al. (2004) regarding tectonic evolution of ZOM and NOC. Firstly, NOC has not suffered any deformation and is devoid of any folds or backthrusts; secondly the Zildat fault present between TMC and ZOM activated as a normal fault but later switched as a thrust (Ravikant 2003) and thirdly ZOM, as a whole, is bounded by two oppositely dipping thrust sheets (Thakur & Mishra 1984) and it also has suffered mild superposed deformation. On the basis of our observations, we propose a two stage model in the following section that explains the structural evolution of this collision zone and explains the exhumation of both TMC and ZOM at crustal level and also the role of NOC as a backstop (please see chapter 7 for details).

Table 4.1: Mineralogical, microstructural and fluid inclusion features of ZOM exotic limestone compiled from selected thin section study (Mineral abbreviation after Kretz 1983; Whitney & Evans 2010)

Sample	Composition	Grain Size & Deformation	Volatile/Fluid Inclusion	Rock	Important Features
JS3A * JS3B *	Cal $_{70-80\%}$, Cal- S $_{5\%}$, Qz $_{5-10\%}$, Qz - S $_{5\%}$	Cal F $_{90\%}$ (G$_{Recrystallized}$) , Cal C $_{10\%}$ (T$_{Thick}$)	S -FI $_d$ in calcite	Limestone / Marble	
JSM1A *	Cal $_{90\%}$, Qz - S $_{5\%}$, Chl $_{5\% (Fracture)}$	Cal F (G$_{Recrystallized}$)	S -FI $_d$ in calcite, Pseudo-S FI in Qz (Zoned)	Limestone / Marble	
JSM1B *	Cal $_{95\%}$, Qz $_{3\%}$, Cpx $_{2\% (clast)}$	Cal F (G$_{Recrystallized}$), Core Mantle microstructure, Book-shelf fracturing	S -FI $_d$ in calcite	Limestone / Marble	Pseudo- Aragonite in SEM
JSM1C *	Cal $_{95\%}$, Qz $_{5\%}$	Cal M (G$_{Recrystallized}$)	S -FI $_d$ in calcite	Limestone / Marble	
JSM2E *	Cal $_{95\%}$, Qz-S $_{5\%}$	Cal C $_{(GBM)}$, Qz C	S -FI $_d$ in calcite, Sigmoidal FI in Quartz	Limestone / Marble	Qz grains show triple junction
JSM2F *	Cal $_{95-100\%}$	Cal M	S -FI $_d$	Limestone / Marble	Weathered and altered
JSM2A **	Cal $_{90-95\%}$, Qz,	Cal C $_{80\% (elongated)}$, Cal M $_{20\%}$	S -FI $_d$	Marble	
JSM2B **	Cal $_{95-100\%}$	Cal C $_{(elongated)}$, T$_{Thick}$	S -FI $_d$	Marble	Twined calcite crystals with high aspect ratio
JSM2C **	Cal $_{95\%}$, Qz $_{5\%}$	Cal M	S -FI $_d$ in calcite, Zoned FI rich qz	marble	
JSM4B ** JSM4C **	Cal $_{95\%}$, Qz $_{5\%}$ (interstitial space)	Cal C, T$_{Thick, curved,}$ recrystallized, patchy	S -FI $_d$ in calcite, Rhombic – Rectangular primary FI in Calcite	Marble	Stretched FI, Brine FI in calcite, Two generation of twining is present.

Notation: S- Secondary, F- Fine, M- Medium, C- Course, G- Grain, T- Twin, FI- Fluid Inclusion, d- dominant. * The carbonates are fine grained, sheared and recrystallized, ** the carbonates are course grained, crystalline with thicker twin lamellae

Table 4.2: Mineralogical & lithological features of various lithounits of ZOM compiled from selected thin section study (Mineral abbreviation after Kretz 1983; Whitney & Evans 2010)

Name	Field Relationship/rock type	Composition	Important Feature
JSM 1D	Red coloured clast within meta-greywacke matrix	fine grained chert with folded calcite veining	
JSM2D ****	Melange conglo-breccia having blocks in matrix	B $_{Cpx, basalt, Opaque, Spn}$, M $_{Chl}$	Cpx are titanaugite, Cpx $_{SiO2\ 40-46\%,\ CaO\ 22-23\%,\ MgO\ 10-13\%,\ Al2O3\ 7-10\%,\ FeO\ 7\%,\ TiO2\ 2-4\%}$
JSM4A ***		M $_{Chl, Talc, Srp}$, R $_{Cpx}$	
JSM4D *****	Conglomerate	B $_{Basalt, Gabbro}$ M $_{Chl}$	
1S59		M $_{Chl, Srp, Talc}$ R $_{Sil?}$	
1S63		M $_{Cal, Qz, Chl}$, R $_{amp}$	
1S64		M $_{Cal,}$ R $_{?}$	
1S65	Carbonate & Melange matrix contact	B $_{Cal, Basalt, ?}$ M $_{Chl}$	
1S66 **	Volcaniclastic	B $_{Cpx, Opaque}$ M $_{Chl}$ S $_{Cal}$	Cpx are titanaugite, Cpx $_{SiO2\ 45-50\%,\ CaO\ 22-23\%,\ MgO\ 8-9\%,\ Al2O3\ 8-9\%,\ FeO\ 7\%,\ TiO2\ 2-3\%}$
1S67	Chlorite schist	M $_{Chl, Qz, Cal, Opeque}$	
1S70 ***		M $_{Chl, Talc, Srp}$, R $_{Cpx}$	
LSM 1A*	Meta-basics	M $_{Chl, Qz}$, S $_{Qz, Cal}$, R $_{Gln?}$	
LSM 1B*			
LSM 1C*			
LSM 1D **	Volcaniclastic	B $_{Cpx, Spn, Opaque}$ M $_{Chl}$	Micro fossil bearing volcaniclastics
LSM 1E *	Meta-basics	M $_{Chl, Qz}$, S $_{Qz, Cal}$, R $_{Gln?}$	Large pyrite crystals
LSM 2A ***	Talc, Chl rich meta- basics	M $_{Qz, Cal, Chl, Talc}$, R $_{Amp}$	
LSM 3A ***		M $_{Qz, Cal, Chl, opeque}$	
LSM 3B ***		M $_{Qz, Cal, Chl, opeque}$	
LSM 4A ****	Matrix of Melange conglo-breccia	M $_{Qz, Chl}$ R $_{Amp}$	
LSM 6A *****	Conglomerate	B $_{Basalt, Gabbro}$ M $_{Chl}$	Post collisional conglomerate
LSM 7 *****			
GN 1 *****			

Notation: B- Blocks, M-Matrix, S-Secondary, R-Relict

* Metabasic unit at the terminal part of mélange towards TMC, ** Volcaniclastic unit associated with metabasics having titan-augite porphyroclasts, *** Talc-Serpentinised phyllitic rock, **** Mélange conglo-breccia, ***** Post collisional conglomerate

Table 4.3: EPMA analysis results of pyroxenes

Point	2	3	4	6	7	8	9	10
Na_2O	0.8	0.56	0.55	0.51	0.56	0.56	0.57	0.6
MgO	12.07	12.06	12.62	12.09	12.37	12.35	12.14	12.51
Al_2O_3	8.56	9	8.14	9.23	8.28	8.2	8.76	8.47
SiO_2	45.88	44.76	46.26	44.54	45.57	45.84	45.32	46.02
P_2O_5	0	0	0.05	0.05	0.04	0	0	0
K_2O	0.01	0	0	0.01	0	0	0.01	0
CaO	22.18	22.74	22.87	22.38	22.76	22.82	22.42	22.28
TiO_2	3.14	3.19	2.61	2.97	2.8	2.67	3.05	2.81
Cr_2O_3	0	0	0.13	0	0.13	0.08	0.05	0.03
MnO	0.07	0.06	0.09	0.11	0	0.06	0.27	0.15
FeO	7.44	7.19	7	7.17	7.36	7.35	7.06	7.18
NiO	0	0.05	0	0	0.05	0	0	0.01
Total	**100.16**	**99.61**	**100.31**	**99.06**	**99.92**	**99.93**	**99.66**	**100.07**

On the basis of 6 O

Na	0.058	0.041	0.04	0.037	0.041	0.041	0.042	0.044
Mg	0.673	0.677	0.702	0.682	0.693	0.691	0.68	0.697
Al	0.377	0.4	0.358	0.412	0.366	0.363	0.388	0.373
Si	1.716	1.687	1.726	1.685	1.711	1.72	1.704	1.72
P	0	0	0.001	0.002	0.001	0	0	0
K	0	0	0	0	0	0	0	0
Ca	0.889	0.918	0.914	0.907	0.916	0.917	0.903	0.892
Ti	0.088	0.09	0.073	0.084	0.079	0.075	0.086	0.079
Cr	0	0	0.004	0	0.004	0.002	0.002	0.001
Mn	0.002	0.002	0.003	0.003	0	0.002	0.009	0.005
Fe	0.233	0.226	0.218	0.227	0.231	0.231	0.222	0.224
Ni	0	0.001	0	0	0.002	0	0	0
Total	**4.036**	**4.043**	**4.038**	**4.041**	**4.044**	**4.042**	**4.036**	**4.036**
$Mg^{\#}$	0.7428	0.7497	0.7630	0.7503	0.7500	0.7495	0.7539	0.7568

Table 4.3 EPMA analysis results of pyroxenes (*Cont….*)

Point	11	12	13	14	15	17	18	19
Na₂O	0.53	0.48	0.51	0.43	0.55	1.09	0.56	0.51
MgO	12.38	12.6	12.01	12.97	12.52	11.69	12.12	12.46
Al₂O₃	8.07	8.13	9.15	7.34	8.11	8.4	8.73	8.58
SiO₂	45.59	45.87	44.89	46.9	46.15	46.25	45	45.41
P₂O₅	0	0.05	0.04	0.08	0	0.05	0.03	0.04
K₂O	0	0.01	0.01	0	0	0	0	0
CaO	23	22.92	23.06	22.86	22.82	21.53	22.72	22.6
TiO₂	2.68	2.84	2.97	2.35	2.73	2.58	2.91	2.81
Cr₂O₃	0.03	0.07	0.09	0.32	0.04	0	0.04	0.17
MnO	0.06	0.13	0.12	0.03	0.1	0.22	0.16	0.18
FeO	7.3	6.91	7.18	6.81	7.18	7.72	7.31	7.23
NiO	0.03	0.01	0	0	0.05	0.12	0	0.07
Total	**99.67**	**100.01**	**100.04**	**100.09**	**100.26**	**99.65**	**99.58**	**100.07**
				On the basis of 6 O				
Na	0.038	0.035	0.037	0.031	0.04	0.08	0.041	0.037
Mg	0.695	0.703	0.672	0.721	0.698	0.655	0.681	0.696
Al	0.358	0.359	0.405	0.323	0.357	0.372	0.388	0.379
Si	1.717	1.717	1.685	1.75	1.724	1.738	1.697	1.702
P	0	0.001	0.001	0.002	0	0.002	0.001	0.001
K	0	0.001	0.001	0	0	0	0	0
Ca	0.928	0.919	0.927	0.914	0.914	0.867	0.918	0.908
Ti	0.076	0.08	0.084	0.066	0.077	0.073	0.082	0.079
Cr	0.001	0.002	0.003	0.009	0.001	0	0.001	0.005
Mn	0.002	0.004	0.004	0.001	0.003	0.007	0.005	0.006
Fe	0.23	0.216	0.225	0.212	0.224	0.243	0.231	0.227
Ni	0.001	0	0	0	0.002	0.004	0	0.002
Total	**4.047**	**4.038**	**4.044**	**4.03**	**4.039**	**4.04**	**4.045**	**4.043**
Mg#	0.7514	0.7650	0.7492	0.7728	0.7570	0.7294	0.7467	0.7541

Point	33	34	35	36	37	38	39	41	42	43	44
Na_2O	0.47	0.51	0.5	0.45	0.49	0.46	0.46	0.44	0.49	0.61	0.48
MgO	12.61	16.11	16.16	16.42	16.05	15.15	12.27	13.9	16.19	16.04	16.01
Al_2O_3	7.76	4.26	4.54	4.47	4.46	5.15	8.08	5.85	4.43	4.21	4.39
SiO_2	46.48	52.03	51.97	51.76	51.52	50.02	45.3	48.5	51.8	52.09	51.38
P_2O_5	0.02	0	0.04	0	0.02	0.02	0.03	0	0	0.01	0.05
K_2O	0.02	0.01	0	0.03	0	0.02	0	0	0	0.01	0
CaO	22.79	22.29	22.12	22.03	22.14	22.57	23.23	23.11	21.99	21.83	22.4
TiO_2	3.09	0.97	1.01	0.97	1.03	1.39	3.47	2.3	0.91	0.94	1.05
Cr_2O_3	0	0.71	0.74	0.87	0.98	0.74	0	0.08	0.71	0.9	0.82
MnO	0.2	0.08	0.18	0.09	0.16	0.2	0.16	0.1	0.11	0.19	0
FeO	7.28	4.94	4.7	4.77	4.84	5.46	7.62	6.98	4.65	4.7	4.67
NiO	0.06	0	0.03	0.06	0.05	0	0	0.13	0.05	0.1	0.01
Total	100.78	101.91	101.99	101.91	101.74	101.18	100.64	101.39	101.34	101.64	101.25
On the basis of 6 O											
Na	0.034	0.036	0.035	0.031	0.035	0.033	0.033	0.032	0.034	0.043	0.034
Mg	0.699	0.865	0.867	0.882	0.865	0.826	0.685	0.764	0.873	0.863	0.866
Al	0.34	0.181	0.193	0.19	0.19	0.222	0.356	0.254	0.189	0.179	0.187
Si	1.728	1.875	1.869	1.865	1.862	1.829	1.695	1.787	1.874	1.88	1.864
P	0.001	0	0.001	0	0.001	0.001	0.001	0	0	0	0.002
K	0.001	0.001	0	0.001	0	0.001	0	0	0	0	0
Ca	0.908	0.861	0.852	0.85	0.857	0.884	0.932	0.912	0.852	0.844	0.871
Ti	0.086	0.026	0.027	0.026	0.028	0.038	0.098	0.064	0.025	0.025	0.029
Cr	0	0.02	0.021	0.025	0.028	0.022	0	0.002	0.02	0.026	0.024
Mn	0.006	0.003	0.005	0.003	0.005	0.006	0.005	0.003	0.003	0.006	0
Fe	0.226	0.149	0.141	0.144	0.146	0.167	0.238	0.215	0.141	0.142	0.142
Ni	0.002	0	0.001	0.002	0.001	0	0	0.004	0.002	0.003	0
Total	4.032	4.016	4.012	4.018	4.018	4.027	4.044	4.037	4.014	4.013	4.017
Mg#	0.7557	0.8531	0.8601	0.8596	0.8556	0.8318	0.7421	0.7804	0.8609	0.8587	0.8591

Point	45.	46	47	48	49	50	51	52
Na$_2$O	0.4	0.46	0.53	0.52	0.49	0.52	0.42	0.48
MgO	13.77	14.36	14.41	12.2	12.58	12.35	14.42	12.04
Al$_2$O$_3$	5.43	5.89	5.96	8.8	8.28	9.06	5.72	9.21
SiO$_2$	47.85	48.82	48.78	45.18	45.73	45.02	48.89	44.78
P$_2$O$_5$	0.09	0.02	0	0	0.03	0.12	0	0.07
K$_2$O	0.02	0	0.03	0.01	0	0.02	0	0.02
CaO	22.4	22.52	22.92	22.79	23.24	22.7	22.59	23
TiO$_2$	2.54	1.63	1.63	3.01	2.63	3.02	1.46	3.08
Cr$_2$O$_3$	0.01	0.31	0.39	0.11	0.31	0.09	0.29	0.09
MnO	0.24	0.07	0.17	0.11	0.14	0.17	0.12	0.11
FeO	7.38	5.9	5.7	7.09	6.88	6.89	5.71	6.87
NiO	0.02	0	0.02	0.12	0.1	0	0.04	0.03
Total	100.16	99.99	100.53	99.95	100.42	99.97	99.65	99.78

On the basis of 6 O

Na	0.029	0.033	0.038	0.038	0.036	0.038	0.03	0.035
Mg	0.767	0.793	0.793	0.683	0.701	0.69	0.799	0.674
Al	0.239	0.257	0.259	0.389	0.365	0.4	0.25	0.408
Si	1.787	1.809	1.801	1.696	1.709	1.687	1.817	1.683
P	0.003	0.001	0	0	0.001	0.004	0	0.002
K	0.001	0	0.001	0	0	0.001	0	0.001
Ca	0.897	0.894	0.907	0.916	0.93	0.911	0.899	0.926
Ti	0.071	0.045	0.045	0.085	0.074	0.085	0.041	0.087
Cr	0	0.009	0.011	0.003	0.009	0.003	0.009	0.003
Mn	0.008	0.002	0.005	0.003	0.004	0.005	0.004	0.003
Fe	0.23	0.183	0.176	0.223	0.215	0.216	0.177	0.216
Ni	0	0	0.001	0.004	0.003	0	0.001	0.001
Total	4.033	4.027	4.038	4.042	4.047	4.04	4.028	4.039
Mg#	0.7693	0.8125	0.8184	0.7539	0.7653	0.7616	0.8186	0.7573

Point	59	60	61	62	64	65	66	67	68	69
Na$_2$O	0.41	0.51	0.52	0.39	0.53	0.42	0.46	0.48	0.52	0.43
MgO	12.51	12.38	12.27	13.61	12.67	13.64	12.27	13.35	13.34	12.38
Al$_2$O$_3$	7.63	8.58	8.51	5.91	7.79	5.18	7.45	5.26	5.22	7.73
SiO$_2$	45.38	45.28	45.31	47.6	45.97	48.01	45.41	48.33	48.61	45.98
P$_2$O$_5$	0.18	0.01	0.01	0	0.02	0.03	0	0	0.01	0
K$_2$O	0.03	0	0.02	0	0.02	0.01	0	0	0.03	0.02
CaO	23.29	22.89	22.62	23.21	23.34	23.04	23.37	23	22.69	22.8
TiO$_2$	2.98	2.88	2.88	2.23	2.77	2.27	3.24	2.23	2.16	3.14
Cr$_2$O$_3$	0.04	0.09	0.1	0.05	0.07	0	0.01	0	0.01	0.05
MnO	0.19	0.2	0.13	0.2	0.15	0.11	0.25	0.19	0.09	0.15
FeO	7.4	7.49	7.08	6.83	6.93	6.94	7.52	7.19	7.62	7.44
NiO	0	0	0.04	0	0	0	0	0.05	0.05	0
Total	100.03	100.3	99.49	100.02	100.27	99.65	99.96	100.09	100.36	100.12
					On the basis of 6 O					
Na	0.03	0.037	0.038	0.028	0.038	0.03	0.033	0.035	0.038	0.031
Mg	0.702	0.692	0.689	0.759	0.707	0.763	0.69	0.744	0.741	0.692
Al	0.338	0.379	0.378	0.26	0.344	0.229	0.331	0.232	0.229	0.342
Si	1.707	1.697	1.707	1.78	1.72	1.801	1.712	1.806	1.812	1.723
P	0.006	0	0	0	0.001	0.001	0	0	0	0
K	0.001	0	0.001	0	0.001	0	0	0	0.001	0.001
Ca	0.939	0.919	0.913	0.93	0.936	0.926	0.944	0.921	0.906	0.916
Ti	0.084	0.081	0.082	0.063	0.078	0.064	0.092	0.063	0.061	0.089
Cr	0.001	0.003	0.003	0.001	0.002	0	0	0	0	0.001
Mn	0.006	0.006	0.004	0.006	0.005	0.004	0.008	0.006	0.003	0.005
Fe	0.233	0.235	0.223	0.214	0.217	0.218	0.237	0.225	0.238	0.233
Ni	0	0	0.001	0	0	0	0	0.002	0.001	0
Total	4.047	4.049	4.04	4.041	4.048	4.035	4.047	4.033	4.031	4.033
Mg#	0.7508	0.7465	0.7555	0.7801	0.7652	0.7778	0.7443	0.7678	0.7569	0.7481

Point	74	75	76	79	80	82	83
Na$_2$O	0.47	0.51	0.55	0.5	0.46	0.54	0.47
MgO	15.98	15.62	15.39	15.36	15.97	15.32	15.5
Al$_2$O$_3$	4.18	4.54	4.75	4.75	4.66	5.12	4.58
SiO$_2$	50.81	50.93	51.02	50.36	50.57	50.2	50.77
P$_2$O$_5$	0	0.04	0	0.01	0.01	0.11	0.04
K$_2$O	0.01	0.02	0	0.02	0	0.03	0.02
CaO	21.63	22.39	22.27	22.1	21.84	21.71	22.06
TiO$_2$	0.96	1.04	1	1.1	1.19	1.18	1.04
Cr$_2$O$_3$	0.65	0.93	0.91	0.96	0.62	0.68	0.77
MnO	0.18	0.07	0.12	0.17	0.08	0	0.06
FeO	4.78	4.95	4.91	4.52	5.1	5.12	5.01
NiO	0.02	0.07	0.08	0.01	0	0	0
Total	**99.67**	**101.1**	**101.01**	**99.87**	**100.51**	**100.02**	**100.3**

On the basis of 6 O

	74	75	76	79	80	82	83
Na	0.033	0.036	0.039	0.036	0.033	0.039	0.033
Mg	0.878	0.849	0.836	0.843	0.871	0.84	0.847
Al	0.182	0.195	0.204	0.206	0.201	0.222	0.198
Si	1.872	1.856	1.859	1.854	1.851	1.846	1.862
P	0	0.001	0	0	0	0.004	0.001
K	0	0.001	0	0.001	0	0.001	0.001
Ca	0.854	0.874	0.87	0.872	0.857	0.855	0.867
Ti	0.027	0.028	0.027	0.03	0.033	0.033	0.029
Cr	0.019	0.027	0.026	0.028	0.018	0.02	0.022
Mn	0.006	0.002	0.004	0.005	0.002	0	0.002
Fe	0.147	0.151	0.15	0.139	0.156	0.157	0.154
Ni	0.001	0.002	0.002	0	0	0	0
Total	**4.018**	**4.021**	**4.018**	**4.016**	**4.023**	**4.016**	**4.015**
Mg#	0.8566	0.8490	0.8479	0.8585	0.8481	0.8425	0.8462

Table 4.4: EPMA analysis results of amphiboles

Spot no.	21	22	23	24	25	26	29	30
Na_2O	4.13	3.82	5.38	3.93	5.32	5.74	4.15	4.81
MgO	7.02	7.16	5.2	5.62	5.98	4.33	6.73	6.13
Al_2O_3	10.63	10.55	12.02	9.73	11.78	11.27	10.69	10.97
SiO_2	41.12	41.47	40.37	36.45	47.07	43.02	40.54	40.84
P_2O_5	0	0.02	0	0.03	0.04	0	0	0
K_2O	0.63	0.64	0.55	0.54	0.52	0.44	0.64	0.6
CaO	9.16	9.41	7.26	12.64	8.03	13.29	8.97	7.86
TiO_2	0.16	0.1	0.24	0.22	0.07	0.09	0.22	0.32
Cr_2O_3	0.03	0	0.02	0	0	0.07	0	0
MnO	0.36	0.19	0.33	0.33	0.39	0.22	0.27	0.32
FeO	22.13	22.47	23.92	21.13	17.84	13.92	22.88	23.56
Total	95.36	95.82	95.3	90.61	97.04	92.38	95.1	95.43
			Cation on the Basis of 23 O					
Na	1.271	1.17	1.67	1.304	1.548	1.77	1.287	1.488
Mg	1.663	1.687	1.24	1.433	1.336	1.027	1.605	1.459
Al	1.989	1.964	2.266	1.96	2.081	2.114	2.016	2.063
Si	6.531	6.551	6.459	6.233	7.058	6.845	6.486	6.516
P	0.001	0.002	0	0.004	0.005	0	0	0
K	0.127	0.129	0.113	0.118	0.099	0.089	0.13	0.123
Ca	1.559	1.593	1.245	2.315	1.29	2.266	1.538	1.344
Ti	0.02	0.011	0.028	0.028	0.007	0.01	0.027	0.039
Cr	0.004	0	0.003	0	0	0.009	0	0
Mn	0.048	0.025	0.044	0.048	0.05	0.029	0.037	0.044
Fe	2.94	2.969	3.201	3.022	2.237	1.853	3.061	3.144
Total	18.151	18.101	18.27	18.464	17.711	18.013	18.188	18.219

Table 4.5: EPMA analysis results of titanites

Element	Titanite	Titanite	Titanite	Titanite	Titanite	Titanite	Titanite
Na_2O	0.06	0.05	0.13	0.08	0.08	0.08	0.08
MgO	0.06	0.28	1.69	1.28	0.29	0.19	0.47
Al_2O_3	1.96	2.17	3	2.84	2.22	1.95	2.2
SiO_2	30.62	30.58	30.46	30.33	30.32	30.32	30.17
P_2O_5	0.02	0	0	0.02	0	0.04	0
K_2O	0.03	0.06	0.5	0.42	0.05	0.04	0.08
CaO	29.02	28.1	24.47	25.84	27.55	27.9	27.44
TiO_2	34.6	34.26	29.99	31.35	33.39	34.39	33.49
Cr_2O_3	0	0.06	0.27	0.11	0.08	0	0.11
MnO	0.11	0	0	0.1	0	0.09	0
FeO	1.98	2.02	3.9	2.98	2.11	1.55	2.02
Total	**98.46**	**97.57**	**94.4**	**95.36**	**96.09**	**96.55**	**96.06**

Table 4.4: EPMA analysis results of albite & epidote

Elements	Albite	Albite	Albite	Albite	Albite	Albite	Epidote
Na2O	12.12	11.75	11.82	10.58	9.67	11.7	0.04
MgO	0.01	0.02	0.25	0.33	1.56	0	0.04
Al2O3	19.3	19.77	19.18	20.27	20.33	18.82	20.15
SiO2	71.2	72.24	69.83	70.51	68.92	68.34	37.49
P2O5	0.03	0	0	0.03	0	0	0.05
K2O	0.07	0.05	0.16	1.05	1.2	0.08	0.01
CaO	0.03	0.1	0.02	0.18	0.25	0.11	23.18
TiO2	0	0	0.08	0.08	0	0.03	0.38
Cr2O3	0.08	0	0	0.03	0.04	0.04	0.11
MnO	0.05	0	0	0	0.12	0.05	0.21
FeO	0	0.14	0.57	0.68	1.75	0.05	14.39
NiO	0.02	0	0.02	0	0	0	0
Total	102.91	104.08	101.93	103.75	103.86	99.23	96.03

CHAPTER 5

Fluid evolution pattern of Zildat Ophiolitic Mélange

FLUID EVOLUTION PATTERN OF ZILDAT OPHIOLITIC

MÉLANGE

5.1.   INTRODUCTION

Fluid-rock mixing or water-rock interaction is commonly used terminology in geology. The study of fluid-rock or water-rock interaction and its importance in geology has evolved extremely in recent years. Initially, it is believed to be more interactive at the sub-surface and with solid crystalline rocks. With time, study reveals fluid do play the major role in complex geological processes, viz; fluid - rock interaction drives the mass geochemical transfer, fluid driven mineralogical alteration, fluid controlled break down reactions at subducting plate in convergent set-up, fluid driven deformation and emplacement processes. The Zildat Ophiolitic Mélange (ZOM) is a disrupted incoherent rock mass varying its composition. It is chaotically deformed and heterogeneously hydrated with three major components; altered oceanic crust, metasediments and ophiolite remnants. The mixing of various components creates assimilation of mélange metasediments with altered oceanic crust and mantle triggers chemical imbalance due to presence of reactivated fluids (Kerrick and Connolly 2001; Gorman et al. 2006). These reactive fluids can enhance the activity of non-volatile masses, generating metasomatic and metamorphic alterations (e.g., Bebout and Barton 1989, 1993, 2002; Manning 1997; King et al. 2003). These alteration processes are equilibrated at different depths inside a subduction pathway (Gansser 1974;

86

Norman 1975; Hall 1976, 1980; Federico et al. 2007). The transportation mechanism is tracked by complex fluid evolution pattern recorded within these rocks (Zack and John 2007). Degree of fluid modification is preferentially controlled by mineral–fluid interaction (Scambelluri and Philippot 2001; Gao and Klemd 2001; Schmidt and Poli 2003; Plank 2005; Kessel et al. 2005). Fluid inclusion study is considered to be one of the strongest tools to envisage multi fluid component system. Further quantification as a resultant of fluid involvement are studied through stable isotope systematic as they reveal information of both early precursor rocks and the modified/ metamorphosed rocks in which fluid plays an important role (Wickham and Taylor 1987; Bouman et al. 1994, 2009; Cartwright et al. 1995; Baumgartner and Valley 2001; Halama et al. 2011). Combining these two systematics can help to construct the complete evolutionary trajectory of a rock with its subsequent emplacement history. To ascertain fluid fluxes and variation in fluid regime across the mélange, exotic carbonate blocks were targeted for analyses. Limestone has distinct isotopic values comparing to their adjacent lithologies, so any kind of fluid modification from its original value can be distinguished easily.

5.2.   GEOLOGY AND SAMPLING STRATEGY

The dismembered and heterogeneously deformed carbonates are collected across the mélange covering its complete lateral extent (Fig. 5.1b). The sampling is done starting from northern end of the mélange in contact with the Nidar Ophiolites to the southern end at the margin of the Tso Morari

Crystallines. The carbonates are compositionally similar but show heterogeneity in intensity of deformation and crystallinity (Fig. 5.2a,b). The limestones blocks are large in size and crystalline in nature towards the northern end of the mélange, while moving towards south these limestone blocks are deformed and brecciated near the Zildat fault zone (Fig. 5.2c).
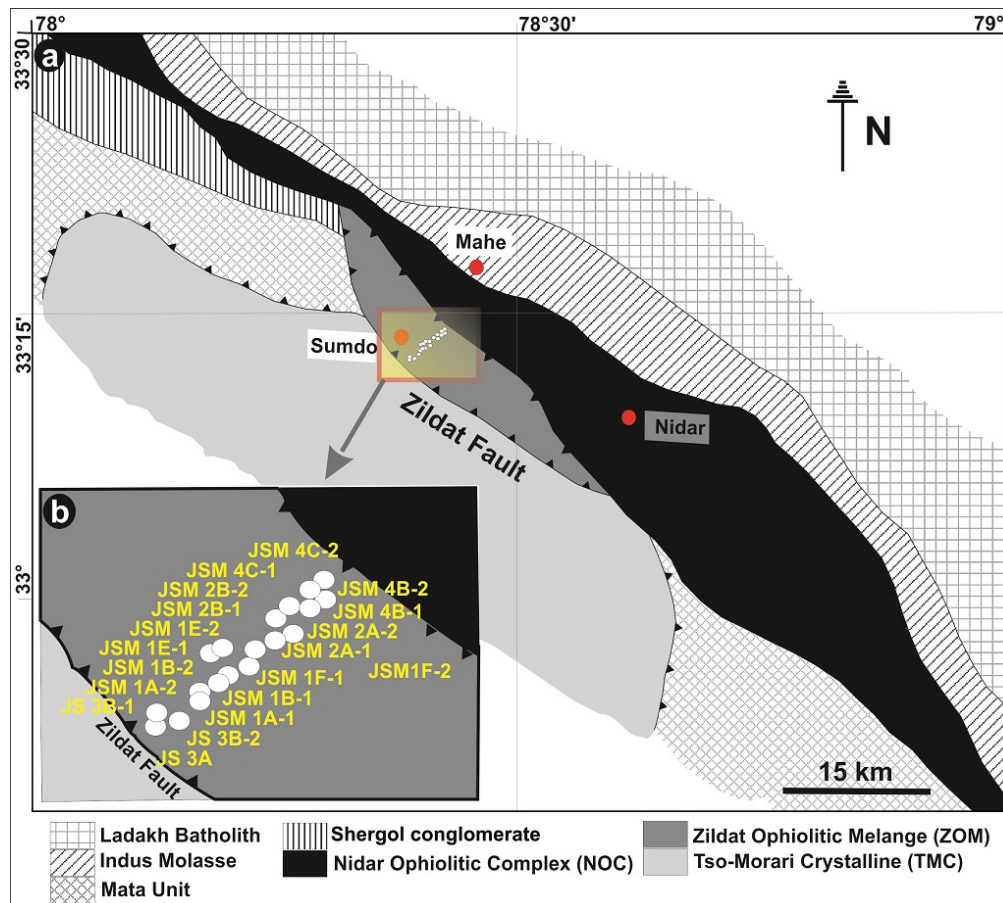
Figure 5.1: (a) & (b) *Simplified geological map of the study area showing location of studied metamorphosed limestone samples distributed within Zildat Ophiolitic Mélange (modified after Thakur & Mishra 1984, Steck et al. 1998, Maheo et al. 2006).*

The mélange near the Zildat fault zone is interestingly characterised by numerous quartz veins concordant with the regional schistosity of the mélange (Fig. 5.2d). The collected carbonate samples were studied under microscope for fluid inclusion petrography and the bulk stable isotope analysis were performed using Isotope Ratio Mass Spectrometer.
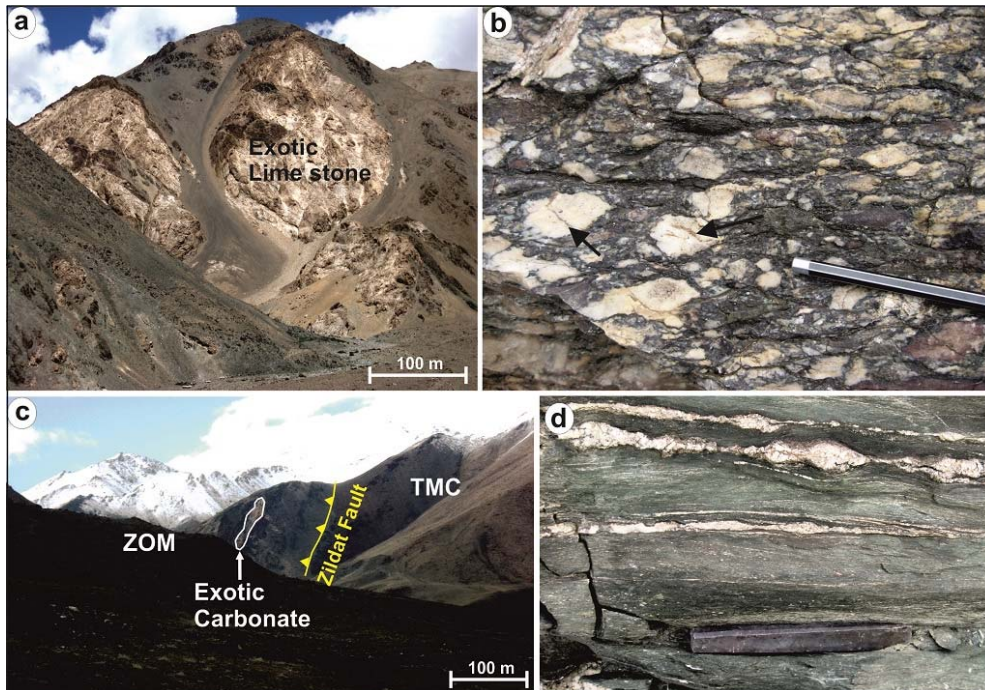
Figure 5.2: *(a) Large scale dismembered exotic limestone within Zildat Ophiolitic Mélange surrounded by heterogeneous metasediments (meta-greywacke) with metabasic clasts. Towards the contact of Nidar Ophiolite, away from Zildat fault, these are distributed as large scale mega-clasts. (b) Sheared and brecciated clasts of limestone mantled by metasediments, nears Zildat Fault Zone. Pencil for scale (c) The Zildat Ophiolitic Mélange and Tso-Morari Crystalline are separated by Zildat detachment fault. (d) Silica vein boudinaged by late deformation, observed at the marginal part of the mélange towards the contact of Tso-Morari Crystalline.*

5.3. FLUID INCLUSION PETROGRAPHY AND EVOLUTION

Despite their tiny appearances, study of fluid inclusions study is proven to be an established research tool extensively used by geologists in various field like economic and petroleum geology for prospecting and exploration of ore deposits and oil fields, genesis of minerals and fluid controlled tectonic processes. Fluid inclusions are fluid-filled vacuoles sealed within minerals. In nature crystal (mineral) can never be developed without imperfection. Such imperfections on the crystal surface are engulfed by the crystal as it grows.

This process creates tiny, commonly tens of microns in size, vacuoles containing the fluid present at the moment of sealing. Fluid inclusions can be described by visual parameters like size, shape, colour, refractive index and particularly by the phases present at room temperature. Fluid inclusions usually contain three phases- liquid (L), gas or vapour (V) and solid (S). The spatial relationships of fluid inclusions provide information about the time of formation with regard to the host mineral. Primary fluid inclusions by definition are trapped during crystal growth, whereas secondary fluid inclusions can be trapped at any time after the growth of the host crystal. Fluid inclusions in microcracks formed during crystal growth are referred to as 'pseudosecondary'. Diagnostic criteria for classifying fluid inclusions as primary or secondary have been proposed by Roedder, 1979. To minimize the emphasis on the primary, secondary and pseudosecondary classification of inclusions, Goldstein & Reynolds (1994) introduced the concept of the Fluid Inclusion Assemblage (FIA) to describe *a group of fluid inclusions that were all trapped at the same time*. An FIA thus defines the most finely discriminated fluid inclusion trapping event that can be identified on the basis of petrography (Goldstein, 2003). This requirement further implies that the inclusions in the FIA were all trapped at approximately the same temperature and pressure, and all trapped fluids are of approximately the same composition. Therefore, the FIA represents a "fluid event" in the history of the system, and the fluid in the inclusions making up the FIA represents the fluid that was present during that event. The requirement that the inclusions within an FIA were all trapped "at the same time" is relative and the absolute amount

of time of the event will vary according to the environment of formation. By systematic study and documentation of fluid inclusion assemblages through petrography, one can decode multiple generation of fluid involvement during the deformation and evolution of a rock even in complex tectonic settings. With these views an attempt is made to categorize different generation of fluids and event of their entrapment during the deformation of Zildat Ophiolitic Mélange (ZOM) zone carbonates.

Fluid inclusion study of ZOM carbonates:

Fluid inclusion petrography of ZOM carbonates display varying mode of occurrences. Based on physical appearances, they are broadly classified into two groups: primary isolated type and secondary trail bound type. In the interior parts of the ZOM (Figs. 5.3a-c), the primary high-saline brine inclusions occur in the calcite grains showing isolated tri-phase morphology (Fig. 5.3a). The tri-phase inclusions are sub-rounded in nature ranging up to ~10 μm in size, containing solid infuse cubic phases of halite (?) along with vapour and liquid phases (Fig. 5.3a). In some places, elongated bi-phase inclusions reveal saline-aqueous nature. These are noticed in patches showing peculiar tubular shape, ~5 μm in size with aspect ratio of ~ 5:1 (Fig. 5.3b). Scarce clusters of unidentified minute trail bound inclusion are also seen, which appears to be modified as primary or pseudo-secondary trails (Fig. 5.3d). The predominant phases of fluid inclusions are mostly secondary in origin, which was trapped during deformation process (Figs. 5.3e-h). These inclusions are randomly oriented arrays and are present either as inter-crystalline or within healed fractures. The majorities of secondary fluid

inclusions are containing liquid and vapour phases in the ratio of 1:4. In places

movement of bubbles are observed within the fluid inclusions, which indicate

low salinity conditions. Re-equilibration textures such as, irregular shapes and

decrepitation in the fluid inclusions are commonly noticed which are present
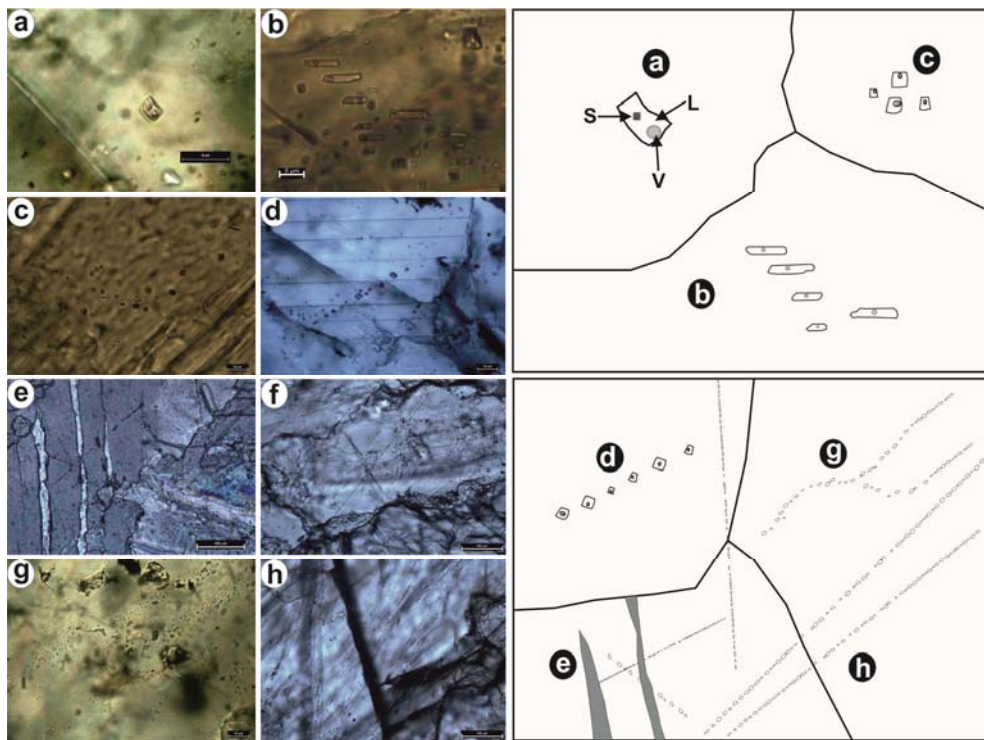
Figure 5.3: *Photomicrographs of fluid inclusions obtained from carbonates of Zildat Ophiolitic Mélange. **(a)** Tri-phase inclusion displaying negative crystal shape. It contains solid (cubic)-liquid and vapor phases which suggest brine fluid inclusion. **(b)** Tube shaped bi-phase fluid inclusions showing preferred orientation. **(c)** Cluster of primary bi-phase fluid inclusions along with diffused crystal phases. **(d)** Intragranular semicircular pseudo-secondary/ modified primary trail bound fluid inclusions. **(e)** & **(f)** Fluid inclusion trails crosscut by thick calcite twining. See corresponding sketch, which shows thick grey color tapered boundary of calcite twins cross cutting array of hollow dots of inclusion trail. **(g)** Bifurcated fluid inclusion trail, showing pseudo-secondary nature. **(h)** Fluid inclusion trails showing secondary fluid entrapment. See corresponding sketch, which shows long array of hollow dots showing fluid inclusion trails cross cutting the grain boundary.*

in the deformed parts of calcite grains. They are inferred to be associated with

mélange deformation preferably at a low temperature condition. No usual

distinction of fluid composition is observed during petrographic observation;

therefore fluid inclusion thermometry could not be deployed to characterize

the fluid inclusions any further. In order to retain the textural relationship of carbonate minerals, destructive experimentation modes were avoided.

5.4. STABLE ISOTOPE GEOCHEMISTRY USING OXYGEN & CARBON ISOTOPE

It was Harold Urey (1947) who first pointed out thermodynamically based estimate of the temperature-dependence of $^{18}O/^{16}O$ fractionation between calcium carbonate and water, and a recognition of how this information might be used to determine the temperatures of ancient oceans launched the science of stable isotope geochemistry. The approach pioneered by Urey has since been used to estimate temperatures for a wide range of geological processes (e.g. Emiliani 1955; Anderson et al. 1971; Clayton 1986).

To compare isotope data, an internationally accepted set of standards is used (NBS- 18). Stable isotope ratios are reported using delta notation (δ). This notation compares the ratio of the heavier isotope to the lighter isotope in a sample to that of a standard. Because the variations are small, we multiply by 1000 and the resulting delta value is therefore in permil (‰).

$$\delta = [\{R(\text{Sample}) - R(\text{Standard})\}/R(\text{Standard})] \times 1000$$

where *R* represents the measured isotope ratio

For carbon and and oxygen stable isotope values the above equation can be written as,

$$\delta^{13}C = \frac{(^{13}C/^{12}C)sample - (^{13}C/^{12}C)PDB}{(^{13}C/^{12}C)PDB} \times 1000$$

$$\delta^{18}O = \frac{(^{18}O/^{16}O)sample - (^{18}O/^{16}O)SMOW}{(^{18}O/^{16}O)SMOW} \times 1000$$

Unmetamorphosed sediments usually have characteristic $\delta^{18}O$ values (e.g. Hoers 1980). In general, limestones have the highest $\delta^{18}O$ values (20-30‰), followed by shales (15-20‰), and quartzites (10-15‰). Relatively large shifts in $\delta^{18}O$ values are, however, documented from metasediments in some regional metamorphic terrains. $\delta^{18}O$ values of sedimentary rocks are sometimes, but not universally, lowered by several permil during regional metamorphism. The $\delta^{18}O$ values are probably lowered by < 1-2‰ by prograde metamorphic devolatilisation (e.g. Chamberlain et al. 1990; Stern et al. 1992), suggesting that closed system reactions are not the major cause of isotopic resetting. This assertion is supported by the fact that rocks in some metamorphic terrains that have undergone prograde devolatilisation retain their oxygen isotope values without much resetting. It is most likely that, as in contact metamorphism (Valley 1986; Nabelek 1991), the lowering of $\delta^{18}O$ values by several permil during regional metamorphism reflects fluid infiltration.

Carbonate samples for stable isotope ratios were measured at Wadia Institute of Himalayan Geology. The detail analytical procedure is mentioned in chapter 3. The conversion equations of $\delta^{18}O(PDB)$ versus $\delta^{18}O(VSMOW)$ is done by following Coplen et al. 1983. A total of 19 representative carbonate samples were selected to analyse $\delta^{18}O$ and $\delta^{13}C$ isotopes. The stable isotope values are displayed in Table 5.1.The oxygen ($\delta^{18}O$) and carbon ($\delta^{13}C$) isotope values of carbonate rocks are not uniform rather they decrease with increasing deformation and shearing approaching to the Zildat fault zone. The

overall $\delta^{13}C$ carbonate values fall in the range of 1 to 4 ‰ which reveals a platform carbonate affinity (Table 5.1).

Sample Name	δ13C vs VPDB	δ18O vs VSMOW	Megascopic behavior of analyzed carbonates
JS 3A	2.45	15.65	Sheared, near TMC
JS 3B_1	0.97	17.20	Sheared, near TMC
JS 3B_2	1.16	16.69	Sheared, near TMC
JSM 1A_1	2.44	17.82	Sheared, near TMC
JSM 1A_2	2.59	17.54	Sheared, near TMC
JSM 1B_1	2.40	17.72	Sheared, near TMC
JSM 1B_2	2.41	17.41	Sheared, near TMC
JSM 2E_1	2.85	18.75	Sheared, near TMC
JSM 2E_2	3.05	18.46	Sheared, near TMC
JSM 2F_1	2.72	18.19	Sheared, near TMC
JSM 2F_2	2.85	17.85	Sheared, near TMC
JSM 2A_1	3.70	23.58	crystalline
JSM 2A_2	3.72	23.27	crystalline
JSM 2B_1	3.49	22.39	crystalline
JSM 2B_2	3.65	22.13	crystalline
JSM 4B_1	2.88	19.32	crystalline
JSM 4B_2	2.97	18.89	crystalline
JSM 4C_1	3.36	20.14	crystalline
JSM 4C_2	3.38	19.73	crystalline

Table. 5.1: *Stable isotope data from exotic carbonates of the Zildat Ophiolitic Mélange*

For the less deformed / crystalline part of mega-boudin carbonates, the values are 3-4 ‰. On the other hand, it varies from 1 to 3 ‰ for heavily deformed and sheared carbonate blocks that suggests metamorphism at crustal level. The absolute values of $\delta^{13}C$ show a steady decrease in the carbonates from interior

to margin nearer to the TMC. The $\delta^{18}O$ values also show two distinct batches of data (Fig. 5.4). For the less deformed carbonates of the interior part, the $\delta^{18}O$ values fall in the range of 20-24‰. This implies marine carbonate signature and indicates influence of ancient sea water (Hoefs, 1980). For the intensely deformed carbonates of the margins, the $\delta^{18}O$ values fall in the range of 15.5 to 18 ‰, which signifies role of external fluids and alteration. The lower values of $\delta180$ isotopic signature of carbonates are caused by alteration indicating modification after depositional marine condition.

5.5. DISCUSSION

The ZOM is a tectonic block situated within ISZ, and confined between the Nidar Ophiolite and the TMC complex. Mélange represents a metagreywacke having substantial fragments of oceanic sediments, volcanics (volcanoclasts) and ophiolite clasts that encompasses exotic marine carbonate blocks. Although tectonically disrupted, carbonate blocks across the mélange leading to marginal parts display a dominance of secondary fluid, bimodal fluid evolution and intense fluid mixing signatures (Fig. 5.3, Fig. 5.4 & Table 5.1). Fluid flow in weakly deformed carbonate blocks reveals limited evidence of brine (Fig. 5.3a), which may have trapped soon after the carbonate deposition. The appearance of brine in the mélange possibly is linked with a high grade metamorphic episode, and this metamorphism may have occurred during subduction of the oceanic crust (Scambelluri et al. 1997). Later inflow of aqueous –saline fluid may have produced at the mineral reaction site during the retrogression. The later inflow of secondary aqueous fluid (Figs. 5.3d-f) can be significantly modified through external fluid flux during emplacement

along the ZOM. At this stage, intense chemical modification of the fluid and its mixing was caused due to influences of external sources from adjacent TMC rocks (Mukherjee & Sachan 2009). Although, entrapment of metasomatic fluids due to interaction of ultramafic and mélange can also cause fluid modification and mixing, the evidences of fluid mixing and input of metamorphic fluids from TMC are well consistent with δ18O isotopic values (Fig. 5.4).

The stable isotope composition of a metamorphosed rock is controlled by six factors: (1) the composition of the pre-metamorphic protolith; (2) the effects of volatilization; (3) the temperature of exchange; (4) exchange kinetics; (5) fluid composition, and (6) fluid flux (Baumgartner & Valley 2001). These factors are best evaluated in studies of contact metamorphism because of the good geologic control and the common occurrence of fluids with distinct initial isotopic compositions are usually available in these systems. Dehydration is the best-known and most common example of metamorphic volatilization. The magnitude of the isotopic effect is controlled by the amounts of water expelled; high-grade rocks contain less water than lower grade equivalents due to progressive dehydration (Spear 1993). The effect of dehydration reactions on the value of δ18O in a rock will always be small, less than 1 permil. Coupled O-C isotope depletions are seen in many metamorphic systems involving carbonate rocks. However, in each area, the magnitude of the depletions is too large to be explained by the closed system the devolatilization processes discussed here. Significant fluid infiltration and exchange involving low δ18O, low δ13C fluids are indicated by the stable

isotope data (see Valley 1986). The magnitude of 18O/16O or 13C/12C depletion caused by volatilization is not sufficient to cause the large isotopic shifts seen in Fig. 5.4. Hence, these shifts must result largely from exchange with infiltrating fluids. The effect of infiltration is greatest when sufficient fluids are available, when contrasts in isotopic composition are great, when permeability is high, and fluid-rock exchange is not slowed by exchange kinetics.
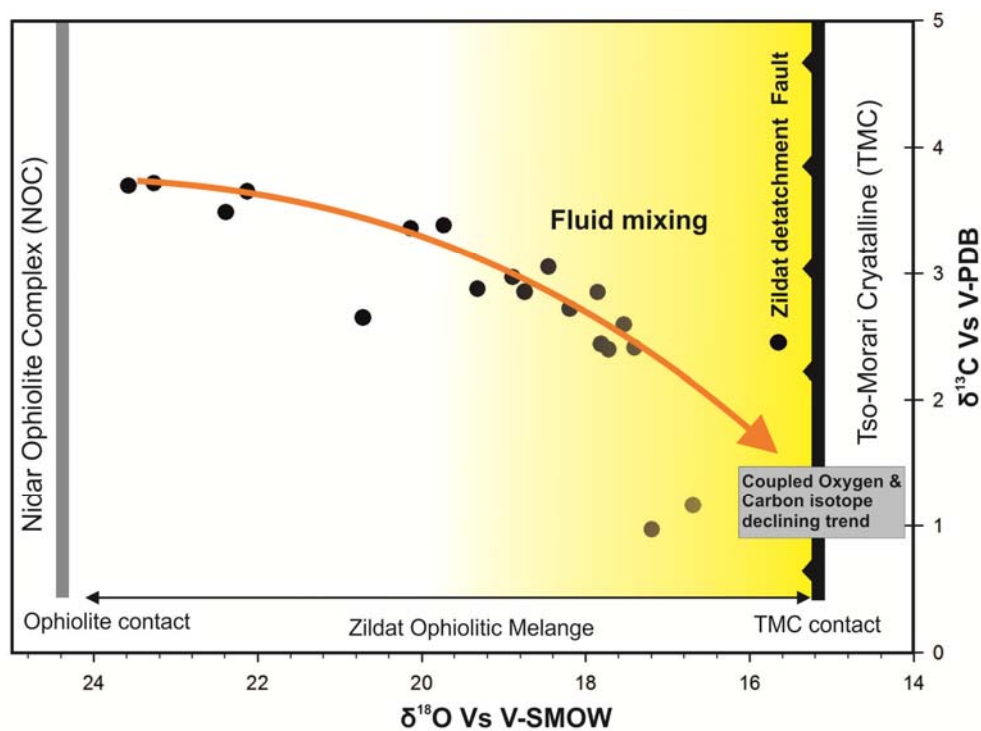
Figure 5.4: *Model showing plots of stable isotope value of exotic limestones distributed through Zildat Ophiolitic Mélange. The corresponding stable isotope data show decreasing trend towards Zildat Fault Zone. Coupled Oxygen & Carbon isotopic trend from the exotic carbonates across the ZOM. The δ18O and δ13C values show decreasing trend from the interior to the leading edge of mélange. The Oxygen values away from the sheared part are of marine carbonate affinity (20-24‰). Depleted values were obtained near the TMC contact that indicates fluid mixing. Shaded part of the diagram represents zone of fluid infiltration. The fluid possibly derived from adjacent TMC unit, guided by Zildat fault.*

The oxygen isotope data from ZOM carbonates show distinct values with respect to the original deposition condition and subsequent alteration. Highly depleted oxygen values from the margin of the ZOM (Fig. 5.4) can be

explained by crustal contamination at low temperature condition (Pálfy et al. 2001). The $\delta18O$ values of crustal fluids are lighter than that of carbonate rocks (Veizer et al. 1999; Wallmann 2001). Hence, it may deplete the initial value of $\delta18O$. The carbonates reflecting high $\delta18O$ values (~24 ‰) from the interior of the mélange indicating early marine condition (Fig. 5.4). The examined $\delta18O$ values show consistency with $\delta13$ C values. This indicates availability of brine fluids which has been provided by high grade metamorphism. In a way, later modifications by lighter isotopes of water can overprint the carbonates, leaving a more depleted signature than the primary signature of deposition (Pálfy et al. 2001). The oxygen and carbon isotope study of carbonate rocks therefore demonstrate syn-depositional conditions and post depositional alteration. Across the mélange, fluid production and oxygen isotopes variation in order of 7-8‰ suggest fluid infiltration from adjacent Tso Morari Gneissic dome. This phenomenon can be supported by the presence of dense network of quartz veins within mélange metasediments, which is more localised near the Zildat fault (Fig. 5.2d). However, this inference can be more precisely constrained by the study of fluid rare earth element analyses.

CHAPTER 6

Origin & Formational Setting of Zildat Ophiolitic Mélange

ORIGIN & FORMATIONAL SETTING OF ZILDAT OPHIOLITIC MÉLANGE

6.1. INTRODUCTION

Plate tectonic processes have generated considerable geological complexities in the zone of plate interfaces which evolved as a resultant litho-unit named Zildat Ophiolitic Melange (ZOM), Indus Suture Zone, NW Himalaya. This region shows evidence of plate convergence involving subduction of an oceanic plate, continent–continent collision, sediment accretion and emplacement of dismembered ophiolites and exhumation of high and ultra-high pressure metamorphic rocks. In general the Mélange rocks display characteristics features of modern and ancient convergent plate boundaries, marked by ophiolite clasts and high to low grade metamorphic rocks signifies the convergent plate margin processes. The ZOM provide detail insight into metamorphic evolution of subducted rocks and large scale element mobility with associated lithologies. The high-pressure rocks of ZOM are considered significant in particular to provide insight into the subduction of ancient oceanic lithosphere. Several oversimplified approach has been made to understand the genetic evolution of ZOM. However, details of the protolith of these complex units and their origin remain unclear. Very few geochemical data are reported from these rocks till now, despite of their potential to provide an important record of pre-subduction tectonic configuration, and hence, the tectonic settings from which their protolith derived. The present chapter attempt to infer the tectonic setting of the precursor rocks of the ZOM to understand its geodynamic evolution in a more comprehensive manner.

Major, trace and rare earth element variation, chemical discrimination diagrams have been used in order to characterize the nature of parent rock and related processes. Geochemical data are plotted and interpreted by discrimination schemes provided by Pearce and Cann (1973), Tribuzio et al. (1996), Winchester and Floyd (1976), Morrison (1978), Vermeesch (2006) and Van Westrenen et al. (2001). In addition, laser Raman spectroscopy study is deployed on the volatile and incipient phases of volcaniclastic rock of ZOM for the characterization of mineral phases and associated texture within.

6.2. SAMPLE SELECTION AND PREPARATION

The ZOM rocks are devided into several sub-units (shown in Figure 4.1 d) which are need to be treated separately for knowing its formational and depositional setting. An attempt has been made through geochemical study of the basic volcanic rocks of ZOM, which are present at the southern end the terminal part of the Mélange. These rocks also show high pressure metamorphic signature (described in chapter 4), appeared as a separate litho-unit, uniform and homogenous in character and less altered compared to other units of ZOM.

Bulk geochemical analyses are carried out on basic and volcaniclastic rocks of ZOM (towards TMC contact shown in Figure 4.1 d) using X-Ray Fluroscence (XRF) and Inductively Coupled Plasma Mass Spectrometer (ICPMS). Raman spectrometric study are done on polished thin sections using argon laser beam. The detail instrumentation description and analytical procedures are discussed in Chapter 3.

6.3. MAJOR, TRACE & RARE EARTH ELEMENTS GEOCHEMISTRY

The representative rock samples are analysed using XRF and ICPMS for major oxide, rare earth elements and trace element analyses. The detail of analyses are compiled in Table 6.1 and 6.2. The basic rocks are basaltic in nature, composed of plagioclase, clinopyroxene, blue amphibole and titanite. The plagioclase grains are albitic in nature. Clinopyroxenes are augite to titanaugite in composition and the amphiboles are Na amphiboles in majority. The quartz, sericite, chlorite, epidote, calcite, and iron oxides are present as secondary minerals.

The standard method of classifying volcanic rocks is the total alkali–silica (TAS) diagram (Le Bas et al., 1986) (Fig. 6.1a). As per the TAS classification, the ZOM rocks are varies from basic to ultra-basic group with majority of rocks falls in the field of basanite and a few falls in basanite-trachyte-andesite series. The analysed results are shown in Table 6.1. It shows range of SiO_2 content (~40-50 wt. %) with overall alkaline character ($Na_2O+K_2O \sim$ 3.5-7.5 wt. %). Most of the samples indicative of silica under saturated except sample no LSM 1D. The plotted data cluster favours alkaline basaltic-basanitic nature. However few of the data plotted in trachyte-andesitic group. Almost all the samples show high fractionated mafic rocks of MgO values ranges from 3.7-14.1 wt. %. The rocks show comparative higher TiO_2 and Na_2O concentration (2.5 to 3.3 wt. % and 1.3-6.5 wt. % respectively).
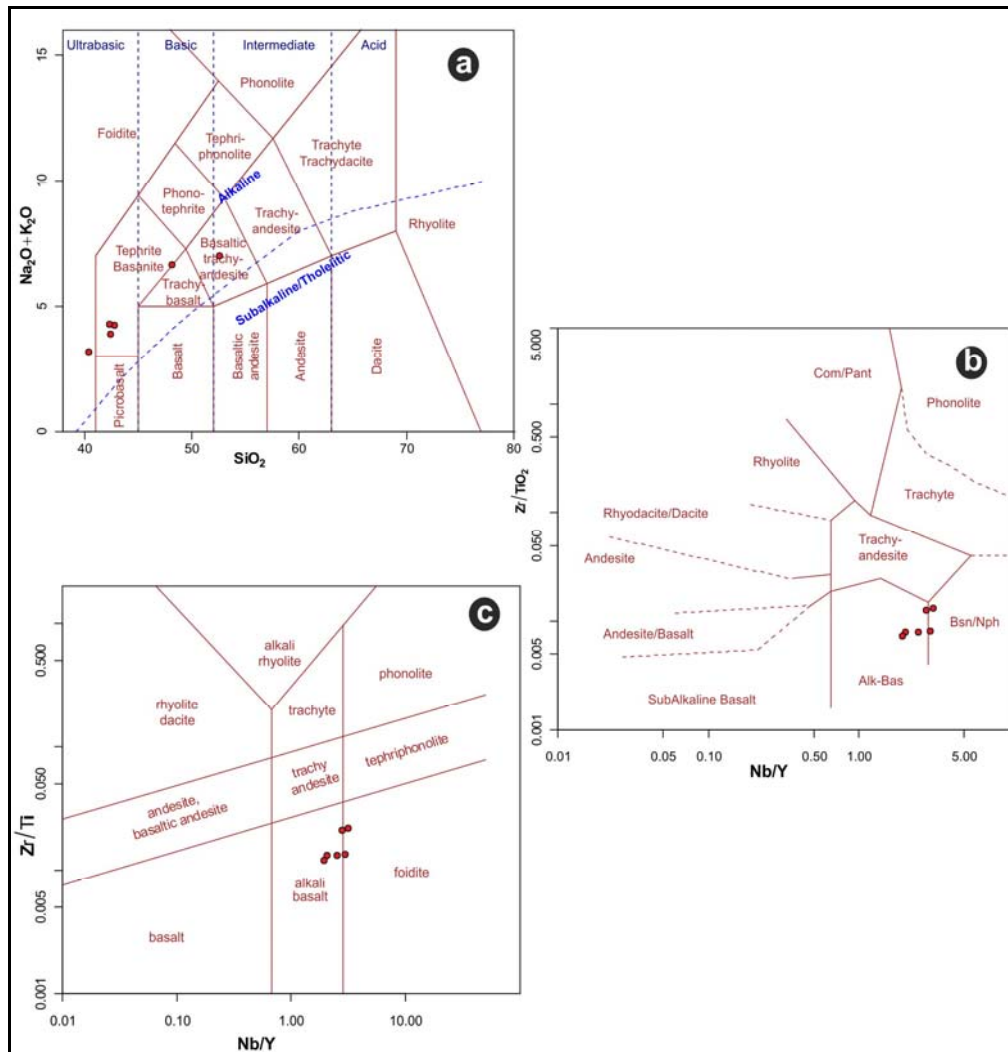
Figure 6.1: (a) *Total alkalis vs. silica classification diagram for ZOM mafic rocks (after Le Bas et al., 1986),* **(b) & (c)** *The classification of volcanic rocks based on immobile elements (after Winchester & Floyd, 1977) modified by Pearce (1996).*

The total alkali (Na$_2$O + K$_2$O) value mainly distinguishes alkalic from sub-alkalic rock types, whereas the silica plot mainly distinguishes primitive from evolved rock types. This classification is not very convincingly attempted in case of rocks suffered alteration process. Thus, the elements Zr, Nb, Y, and Ti are also used for classification purpose following Winchester & Floyd, (1977) and Pearce (1996)'s classification scheme (Fig. 6.1b,c),

Table 6.1: *Whole-rock major oxides and trace element compositions of basic rocks from Zildat Ophiolitic Mélange, Indus Suture Zone, Himalaya. (Analysis done using XRF, Oxide values are in wt.%, Rest elements are in ppm.)*

Sample	LSM1	LSM1A	LSM1D	LSM1E	LSM3A	1S66
Na_2O	3.43	3.53	6.50	3.28	5.70	1.34
MgO	6.34	6.97	3.76	6.88	7.05	14.10
Al_2O_3	11.68	13.20	12.22	12.57	14.86	13.03
SiO_2	40.11	40.20	51.74	39.83	47.04	38.70
P_2O_5	0.72	0.78	0.76	0.70	0.84	0.31
K_2O	0.68	0.19	0.64	0.84	0.84	1.67
CaO	15.17	12.28	10.54	13.40	6.39	7.13
TiO_2	2.89	3.36	2.54	3.10	3.22	3.31
MnO	0.19	0.21	0.14	0.19	0.18	0.16
Fe_2O_3	12.64	14.15	9.75	13.49	11.68	16.04
Total	**93.85**	**94.87**	**98.59**	**94.28**	**97.80**	**95.79**
LOI	6.74	4.79	2.69	5.71	2.95	4.10
Ba	353	134	555	411	340	178
Cr	40	52	58	48	31	529
V	315	303	244	322	243	289
Sc	24	23	17	26	16	31
Co	47	43	41	47	48	72
Ni	24	33	37	27	15	231
Cu	54	52	28	52	60	96
Zn	101	114	59	114	140	129
Ga	19.96	22.03	13.73	22.29	21.01	24.06
Pb	4.6	5.4	3.6	4.4	7.0	3.5
Th	5.97	3.01	5.44	3.94	8.10	3.43
Rb	11	3	9	14	18	39
U	0	0	0.68	1.21	0	0
Sr	686	588	262	820	578	250
Y	23	27	24	26	31	36
Zr	230	271	335	246	406	241
Nb	61.8	70.3	88.3	65.8	104.4	56.6

as these elements are immobile and are not affected by alteration and metamorphism of rocks. The classification diagrams (Fig. 6.1) suggest there is a certain amount of alteration while following the Le Bas et al., (1986) classification scheme. The samples are plotted in a scattered way considering

the silica and alkali content, though the overall rocks are suggestive of their alkaline characteristics. On the other hand, the classification schemes based on immobile trace elements (Winchester & Floyd, 1977; Pearce 1996) suggest alkaline basalt affinity.
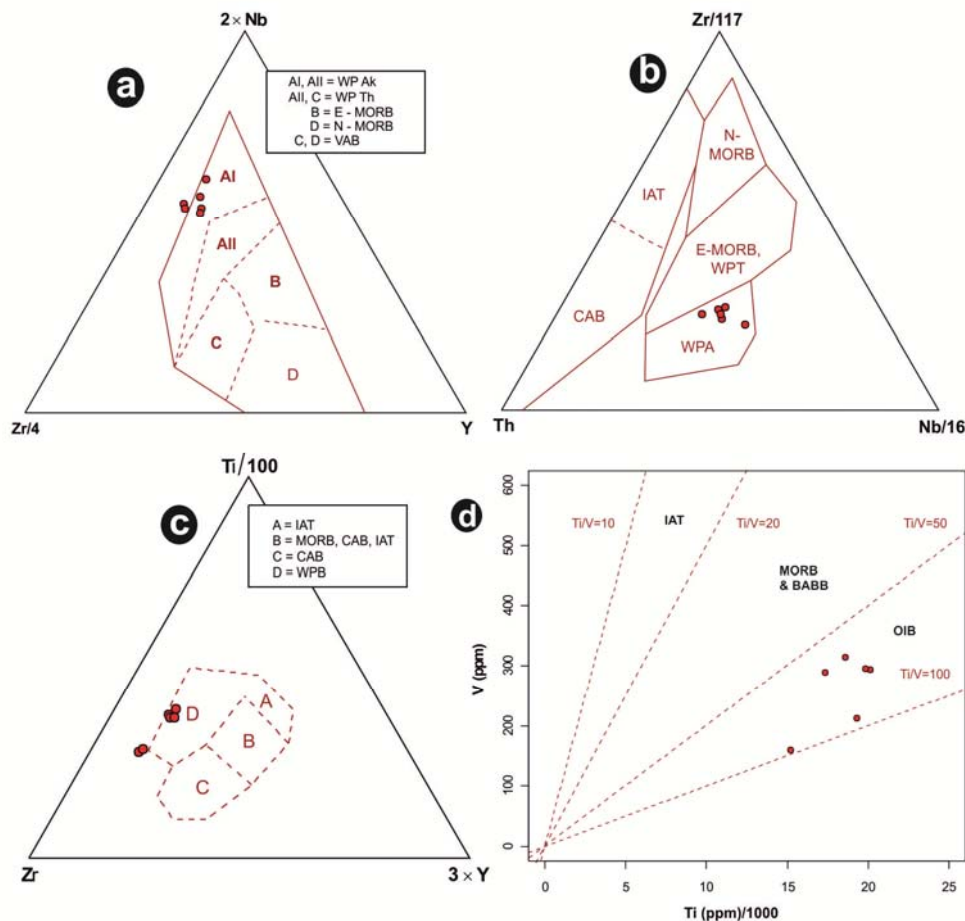
Figure 6.2: (a) *Discrimination Nb-Zr-Y diagram (Meschede, 1986) for basalts from ZOM. AI, AII = within plate alkali basalts; AII, C = within plate tholeiites; B = E-type MORB; D = N-type MORB; C, D = volcanic arc basalts.* ***(b)*** *tectonic discrimination diagram of Wood (1980). MORB=mid-ocean ridge basalt; WPT=within plate tholeiite; WPA=within plate alkaline basalt; IAT=island-arc tholeiite; CAB=calk-alkaline basalt.* ***(c)*** *Ti–Zr–Y discrimination diagram of Pearce and Cann (1973). A—island arc tholeiites, C—calc-alkali basalts, D—within plate basalts, B—MORB, island-arc tholeiites, and calc-alkali basalts. A and C are the IAB fields, D the OIB field, and B a mixed field of MORBs and IABs.* ***(d)****The data plotted on the Ti-V discrimination diagram of Shervais (1982). IAT- island arc tholeiite basalt, MORB- mid oceanic ridge basalt, BABB = backarc basin basalt, OIB- ocean island basalt.*

Many of the immobile trace element classification diagrams, such as those of Pearce & Cann (1973), Wood et al. (1979), Norry (1979), Shervais

(1982) and Meschede (1986) are used to infer the tectonic setting of the alkaline basalts of ZOM. Immobile trace elements Nb, Zr, Y, Th, Ti and V are used in various combinations for tectonic classification scheme which are shown in Fig. 6.2. Applying discrimination Nb-Zr-Y diagram (Meschede, 1986), Zr-Th-Nb diagram Wood (1980), Ti-Zr-Y diagram Pearce & Cann (1973) and Norry (1979) suggest that the basalts are within plate alkali basalts (Fig. 6.2 a-c, e). Whereas Ti-V discrimination diagram (Shervais, 1982) indicates that the basalts showing ocean island basalts (OIB) trend (Fig. 6.2d). The basic rocks of ZOM have inclined REE patterns that are LREE-enriched. This geochemical signature is typical of ocean-island basalt (OIB) (Nakamura 1974; Sun and McDonough, 1989) (Fig. 6.3).
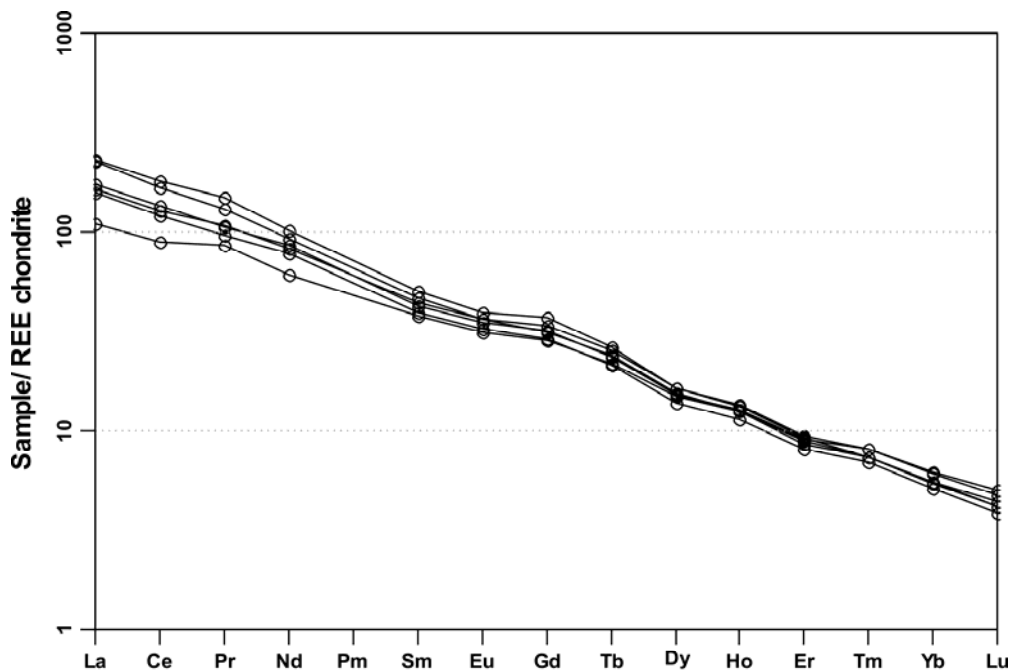
Figure 6.3: *Rare earth element patterns of ZOM basalts from the Indus Suture Zone. Normalization values are from Nakamura (1974).*

Table 6.2: *Whole-rock rare earth and trace elements compositions of basic rocks from Zildat Ophiolitic Mélange, Indus Suture Zone, Himalaya. (Analysis done using ICPMS, K2O value in wt.%. Rest elements are in ppm.)*

Sample	LSM 1	LSM 1A	LSM 1D	LSM 1E	LSM 3A	1S 66
La	52	57.4	75.9	54.2	75.3	36.3
Ce	104	116.6	155.8	110.7	145.7	76.6
Pr	10.8	11.9	16.7	12.1	14.7	9.6
Nd	49.4	54.6	64.4	51.9	58.8	38.1
Sm	7.95	8.68	10.23	8.93	9.4	7.71
Eu	2.49	2.69	3	2.82	2.83	2.42
Gd	7.97	8.77	10.23	8.61	9.4	7.79
Tb	1	1.11	1.23	1.12	1.2	1.03
Dy	4.69	5.2	5.66	5.25	5.63	5.12
Ho	0.8	0.89	0.93	0.88	0.94	0.87
Er	1.81	2.05	2.07	1.99	2.13	1.92
Tm	0.21	0.24	0.22	0.22	0.24	0.22
Yb	1.12	1.33	1.21	1.22	1.36	1.19
Lu	0.13	0.16	0.14	0.15	0.17	0.14
Y	20.4	24.7	20.1	24.4	26.1	23.8
Sc	18.1	19.8	9.7	19.7	11.9	32.6
K_2O	0.55	0.17	0.39	0.75	0.8	1.7
Rb	14.2	7	8.4	19.2	18.9	40.8
Sr	700	564	214	850	558	233
Ba	228	50	205	281	303	423
Nb	50.8	73	62.6	49.7	73.2	46
Hf	1.2	1.8	2	1.3	1.6	1.6
Th	3.1	3.4	4	3.1	5.7	2.7
U	1.5	1.8	1.7	1.3	1.1	0.7
Li	14.4	17.7	4	15.6	35.6	27.2
Be	1.5	2.1	4.3	1.2	1.4	1.4
V	289.5	294	159	314	212	296
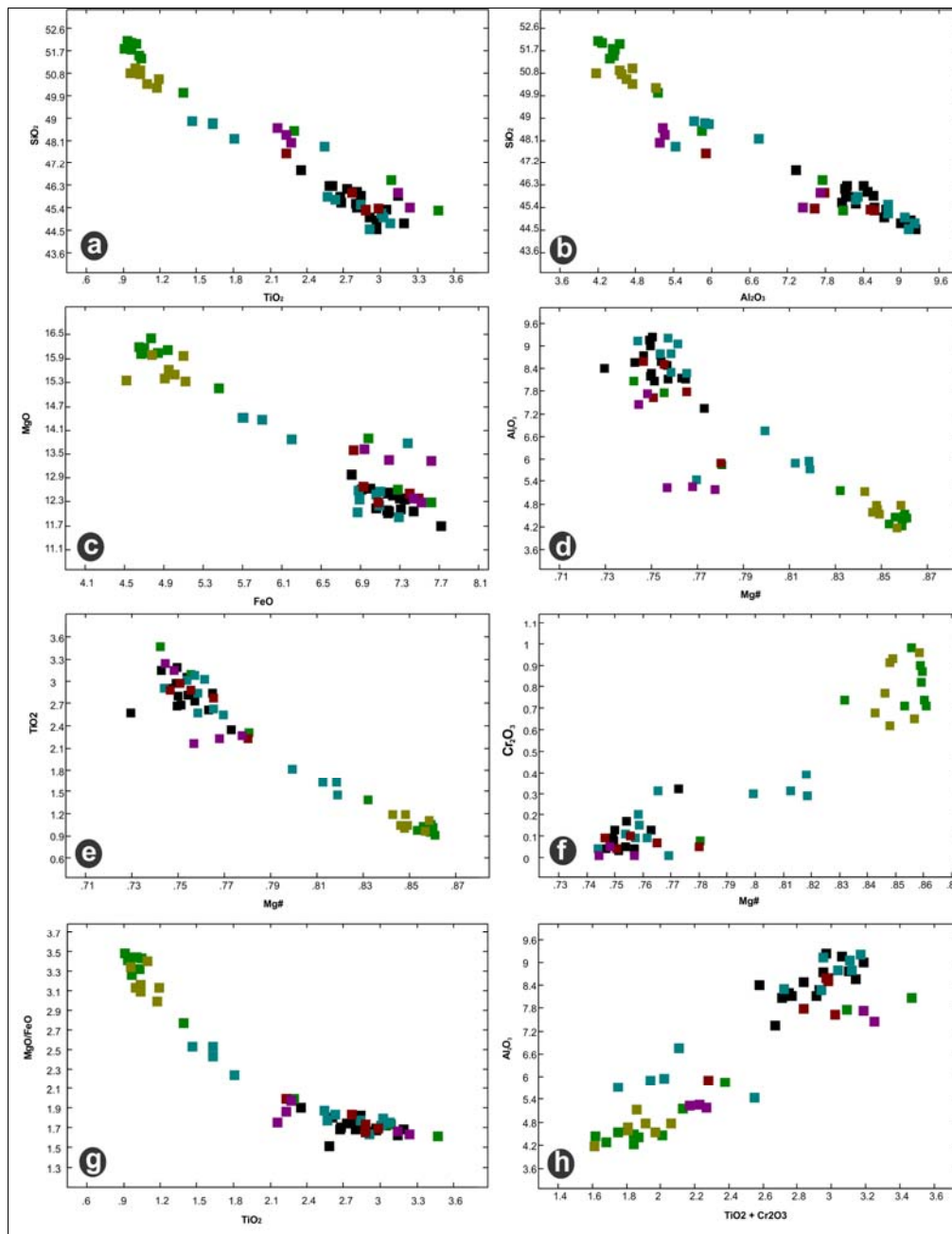
Figure 6.4: (a) *SiO2–TiO2,* **(b)** *SiO2–Al2O3,* **(c)** *MgO-FeO,* **(d)** *Al2O3–Mg#,* **(e)**
TiO2–Mg#, **(f)** *Cr2O3–Mg#,* **(g)** *MgO/FeO - TiO2 and* **(h)** *Al2O3– TiO2 + Cr2O3*
*variation diagrams for a range of elements plotted to show a linear trend among
major element of different pyroxenes pyroxene grains at different spots. The
pyroxenes are analysed for mineral chemistry using EPMA, the results and analysis
spots are shown in chapter 4. Different colours are used for different pyroxene grains.
Variation among a single colour indicate inhomogeneous distribution of elements
within same pyroxene grain from core to rim.*

The geochemical analyses show variability in major oxides and mobile

elements which is indicative of metamorphic alteration. Relative enrichment

of HFSE (High Field Strength Elements) are noticed which tend to behave

immobile may indicate bulk mass loss due to alteration. The Ti concentration is comparatively higher, which reflects partial replacement of pyroxene and rutile to titanite. Higher concentration of Sr in the basics fall in the renge of 250-820 ppm). The higher Sr concentration indicate high grade metamorphic signature. The concentration of Li may reside at amphibole, phengite. High Co, Ni concentration may drive through metasomatism of hydrated ultramafics. Detail mineral chemistry is also done for these rocks using EPMA. The pyroxenes are commonly observed in ZOM, it has higher TiO_2 and Al_2O_3, indicating titan-augite which is generally found in alkaline rocks. SiO_2–TiO_2, SiO_2–Al_2O_3, MgO-FeO, Al_2O_3–$Mg^\#$, TiO_2–$Mg^\#$, Cr_2O_3–$Mg^\#$, MgO/FeO - TiO_2 and Al_2O_3– TiO_2 + Cr_2O_3 variation diagrams are plotted to show a linear trend among major element of pyroxenes (Fig. 6.4), indicating a continuous evolution of magma. The detail results and analysis spots are shown in chapter 4.

6.4. VOLATILE PHASES IDENTIFICATION USING LASER RAMAN SPECTROSCOPY

Laser Raman Spectroscopy is mainly used to characterise some unusual mineral phases which are associated with the volcaniclastic rock of ZOM. This volcaniclastic layer consists of angular fragments of predominantly Ti-rich pyroxene (titan-augite), titanite, albatic plagioclase lath and fine-grained altered glassy matrix (<3 microns) (Fig. 6.5 a,b). The shape of the titanite is unusual type, they do not look like inorganic substance and are appear to be organic microfossils (?) (Fig. 6.5 c-h). These fossil like substances are 200-500 µm in size, display elliptical to sub-rounded in shape.
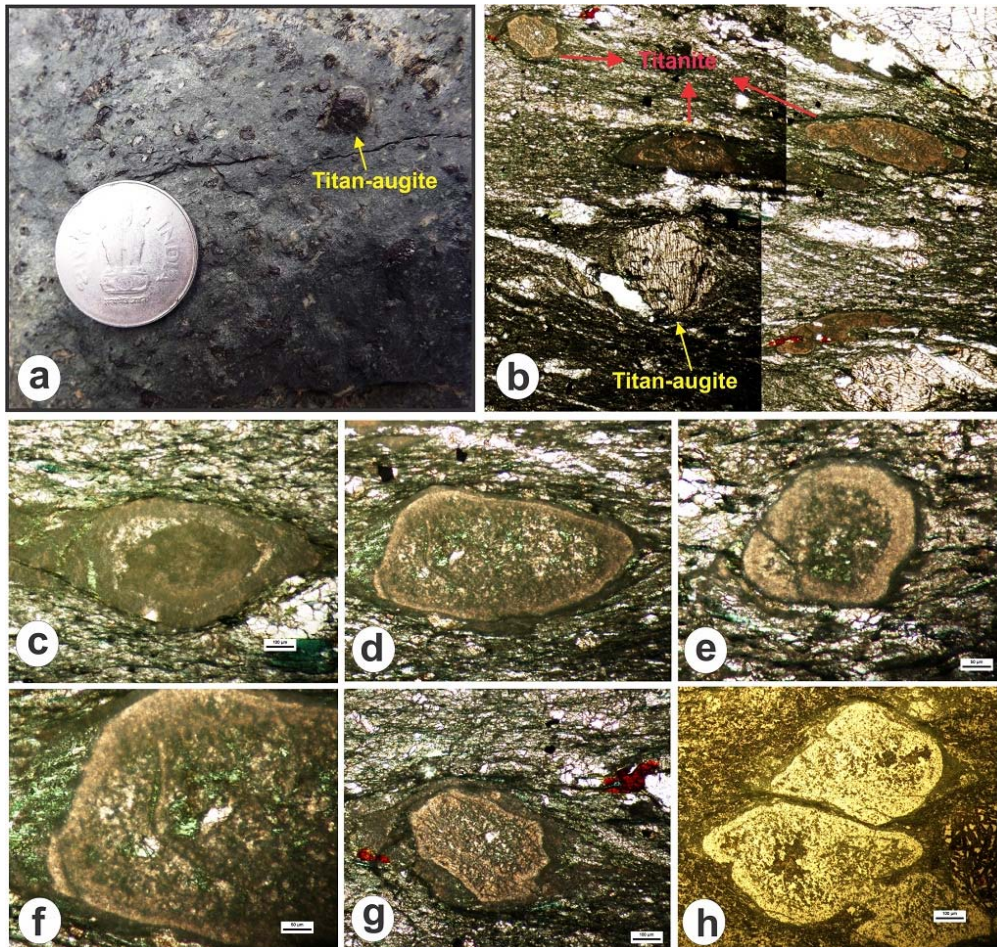
Figure 6.5: (a) *Mesoscopic view of studied volcanicalastic rock sample from the Zildat Ophiolitic Mélange. Yellow arrows show the euhedral pyroxene (titan-augite) clast set in a fine grained basic matrix.* ***(b)*** *Photomicroscopic mosaic of volcaniclastics rock showing titan-augite and fossil like titanite clasts.* ***(c-h)*** *Photomicrographic details of microfossil from the volcaniclastic unit showing preserved test part and variation of shape due to deformation.*

Their major axis is oriented along the foliation and the tectonic foliation warps around the microfossils (Fig. 6.5c). The microfossils contain a distinct outer rim, which is made up of very fine grained minerals and can be easily distinguished from the inner part of the fossil (Fig. 6.5d & e). This is considered to be the test part of the organism and has more or less consistent thickness of ~30 micron. High resolution image reveals that the test is ornamented with a thin layer of dark carbonaceous matter, which is circular in shape and continuous throughout the peripheral part (Fig. 6.6). The

110

composition of the microfossils has been almost replaced due to chemical and mineralogical alteration. Their inner parts are filled by minerals from the surrounding matrix. The comparatively robust rim part has been affected by late stage chemical replacements. Both the rim and inner part of these microfossils shows abundance of titanite. However, the original structure of these microfossils is retained to a large extent despite deformation.

Low intensity Raman spectroscopy (514 nm) was employed on this peculiar volcaniclastic rock to characterize the incipient and volatile phases present within the sample. The Raman spectra from the pyroxene and titanite are shown and discussed in Chapter 4 (Fig. 4.). The pyroxene spectra show a stretched and broad peak infer to be the presence of glassy and/or pyroclastic phases within pyroxenes. Whereas the outer part of the microfossil (?) shows presence of carbonaceous matter (Fig. 6.6). It show Raman spectra at 1560 – 1600 cm^{-1} G band region and a weak D band hump at around 1320 cm^{-1}. There are some weak second order S peak around 2704 cm^{-1}. The first and second order Raman spectra indicate presence of disordered or microcrystalline carbonaceous material. The Raman band around 3072 – 3077 cm^{-1} indicate presence of hydrocarbons as 3000 – 3100 cm^{-1} is the region of weak arena bands (Larkin 2011). The 3552 – 3577 cm^{-1} and 3674 cm^{-1} band indicates OH stretching vibrations (Larkin 2011).
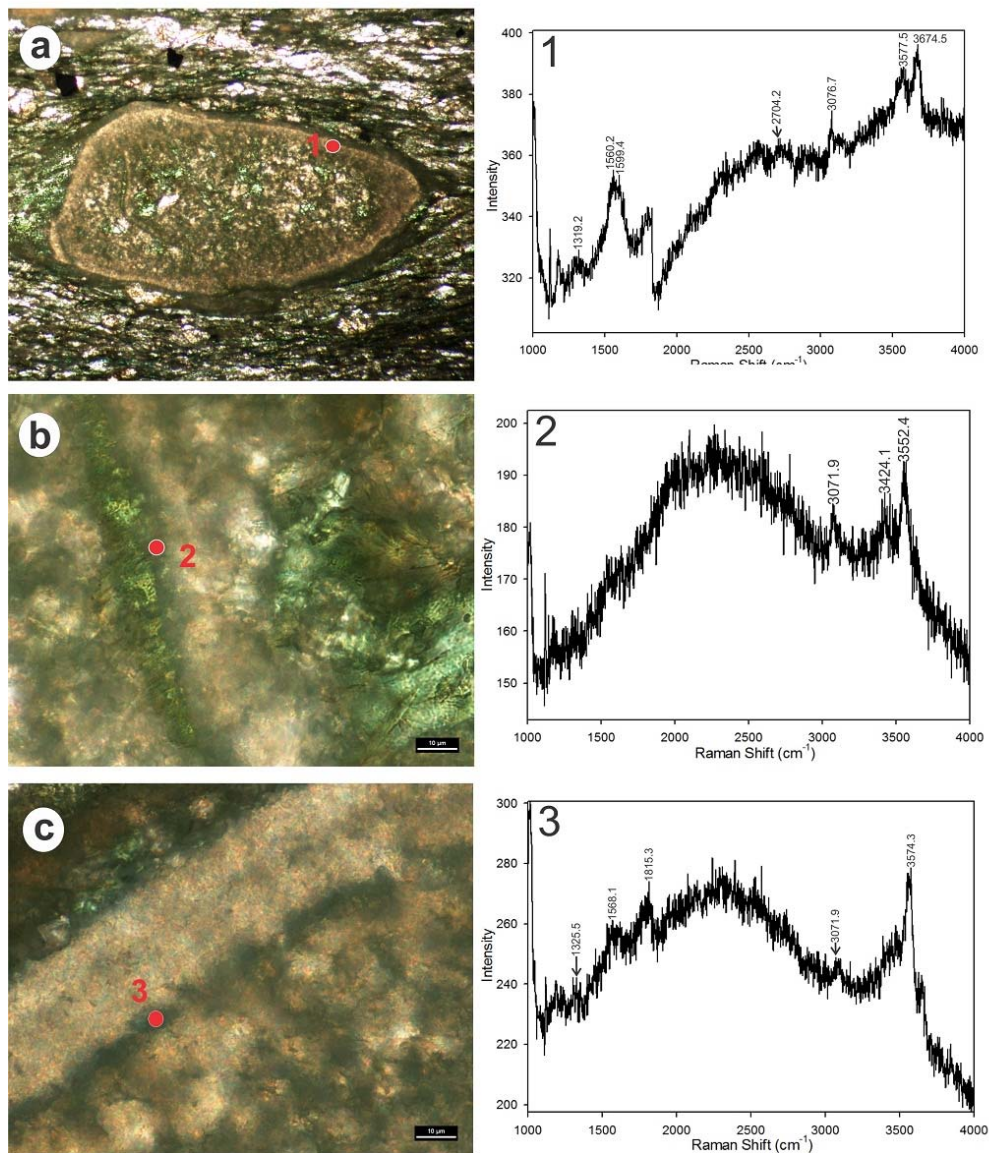
Figure 6.6: *Combined photomicrograph and raman spectra of microfossil found in ZOM volcaniclastic unit.* ***(a-c)*** *photomicrograph of microfossil in different scale opted for raman spectroscopic study. Raman laser spot are taken from different parts shown as **1,2,3**. The respected raman spectra are shown in right side of the diagram indicating presence of carbonaceous matter and hydrocarbon signature. Please gone through the text for details.*

6.5. DISCUSSION

The Zildat Ophiolitic Mélange of Indus Suture Zone is considered as remnants of Neo-Tethyan sea mounts accreted at the northern margin of

Indian continent (Sigoyer et al. 2004). It represents relict of subducted oceanic crust and preserves signatures of past volcanic events caused by subduction process. These oceanic fragments along the suture have been interpreted in an intra-oceanic or supra-subduction zone context (Hébert et al., 2000, 2001, 2003; Aitchison et al., 2000; Huot et al., 2000, 2003; Dubois-Coˆ teʹ et al., 2003, Mahéo et al., 2004., Ahmed et al 2008). The present study suggests the oceanic fragment mixed-up in Zildat Ophiolitic Mélange is not entirely supra-subduction related volcanic rocks but also bears signature of pristine phase volcanic activity that may indicate pre-subduction ocean floor volcanism during the opening of the Neo-Tethyan Ocean. It is believed that the major and trace element geochemistry of basic rocks can potentially reveal much about the protolith. Studies have demonstrated the value of immobile trace elements such as Zr, Y, Hf, Th, Nb, and Ta as indicators of magma types and tectonic settings [e.g., Pearce and Cann, 1973; Pearce and Norry, 1979; Wood et al., 1979; Wood, 1980]. These elements are useful to characterize the basalts from a complicated tectonic setting. There are evidences that HFSE such as Ti, Zr, Nb Y, and REE are effectively insoluble and immobile during subduction and metamorphism (Thompson 1973; Sheraton 1984; McCulloch & Gamble 1991; Pearce et al. 2000; Zhao et al. 2007). Hence, these elements retain their original contents and ratios, and provide insight into the pristine petrological characteristics of the subducted rocks (Pearce & Norry 1979; White 2007). On the basis of HFSE elements, all the basic rock samples from ZOM falls in the within plate alkaline basalt field. The REE data shows OIB signature, which indicate oceanic volcanism prior to the subduction of the oceanic crust. Thus

the mineralogical and chemical signature of ZOM mimics the entire history of the Neo-Tethys oceanic basin environment prior to the India–Asia suturing. The alkaline volcaniclastic unit preserves organic remnants in the form of microfossils. These microfossils lost their original morphological features due to post depositional deformation. So, identification of these microfossils could be a tough task. However, Raman spectroscopy analyses detected titanite test of these microfossils and this titanite signature is also noticed in the matrix and the interior parts of the microfossils. Hence it can be inferred that since the volcaniclastic was already enriched in TiO_2 (Table. 6.1), late incorporation of silicic and calcic fluids have reacted to form this secondary titanite throughout the rock. Breakdown of calcic plagioclase and volcanic glass also have contributed to the formation of secondary titanite (Jefferson, 1982). Therefore the titanite we detected at the test part of these microfossils is a secondary replacement. Despite of heavy deformation and alteration in ZOM, some characteristic features helped us to establish these unique features as microfossils. The presence of carbonaceous matter within this organic features provides further strength to our view (Fig. 6.6). Nevertheless, occurrence of radiolarian and similar marine microfossils are usual in mélange rocks. In (2001) Satoru et al. reported early Cretaceous radiolarians from the radiolarian chert of the Nidar Ophiolitic Complex in the Indus Suture Zone. Fragments of cherts containing radiolarian are also observed within the ZOM as rediolarite way back in 2004 by De Sigoyer et al. Similarly, observations also made in late Cretaceous radiolarians from Saiqu Mélange of southern Tibet (Li et al., 2009) and Cretaceous radiolarians from Yarlung-Zangbo suture of Tibet

(Wang et al., 2000). Danelian & Robertson (1997) reported occurrence of mid-Jurassic, mid-Cretaceous and late-Cretaceous radiolarians from Karamba Basin of Indus Suture Zone and early Cretaceous radiolarians were also reported from the Spontang massif of Ladakh Himalaya (Baxter et al., 2010). However, all these reported occurrence of radiolarians are typically in sedimentary environments. In the present study, the occurrence of microfossil is unique and is found within an alkaline basic volcaniclastic rock. In the geological past researchers have lead to correlate large scale magma emplacement with extreme biological crisis (Courtillot, 1999; Hallam, 2005; Hough et al., 2006; Blackburn et al., 2013). Based on the unusual occurrence of these microfossils within the volcanoclastics it can be assume that ocean floor magmatic activity may cause major catastrophe. However, more extensive work is needed to see whether presence of these microfossils within volcaniclasts indeed indicate marine biota crisis caused by sub-marine volcanism.

CHAPTER 7

Evolution of Zildat Ophiolitic Mélange & Model Reconstruction

EVOLUTION OF ZILDAT OPHIOLITIC MÉLANGE &

MODEL RECONSTRUCTION

(Zildat Ophiolitic) Mélange- by the very characteristic feature of their 'block-in-matrix' fabric and incoherent nature of the sediments are zone of pervasive internal deformation, varied range of chemical inhomoginity and complex metamorphic history. ZOM is defined by heterogeneous tectonic slices composed of ophiolite fragments, volcaniclastic sediments and reworked clasts of varied composition. Mélange rocks rank with high pressure-low temperature to moderately high temperature metamorphic rocks demonstrate the records of a convergent plate margin processes. The evolution of ZOM includes remnants of an early high P-low T metamorphism, would possibly associated with initiation of subduction event, followed by internal deformation and mixing of three components system; ophiolite clasts, metavolcanics and oceanic sediments. The geochemical data suggests large scale mass movement (fluid-rock interaction) was aid by serpentine-talc matrix, consequently attributed to positive volume changes during the ZOM emplacement in a confined zone.

7.1. SUMMARY OF THE RESEARCH WORK

This chapter synthesises the present research work on mélange evolution in subduction complex in collisional setting. It broadly discussed in

five subtitles in the context of Zildat Ophiolitic Mélange, Indus Suture Zone, Himalaya.

7.1.1. NATURE OF ZILDAT OPHIOLITIC MÉLANGE

A disrupted multi-layered composite unit, the ZOM has been observed in subduction complex of NW Himalaya. The composite unit comprises pieces of wide range of meta-sedimentary and meta-igneous lithology covering of 4 km thick unit show NW-SE trend. The contact mélange rocks terminated at its contact with TMC of continental affinity, display intense shearing and thinly foliated low density sediments with signature of late reactivated thrusting. The ZOM mapped as number of tectonic slices with mega sized carbonate boudins, were assembled during the exhumation of TMC at 30 Ma onward (de Sigoyer et al 2000; Epard & Steak 2008). Each tectonic slices of mélange subunit manifested relative movement and intense shearing. The best preserved lithounit occur in the centre part of mélange appear to be conglomeritic in nature with many reworked clasts and exotic carbonates. The field observations and detail microscopic study interpret early sedimentary mixing of the mélange which show unique mega scale texture of block-in-matrix fabric in ZOM. The huge range of pervasively deformed clasts of chert, carbonate, basics, volcaniclastics and serpentine vindicate three component mixing of oceanic sediments, ophiolite and volcaniclastics during the formation of ZOM. The nature of development of mélange lithounits with evidences of early signature of mixing, the ZOM is classified as tectonic ophiolitic mélange.

7.1.2. MINERALOGICAL EVOLUTION AND METAMORPHIC HISTORY OF ZOM

The ZOM is a disrupted package of various sedimentary and igneous fragments. Each fragments of mélange lithounits show wide range of mineralogical variation and complex metamorphic histories. These lithounits were supposedly formed in a heterogeneous manner. In such heterogenous nature of ZOM rocks, the metamorphic history of each subunit was ascertained with the help of first order field observation and petrographic analyses. By reflection of ZOM recorded polymetamorphic histories, the metamorphic history of individual clasts are not directly correlated to the overall mélange metamorphism. This section aims to describe the metamorphic history of ZOM is mainly deduced from the overall matrix mineralogy which however show intense retrogression and fluid-rock interaction at the expense of mélange emplacement. The evolution of metamorphism in ZOM rocks are broadly classified in three metamorphic episodes, categorises as M1, M2 & M3. M1 is revealed from the basic volcanic rocks and margin of the carbonates blocks were metamorphosed under transitional condition between blueschist to epidote-amphibolite facies. M2- metasedimentaries from oceanic segment aided with metasomatism of mafic show epidote-amphibolite to amphibolite metamorphism. Whereas wide spread M3 show greenschist metamorphism as the presence of chlorite-phyllite schist and calcium rich basic volcanics, gabbro and serpentinite and their metamorphic equivalents. The evolution of mélange includes an early blueschist assemblages of high pressure metamorphic event at around 450-

500°C (Fig. 7.1) with relict signature of an early eclogite imprint of Na-clinopyroxe fragments. The prevailed metamorphic condition may also be noticed at the margin of exotic limestone blocks in the presence of pseudo-aragonite phase (Fig. 4.7). This event possibly associated with the initial subduction and burial of ZOM carbonates followed by considerable deformation and fluid interface mixing at the early stage evolution of ZOM. A loosely associated blocks of green colour in the mélange show evidences of epidote-amphibolite condition formed at moderately high temperature condition upto 600°C. The mentioned lithotectonic unit of ZOM show mixing of metasomatic fluid from serpentinised ultramafic, this view is looks plausible in concurrence of present interpretation of ophiolite (Dilek 2003). Most of the lithounits of ZOM show significant amount of recrystallization and relict imprint of poly-metamorphism. To recognize the complete metamorphic history of each of these lithounit is difficult is difficult to demonstrate (in chemical analyses), since the original mineralogy and chemical signatures are completely overprinted by later stage metamorphism and tectonism. However, a linking thread of these early events can be seen through pyroxene phases which is most commonly observed in these lithounits of ZOM. In continuation of the above metamorphism, a wide spread amphibolite to greenschist facies condition is noticed with low pressure, below 400°C with the development of penetrative schistosity. This event characterised by appearance of Ca-amphibole and relict Ca-plagioclase to talc-tremolite-chlorite to phyllite grade even further lower metamorphic condition (Fig. 7.1).
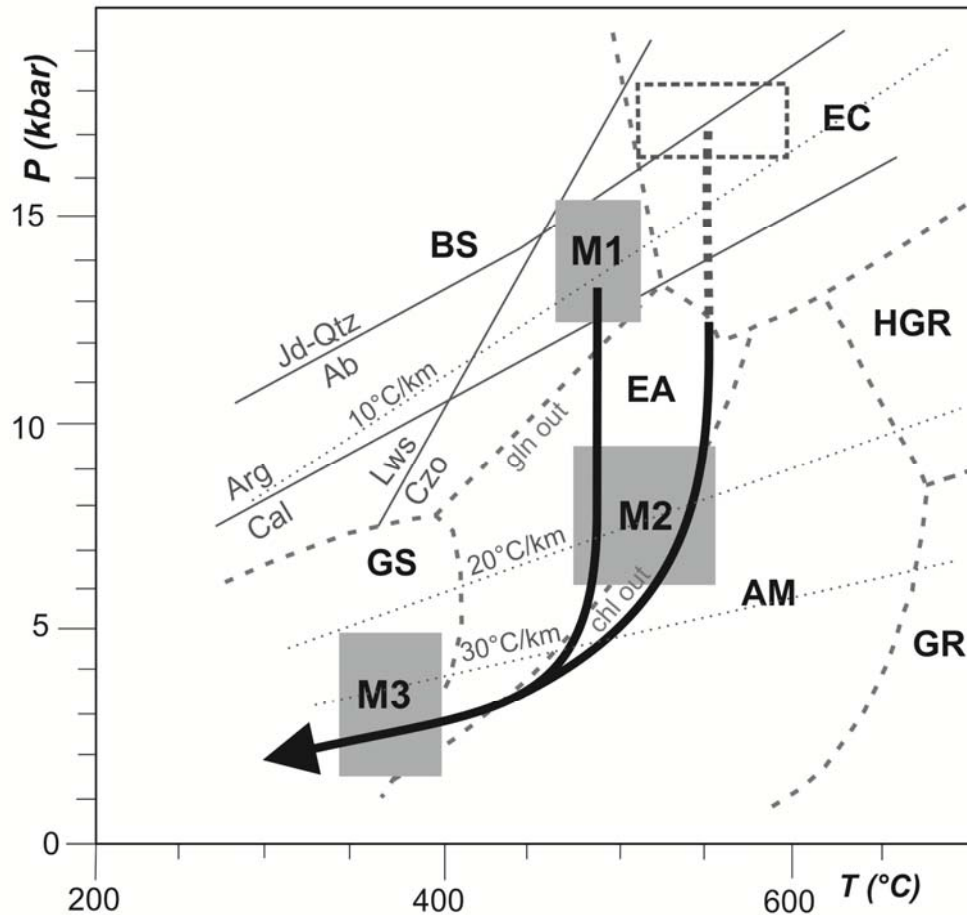
Figure 7.1: *Hypothetical P-T trajectory of ZOM showing two clock wise metamorphic path. One path follows blueschist to medium grade greenschist facies via moderate epidote-amphibolite to lower amphibolite-facies condition. The alternate path that might follow eclogite to greenschist condition via high temperature epidote-amphibolite to amphibolite condition.*

By studying the basic-ultrabasic and metasedimentary of ZOM unit, it show three prominent metamorphic events passing through high pressure to moderately high temperature-low pressure to low temperature-low pressure condition. The hypothetical P-T trajectory of ZOM suggests two clock wise metamorphic path (Fig. 7.1). One path is following high pressure blueschist to mediam grade greenschist facies via lower amphibolite condition. The alternate path may following high temperature-high pressure relict eclogite to high temperature greenschist condition via high temperature epidote-

amphibolite condition with excess of CO_2 condition in consequence of amphibolite grade metamorphism of TMC. The metamorphic evolution of ZOM starts soon after the mélange formation 'block-in-matrix' fabric, indicate initial subduction-burial of the blocks and subsequent exhumation and exposes blueschist- epidote (amphibolite) and greenschist metamorphic rocks, at the last stage exhumation of mélange rocks following normal geothermal gradient at 10-15°C /km.

7.1.3. BIMODAL STABLE ISOTOPE DISTRIBUTION OF MÉLANGE CARBONATES

The fluid evolution pattern is tracked through stable isotope study of ZOM carbonates. The evidences of fluid mixing and input of metamorphic fluids from TMC are well consistent with d18O isotopic values (Fig. 7.2). The oxygen isotope data show distinct values with respect to the original deposition condition and subsequent alteration. Highly depleted oxygen values from the margin of the ZOM can be explained by crustal contamination at low-temperature condition (Pa´lfy et al. 2001). The d18O values of crustal fluids are lighter than that of carbonate rocks (Veizer et al. 1999; Wallmann 2001). Isotopic signatures indicate 7-8‰ reduction of δ18O values from the interior part of the mélange to the terminal part towards Zildat fault zone which is consistent with reduction of δ13 C values. The shift of δ18O values from 24‰ to 16‰ indicate a modifications of stable isotope values from marine carbonate to a modified one due to fluid infiltration from adjacent Tso Morari Gneissic dome.
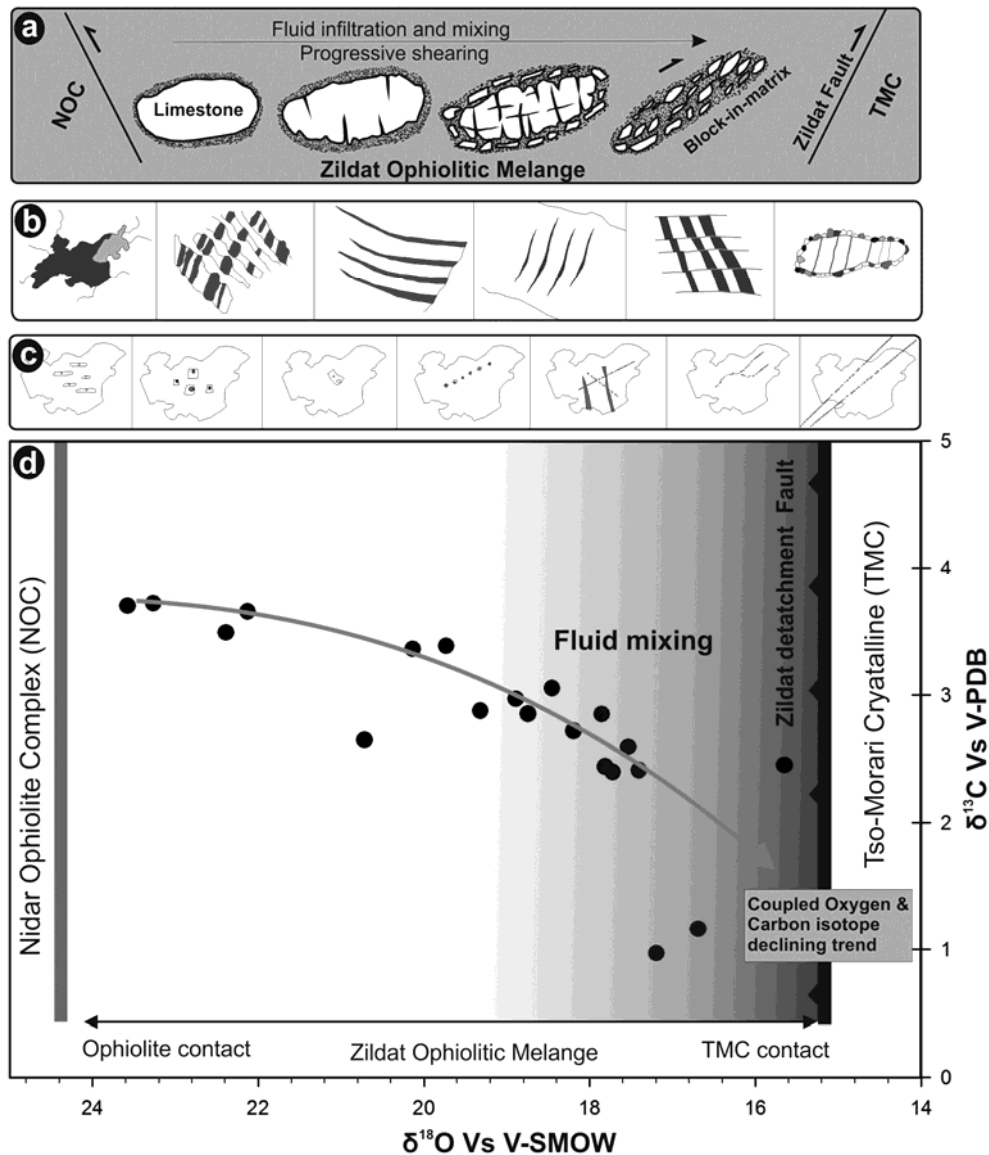
Figure 7.2: *Deformation & fluid mixing signature from the carbonates across ZOM. The range of deformation stages are derived on the basis of field distribution of exotic carbonate blocks and micro-structural observations of calcite twinning. Fluid activity is studied through fluid inclusion petrography and stable isotopic variation across the Mélange.* ***a)*** *sketch showing distribution and orientation of exotics within mélange.* ***b)*** *Schematic diagram of calcite microstructure & twining reflecting different deformation stages. All the evidences suggest a peak to post metamorphic condition from high to low temp episodes reflecting different deformation stages.* ***c)*** *Schematic diagram of fluid inclusion arrangement at different stage. H2O-Nacl fluids are showing their primary signature whereas the secondary fluids are aquous-carbonic. These secondary trails are dominated at the sheared part of the mélange.* ***d)*** *Coupled Oxygen & Carbon isotoic trend from the exotic carbonates across the ZOM, interpreted as fluid infiltration from TMC. The shaded portion represents the mixing of fluid.*

The fluid exchange between TMC and ZOM is prominent at its contact

which indicates synchronous exhumation of both the unit at the final stage.

Guillot et al. (1997) and de Sigoyer et al. (1997) characterized multiphase metamorphic events in the TMC area. The latest stage is marked by heating during decompression (Guillot et al. 1997; de Sigoyer et al. 1997). This heating process can reequilibrate high density fluids that migrate through weaker zones of adjacent mélange rocks. These volatile rich fluids were possibly re-modified during the emplacement of ZOM. Numerous quartz veins intruding the mélange metasediments display brittle-ductile deformation features. They also suggest that silica rich highly volatile fluids were generated from TMC at the expense of high temperature mineral alteration (Mukherjee & Sachan 2009). This migrated fluid mixed with the mélange carbonates that caused the depletion of stable isotope values at the marginal parts of the mélange. The fluid mixing signatures with increasing deformation trend is shown in Figure 7.2.

7.1.4. GEOCHEMICAL TRACERS OF ZOM

Regarding the formation of ZOM in tectonic point of view the previous study suggested that the ZOM rocks are remnants of Neo-Tethyan Sea mounts accreted at the northern margin of Indian continent (Sigoyer et al. 2004). The oceanic fragments along the Indus Suture Zone are interpreted in intra-oceanic or supra-subduction zone context (Hébert et al., 2000, 2001, 2003; Aitchison et al., 2000; Huot et al., 2000, 2003; Dubois-Coˆteˊ et al., 2003, Mahéo et al., 2004., Ahmed et al 2008). In addition to this, few literatures also suggest that the protolith of suture zone blueschist are of N-MORB and OIB affinity (Honegger et al 1989, Ahmed et al 1996, Maheo et al 2006). Majority of the

above information are obtained from the Sapi-Shergol mélange zone (except Ahmed et al., 1996), which is far west from the present study area. To infer the nature of protolith and tectonic setting of the metabasics rocks present within the ZOM, major and trace element geochemistry were carried out. However, some potential biases and limitations need to be taken care of before interpreting the geochemical data: (i) whether the hand specimen to be analysed truly representative of that particular litho-unit. (ii) How far have the elemental contents of the rock been changed from their pristine igneous values as a result of alteration on the seafloor and during subduction. To counter these problems, less altered uniform basaltic rocks are chosen for analysis and the geo-tectonic interpretations are made considering the HFSE and REEs. As the HFSE elements such as Ti, Zr, Nb Y, and REE remain insoluble and immobile during alteration and metamorphism (Thompson 1973; Sheraton 1984; McCulloch & Gamble 1991; Pearce et al. 2000; Zhao et al. 2007). Hence, these elements preserve their primordial characteristics to provide insight into the originality of the subducted rocks (Pearce & Norry 1979; White 2007). Based on chondrite normalised REEs and various tectonic discrimination diagrams (e.g., Pearce and Cann, 1973; Pearce and Norry, 1979; Wood et al., 1979; Wood, 1980) it can be inferred that the basic rocks of ZOM are within plate type alkaline basalts, which shows OIB affinity. This can be related to a pre-subduction volcanism that formed oceanic lithosphere during the rifting stage of Neo-Tethys. In general, protoliths of blueschist are considered to be MORB rocks (see Becker et al., 2000 for review). However, in case of ZOM, the protoliths of blueschists are OIB and not MORB.

7.1.5. STRUCTURAL EVOLUTION AND EMPLACEMENT PATTERN OF ZOM

The present study have identified at least three deformation events in the ZOM. De Sigoyer et al., 2004 suggested the latest stage of deformation of ZOM is co-genetic with the adjoining TMC unit and the ZOM rocks are thrusted over TMC along Zildat fault during this deformation event. Towards the other side of ZOM contact, it's been stated that the NOC rocks also suffered the deformation and developed NE verging backthrusts. Contrary to De Sigoyer et al. (2004), the present study suggests NOC is devoid of any deformation signature in the form of penetrative tectonic fabric, folds or backthrusts. The Zildat fault shows evidences of an early extensional shearing event followed by reverse movement, which indicates that the Zildat fault initiated as a detachment fault and later reactivated as a thrust. Calcite microstructures of exotic carbonate blocks of the ZOM also indicate a strain gradient across the ZOM, with maximum intensity of deformation localized along the Zildat fault near the contact between ZOM and TMC. Reduction of grain size of exotic carbonate blocks is observed across the mélange with increasing fluid activity that gave rise to block-in matrix texture. In the interior parts of the ZOM, away from the Zildat fault, large grain size of the calcite marbles are observed. This can be correlated with high temperatures deformation under high grade metamorphic conditions (Covey-Crump and Rutter, 1989). Moving towards the fault zone, carbonates show reduction in grain size due to dynamic recrystallization, at 300°–350°C, i.e. under lower

greenschist-facies conditions (Bestmann et al. 2000), achieved during emplacement.
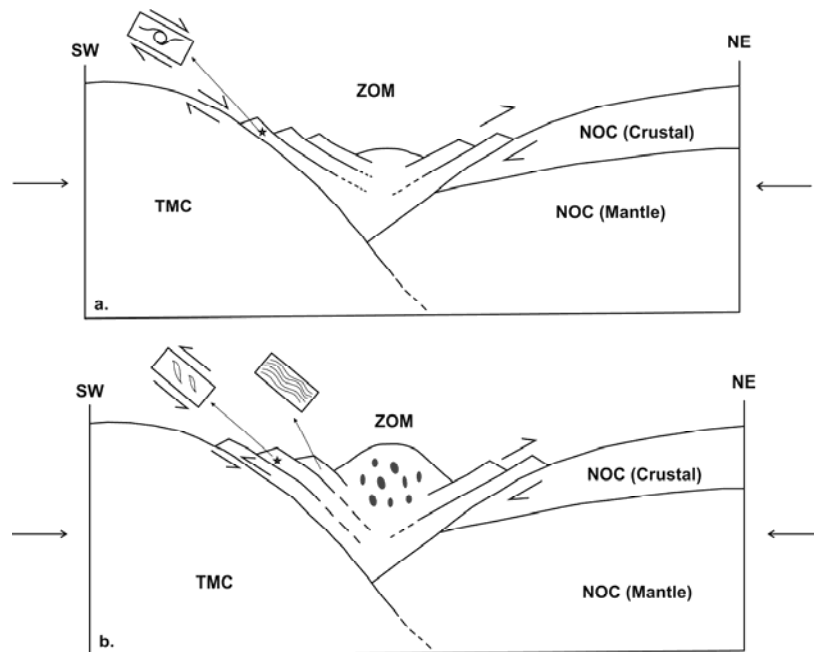
Figure 7.3: *Cartoon showing exhumation of TMC and ZOM and formation of present day configuration of ZOM, in two stages [not to scale].* ***a)*** *Continued northward propagation of the Indian plate and compression against the rigid NOC ['fixed boundary] causes late stage crustal scale exhumation of TMC with respect to ZOM. The Zildat fault activates as a normal fault [note the 'top-to-the-north' shear sense indicated by mylonitized quartz veins, TMC moves upward relative to ZOM and ZOM extends with asymmetric detachments. Due to space problem and having the rigid NOC in one side, ZOM thrusts over NOC.* ***b)*** *With continued convergence, TMC suffers gravity driven collapse after completion of exhumation. Due to this, the Zildat fault re-activates as thrust [not the 'top-to-the-south' shear sense indicated by imbrications of chert and carbonate clasts. ZOM suffers mild superposed deformation and gets bounded by two oppositely dipping thrusts and attains the present day divergent wedge shape.*

With ongoing northward convergence of the Indian continent and presence of NOC as a 'fixed boundary', both TMC and ZOM have squeezed up, as they were both comparatively less dense than NOC. This late stage exhumation of these two units at crustal scale occurred in two stages (Figure 7.3). The quartz veins present in ZOM, along the Zildat fault indicate normal

sense of movement. This indicates that initially TMC has gone relatively upwards with respect to ZOM. ZOM accommodated TMC within this fixed boundary region by forming extensional detachments and by thrusting over NOC. This event can be correlated with the 'D2' deformation suggested by de Sigoyer et al. (2004) at ~47 Ma at amphibolite facies condition. The amphibolite facies condition for this event can also be corroborated by the presence of mylonitized quartz veins giving indications of extensional shearing. In the next stage, TMC underwent 'gravitational collapse'. Due to this, materials are transported away from the elevated, thickened TMC crust by virtue of gravity sliding and the adjacent ZOM accommodated this by re-activation of extensional detachments as thrust slices. The quartz veins showing normal sense of shear got imbricated due to this compressional event and the pre-existing foliation within ZOM suffered mild superposed deformation. The chert and carbonate clasts present within the metagreywacke of ZOM, which have undergone greenschist metamorphism, also indicate this thrusting movement. As the asymmetric extensional detachments formed within ZOM during earlier amphibolite facies condition got imbricated over TMC, ZOM attained the present day bivergant wedge shape. This event relates to the 'D3' event of de Sigoyer et al. (2004) at ~30 Ma at greenschist conditions. However, contrary to de Sigoyer et al. (2004), NOC did not take any part in this deformation and rather it acted as a backstop. Therefore the crustal scale exhumation of TMC and ZOM occurred synchronously with a relative movement. NOC played a crucial role as backstop that facilitated this compression assisted upward movement.

7.1.6. FORMATIONAL AND EVOLUTIONARY STAGES OF ZILDAT

OPHIOLITIC MÉLANGE (ZOM)

The evolution of a mélange is proven to be a tough task to the earth science community around the globe mainly because of diverse lithological mixing of different masses to form an incoherent litho unit. The ZOM is typical of most mélanges associated with the Tethyan ophiolites in the Indus Suture Zone, and therefore represents a formational mechanism that involves subduction-obduction-collision tectonics. Though the ZOM is characterize by different lithologies arranged in a block-in-matrix manner with varying its clast composition and matrix contain. The individual components of this chaotic unit is tried to un-mix in a simplified manner which is described a tabular form explained in Table 7.1.

Zildat Ophiolitic Melange			
Clasts		**Matrix**	**Metasomatic Fluid**
High grade	Blueschists, Limestone-marble (pseudo-aragonite)	Glaucopphene, Epidote	Serpentine (mantle wedge), Silica rich fluid (through TMC)
Low Grade	Chert, Basalts, Gabbro, Basic, Volcaniclastics, Ultramafic (serpentine)	Graywacke, greenschist (chlorite-quartz-albite- titanite-talc-serpentine)	
Mixing & Formation of Melange	Platform sediments (limestone), Ancient sea-mounts (alkaline volcanism -OIB), Ophiolitic clasts (Bonititic magma - MORB)	Basic oceanic magma metamorphosed to blueschist-greenschists	Received fluid from mantle level (serpentine) and crustal level (silica rich) at later stage which is prominent at TMC contact.

Table 7.1: *Table showing different components of ZOM mixed together; un-mixing the clasts-matrix components of varying metamorphic grade affected by continuous fluid supply*

ZOM contain clasts of gabbro, serpentine, radiolarian chert, which have derived from the adjacent ophiolites and also clasts of blueschists. Sm-Nd whole rock dating of gabbro from NOC gives an age of ~140 Ma (Ahmed et al., 2008). Kojima et al. (2001) inferred an age of ~134 Ma to 113 Ma for the radiolarian cherts of the NOC. Honegger et al. (1989) carried out K-Ar dating on the blueschist clasts present within the Indus Suture Zone and obtained an age of ~98 Ma for blueschist metamorphism. Based on these available dates of litho-units which contributed to form clasts of ZOM, we can assume that the formation of this ophiolitic mélange cannot be older than ~140 Ma and probably it started later than ~98 Ma. Surprisingly ZOM is devoid of any clast from TMC or the Indian continental part, apart from siliceous veins along the Zildat fault. So, it can be envisaged that the formation of ZOM was completed before the final exhumation of TMC. The final deformational stage is coeval for ZOM and TMC, where ZOM rocks are juxtaposed over TMC along Zildat fault (Ravikant., 2003). Based on these, a formational and evolutionary model of ZOM is drawn in a tectonic framework which shows different tectonic stages right from the initial condition to final phase deformation of ZOM (Fig. 7.4).

a. Oceanic subduction and proto- ZOM condition, showing subduction of oceanic lithosphere along with platform carbonates and ancient seamounts which are metamorphosed to the blueschist-facies condition.

b. Formational stage of ZOM, involve accretion of material derived from NOC, off scrapped subducted oceanic lithospheric fragments and blueschist clasts.

c. TMC exhumation and development of ZOM, indicate exhumational stage of TMC releases high temperature fluid due to decompressional melting which infiltrated to ZOM.

d. Final stage deformation and exhumation of TMC and ZOM along Zildat fault. In this final deformation stage ZOM rocks are thrusted over TMC along Zildat fault zone.
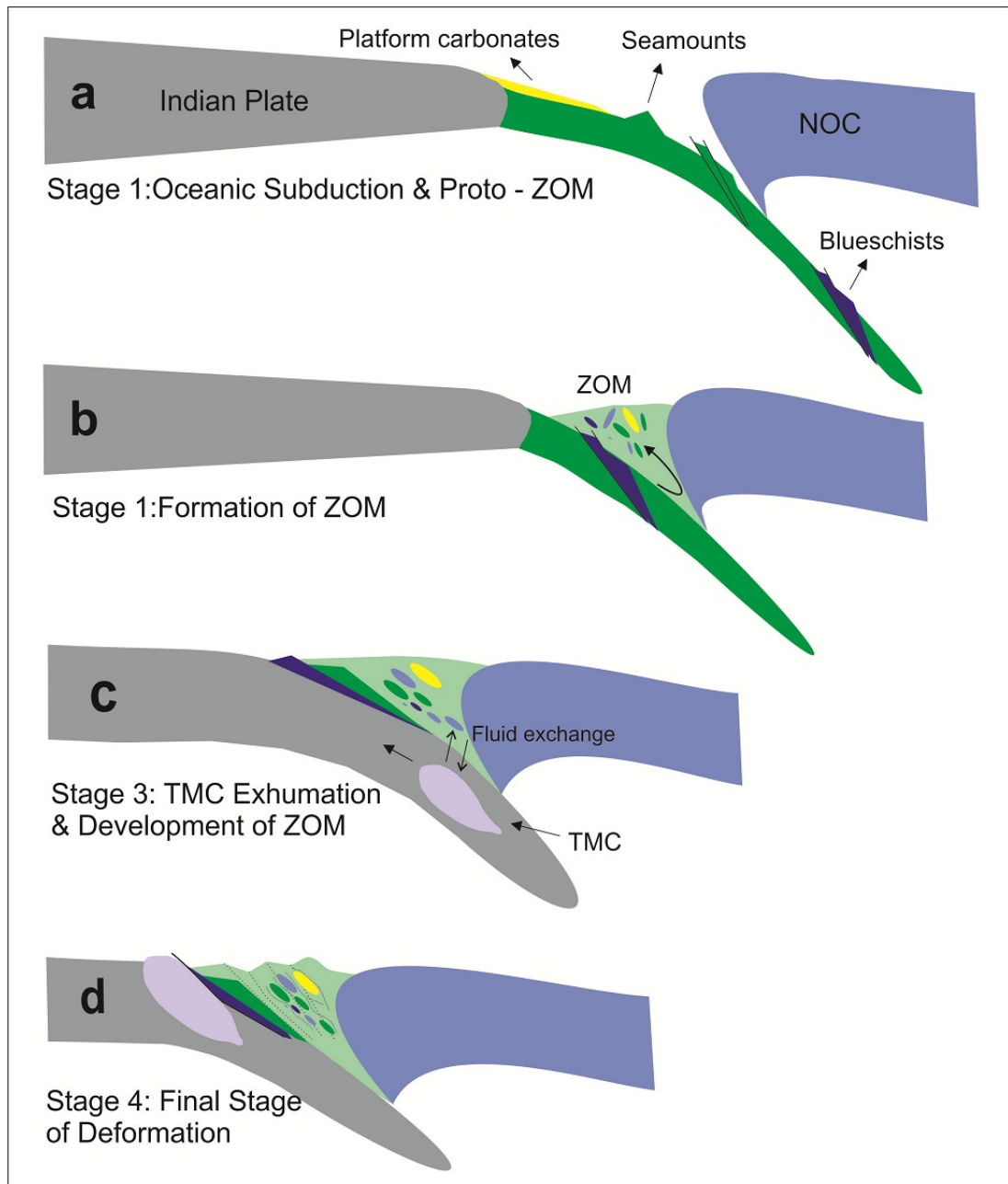
Figure 7.4: *Schematic model showing evolution of the Zildat Ophiolitic Melange*

7.2.   MAJOR OUTCOME AND CONCLUDING REMARKS

On the basis of the present study, following conclusions can be drawn:

➢ The Zildat Ophiolitic Mélange (ZOM) spread over ~ 4-5 km stretch is a mixture of multilayer thin slices of various lithounits.

➢ ZOM is characterised by block-in-matrix texture. The nature of ZOM is characterised as tectonic mélange.

➢ The ZOM is bounded by two oppositely dipping thrusts in between NOC and TMC. In south-eastern extend ZOM pinched out completely where NOC rocks are found in direct contact with TMC.

➢ Zildat fault is considered to be one of the important features of the study area, which lies in between TMC and ZOM. The fault initiated as a normal fault and later reactivated as a thrust due to continuous convergence.

➢ A progressive shearing intensity is present across ZOM moving from north to south margin.

➢ Calcite microstructures of exotic carbonate suggests a strain gradient across the ZOM. The intensity of deformation increases nearer to Zildat fault at the TMC contact.

➢ The coloured multi-layered ZOM is divided into five major subunits; volcaniclastic, sheared basic, talc-serpentine rich phyllite, brecciated meta-greywacke and polygenic conglomerate.

➢ In ZOM, three major metamorphic events are recorded which is characterised- high to low pressure metamorphism.

➢ A clockwise P-T evolution path is drawn from high pressure blueschist to mediam grade greenschist facies condition via epidote-amphibolite to lower amphibolite condition.

➢ Signature of relict eclogite facies metamorphism is thoroughly overprinted by blueschist and amphibolite facies metamorphism.

➢ The metamorphism of individual lithounits and exotic blocks of ZOM cannot be correlated with the overall metamorphism of mélange. The ZOM rock show poly-metamorphic histories.

➢ Bimodal stable isotopic distribution of mélange carbonate demarcate depositional condition of platform carbonate to post depositional fluid induced alteration.

➢ Heavy fluid flux is noticed at the last stage of ZOM evolution. The fluid supplied from the TMC was introduced in the mélange at lower amphibolite facies condition.

➢ Tectonic discrimination plots suggests the basic rocks present at the terminal part of ZOM are alkaline in nature.

➢ Chondrite normalised REEs pattern indicating OIB affinity of alkaline basalt in ZOM.

➢ The NOC played an important role for the exhumation of mélange at the shallow subsurface level. NOC also acted as a fixed boundary rigid back-stop. This helped exhuming the mélange and associated TMC.

➢ The ZOM and TMC are synchronously deformed at final stage of emplacement along the Zildat fault.

7.3. SCOPE OF FUTURE WORK

The present study has extended the understanding of evolutionary aspect of ophiolitic mélange formation in subduction-collision orogeny. It creates new avenues to understand the formation of mélange in convergent set-up. Though, no study is complete in itself and the present one is no exception. There are certain aspects of the Zildat Ophiolitic Mélange and its adjacent rocks, which if investigated, can provide even more details about complete geometry of suture zone mélange.

Further to the present study, each and individual sub-units of the ZOM needed to study even at mineral scale to understand the entire metamorphic history. In-situ geochemistry and geochronology for each subunit is very much recommended. The fluid infiltration inferences form the present study can be more precisely constrained by fluid rare earth element analyses. The presence of abundant pyroxene (titanaugite) in alkaline rocks of ZOM need advance mineralogical and geochemical study to understand early volcanism source prior to mélange formation.

References

Aalto, K.R., (1982). The Franciscan complex of northernmost California: Sedimentation and tectonics. In: Leggett, J.K. (Ed.), Trench-forearc geology: Sedimentation and tectonics on modern and ancient active plate margins: Geol., Soc. London, Spec. Publ., 10, pp. 439–457.

Ahmad, T., Islam, R., Khanna, P., Thakur, V.C., (1996) Geochemistry, petrogenesis and tectonic significance of the basic volcanic units of the Zildat ophiolite me´lange, Indus suture zone, eastern Ladakh (India). Geodinamica Acta 9, 222–233.

Ahmad, T., Tanaka, T., Sachan, H.K., Asahara,Y., Islam, R. Khanna., P.P. (2008) Geochemical and isotopic constraints on the age and origin of the Nidar Ophiolitic Complex, Ladakh, India: implications for the Neotethyan subduction along the Indus Suture Zone. Tectonophysics, 451, pp. 206–224

Aitchison, J.C., Badengzhu, Davis, A.M., Liu, J., Luo, H., Malpas, J., McDermid, I., Wu, H., Ziabrev, S., Zhou, M.F., (2000) Remnants of a Cretaceous intra-oceanic subduction system within the Yarlung-Zangbo suture (southern Tibet). Earth and Planetary Science Letters 183, 231–244.

Alonso, J.L., Gallastegui, J., García-Sansegundo, J., Farias, P., Rodrìguez Fernández, L.R., Ramos, V.A., (2008) Extensional tectonics and gravitational collapse in an Ordovician passive margin: the Western Argentine Precordillera. Gondwana Research 13, 204–215.

Altunkaynak, S., Dilek, Y., (2006) Timing and nature of post-collisional volcanism in western Anatolia (Turkey) and geodynamic implications. Geological Society of America Special Paper 409, 321–351.

Anczkiewicz, R., Burg, J.P., Villa, I.M., and Meier, M., (2000) Late Cretaceous blueschist metamorphism in the Indus Suture Zone, Shangla region, Pakistan Himalaya: Tectonophysics, v. 324, pp. 111–134

Argand, E (1924) La tectonique del Asie. C.R.B. Cong. Int. 169. 123-167.

Arita, K., (1983) Origin of the inverted metamorphism of the Lower Himalayas Central Nepal. Tectonophysics 95, 43– 60.

Arita, K., Dallmeyer, R.D., Takasu, A., (1997) Tectonothermal evolution of the Lesser Himalaya, Nepal: constraints from Ar/Ar ages from the Kathmandu Nappe. The Island Arc 6, 372– 385.

Baud, A., Gaetani, M., Garzanti, E., Fois, E., Nicora, A., Tintori, A., (1984) Geological observations in southeastern Zanskar and adjacent Lahul area (northwestern Himalaya). Eclogae Geologicae Helvetiae 77, 171–197.

Baumgartner LP, Valley JW (2001) Stable isotope transport and contact metamorphic fluid flow. In: Valley JW, Cole D (ed) Stable isotope geochemistry, Min Soc Am. Rev Mineral Geochem 43:415–467

References

Baxter, A.T., Aitchison, J.C., Ali, J.R., Zyabrev, S.V., (2010) Early Cretaceous radiolarians from the Spongtang massif, Ladakh, NW India: implications for Neo-Tethyan evolution. Journal of the Geological Society of London 167, 511–517.

Beaumont, C., (1981) Foreland basins. Geophysical Journal of the Royal Astronomical Society, 65, 291–329.

Bebout GE, Barton MD (1989) Fluid flow and metasomatism in a subduction-zone hydrothermal system: Catalina Schist terrane, California. Geology 17:976–980.

Bebout GE, Barton MD (1993) Metasomatism during subduction: Products and possible paths in the Catalina Schist, California. Chem Geol 108:61–92

Bebout GE, Barton MD (2002) Tectonic and metasomatic mixing in a high-T, subduction-zone mélange—insights into the geochemical evolution of the slab–mantle interface. Chem Geol 187:79–106

Becker, H., (2000) Re–Os fractionation in eclogites and blueschists and the implications for recycling of oceanic crust into the mantle. Earth and Planetary Science Letters 177, 287–300.

Bestmann M, Kunze K, Matthews A (2000) Evolution of a calcite marble shear zone complex on Thassos Island, Greece; microstructural and textural fabrics and their kinematic significance. J Struct Geol 22(11-12):1789-1807.

Blanco-Quintero, I.F., García-Casco, A., Rojas-Agramonte, Y., Rodríguez-Vega, A., Lázaro, C., and Iturralde-Vinent, M.A., (2010a) Metamorphic evolution of subducted hot oceanic crust (La Corea mélange, Cuba): American Journal of Science, doi: 10.2475/11.2010.01

Blanco-Quintero, I.F., Proenza, J.A., García-Casco, A., Tauler, E., and Galí, S., (2010b) Serpentinites and serpentinites within a fossil subduction channel: La Corea mélange, eastern Cuba: Geologica Acta

Blanco-Quintero, I.F., García-Casco, A., Gerya, T.V., (2011) Tectonic blocks in serpentinite mélange (eastern Cuba) reveal large-scale convective flow of the subduction channel. Geology, 39 (2010), pp. 79–82

Brookfield, M.E., Reynolds, P.H. (1981) Late Cretaceous emplacement of the Indus suture zone ophiolitic mélanges and an Eocene-Oligocene magmatic arc on the northern edge of the Indian plate. Earth Planet. Sci. Lett., 55, pp. 157–162.

Brookfield, M.E., (1993) The Himalayan passive margin from Precambrian to Cretaceous. Sedimentary Geology 84, 1–35.

Brookfield, M.E., (1998) The evolution of the great river systems of southern Asia during the Cenozoic India–Asia collision: rivers draining southwards. Geomorphology 22, 285–312.

References

Burkhard, M. (1993). Calcite twins, their geometry, appearance and significance as stress–strain markers and indicators of tectonic regime: a review. J Struct Geol 15:351–368.

Burg, J.P., Chen, G.M. (1984). Tectonics and structural zonation of southern Tibet, China. Nature 311:219–223.

Cannat, M., Mascle, G., (1990). Réunion extraordinaire de la Société géologique de France en Himalaya du Ladakh. Bulletin de la Société Géologique de France 4, 553–582.

Cartwright I., Vry J., Sandiford, M. (1995). Changes in stable isotope ratios of metapelites and marbles during regional metamorphism , Mount Lofty Ranges , South Australia : implications for crustal scale fluid flow. Contrib Mineral Petrol 120:292-310.

Chang, C., (1984) Les caracte´ristiques tectoniques et l'e´volution de la zone de suture du Yarlung-Zangbo. In: Mercier, J.L., Li, G.C. (Eds.), Mission franco-chinoise au Tibet 1980: E ´ tude ge´ologique et ge´ophysique de la crouˆte terrestre et du manteau supe´rieur du Tibet et de l'Himalaya. E´ditions du Centre National de la Recherche Scientifique, Paris, pp. 341–350.

Chang, C.P., Angelier, J., Huang, C.Y. (2000) Origin and evolution of a melange: the active plate boundary and suture zone of the Longitudinal Valley, Taiwan. Tectonophysics, 325, 43-62.

Clark, M.K., Schoenbohm, L.M., Royden, L.H., Whipple, K.X., Burchfiel, B.C., Zhang, X., Tang, W., Wang, E., Chen, L., (2004) Surface uplift, tectonics, and erosion of eastern Tibet from largescale drainage patterns. Tectonics 23, TC1006.

Cloos M (1982) Flow melanges: Numerical modelling and geologic constraints on their origin in the Franciscan subduction complex. Geol Soc Am Bull 93:330- 345.

Codegone, G., Festa, A., Dilek, Y., Pini, G.A. (2012). Small-scale polygenic mélanges in the formation of the ancient Ligurian accretionary wedge (Northern Apennines, Italy) In: Dilek Y, Festa A, Ogawa Y, Pini GA (eds) Chaos and Geodynamics: Mélanges, Mélange forming processes and their significance in the geological record. Tectonophysics, vol 568–569, pp 170–184.

Colchen M, Mascle G, Delaygue G (1994) Lithostratigraphy and age of the formations in the Tso Morari dome (abstract). J Nepal Geol Soc 10:23

Corfield R, Searle M, Owen G (1999) The Photang Thrust Sheet: a subduction - accretion complex beneath the Spontang ophiolite, Ladakh Himalaya. J Geol Soc 156:1031-1044

Courtillot, V., (1999) Evolutionary Catastrophes: The Science of Mass Extinction. Cambridge University Press, Cambridge, 173 pp.

References

Covey-Crump S.J., Rutter, E.H. (1989). Thermally-induced grain growth of calcite marbles on Naxos Island Greece. Contrib Miner Petrol. 101(1):69–86.

Cowan, D.S., (1982). Deformation of partly dewatered and consolidated Franciscan sediments near Piedras Blancas Point, California. In: Leggett, J.K. (Ed.), Trenchforearc geology: Sedimentation and tectonics on modern and ancient active plate margins: Geol. Soc. London, Spec. Publ., 10, pp. 419–432.

Cowan, D.S., 1985, Structural styles in Mesozoic and Cenozoic mélanges in the western Cordillera of North America: Geological Society of America Bullettin, v. 96, p. 451–462.

Critelli, S., Garzanti, E., (1994) Provenance of the lower Tertiary Murree redbeds (Hazara–Kashmir syntaxis, Pakistan) and the initial rising of the Himalayas. Sedimentary Geology 89, 265–284.

Danelian T. and Robertson, A. H. F. (1997). Radiolarian evidence of the stratigraphy and palaeo-oceanography of the deep-water passive margin of the Indian plate (Karamba Formation, IndusSuture Zone, Ladakh Himalaya). Marine Micropaleontology 30, 171-195.

Dewey, J.F., Bird, J.M., (1970) Mountain belts and the new global tectonics. Journal of Geophysical Research 75, 2625–2647.

Dewey, J.F. & Burke, C.A., (1973) Tibetan, Variscan, and Precambrian basement reactivation: products of continental collision. Jour. Geology 81, 683-692.

Dewey, J.F., Cande, S., Pitman, W.C., (1989) Tectonic evolution of the India–Eurasia collision zone. Eclogae Geologicae Helvetiae 82, 717–734.

Desio, A., (1977) The occurrence of blueschists between the middle Indus and the Swat Valleys as an evidence of subduction (North Pakistan). Academia Nazionale dei Lincei 8 (219), 1–9.

De`zes, P.J., Vannay, J.C., Steck, A., Bussy, F., Cosca, M., (1999) Synorogenic extension: quantitative constraints on the age and displacement of the Zanskar shear zone (northwest Himalaya). Geological Society of American Bulletin 111, 364– 374.

de Sigoyer J, Guillot S, Lardeaux JM, Mascle G (1997) Glaucophane-bearing eclogites in the Tso Morari dome (eastern Ladakh, NW Himalaya). Eur J Mineral 9:1073-1083

De Sigoyer, J., Chavagnac, V., Blichert-Toft, J., Villa, I.M., Guillot, S., Luais, B., Cosca, M., Mascle, G., (2000) Dating of the Indian continental subduction and collisional thicken ing in the northwest Himalaya: Multichronology of the Tso Morari eclogites. Geology 28, 487–490.

de Sigoyer J, Gulliot S, Dick P (2004) Exhumation of ultrahigh-pressure Tso Morari unit in eastern Ladakh (NW Himalaya): a case study. Tectonics 23:TC3003. doi:10.1029/2002TC001492

References

Dilek, Y., Thy, P., Hacker, B., and Grundvig, S., (1999) Structure and petrology of Tauride ophiolites and mafic dike intrusions (Turkey): Implications for the Neo-Tethyan ocean: Geological Society of America Bulletin, v. 111, no. 8, p. 1192–1216.

Dilek, Y., Robinson, P.T., (2003) Ophiolites in Earth history. In, Geological Society of London Special Publication 218, 1–8. http://dx.doi.org/10.1144/GSL.SP.2003.218.01.01.

Dilek, Y., Shallo, M., and Furnes, H., (2005) Rift-drift, seafloor spreading, and subduction zone tectonics of Albanian ophiolites: International Geology Review, v. 47, p. 147–176. DOI: 10.2747/0020-6814.47.2.147.

Dilek, Y., (2006) Collision tectonics of the Eastern Mediterranean region: causes and consequences. Geological Society of America Special Paper 409, 1–13.

Dilek, Y., Furnes, H., and Shallo, M., (2007) Suprasubduction zone ophiolite formation along the periphery of Mesozoic Gondwana: Gondwana Research, v. 11, p. 453–475.

Dilek, Y., Furnes, H., (2009) Structure and geochemistry of Tethyan ophiolites and their petrogenesis in subduction rollback systems. Lithos 113, 1–20.

Dilek, Y., Furnes, H., (2011) Ophiolite genesis and global tectonics: geochemical and tectonic fingerprinting of ancient oceanic lithosphere. The Geological Society of America Bulletin 123, 387–411.

Ding, L., Zhong, D.L., Yin, A., Kapp, P., Harrison, T.M., (2001) Cenozoic structural and metamorphic evolution of the eastern Himalayan syntaxis (Namche Barwa). Earth and Planetary Science Letters 192, 423–438.

Di Pietro, J.A., Pogue, K.R., (2004) Tectonostratigraphic subdivisions of the Himalaya: a view from the west. Tectonics 23, TC5001.

Donaldson, D.G., Webb, A.A.G., Menold, C.A., Kylander-Clark, A.R.C., Hacker, B.R. (2013) Petrochronology of Himalayan ultrahigh-pressure eclogite. Geology, 41, pp. 835–838

Ernst, W.G., (1970). Tectonic contact between the Franciscan melange and Great Valley sequence, crustal expression of a Late Mesozoic Benioff zone. Journal of Geophysical Research 75, 886–902.

Epard, J.L., Steck, A., (2008). Structural development of the Tso Morari ultra-high pressure nappe of the Ladakh Himalaya. Tectonophysics, 451, 242–264

Federico, L., Crispini, L., Scambelluri, M., Capponi, G. (2007). Ophiolite mélange zone records exhumation in a fossil subduction channel. Geology 35:499-502

Festa, A., (2010) Tectonic, sedimentary, and diapiric formation of the Messinian melange: Tertiary Piedmont Basin (northwestern Italy), *in* Wakabayashi, J., and

References

Dilek, Y., eds., Melanges: Processes of formation and societal significance: Geological Society of America Special Paper, 480, 215–232.

Festa, A., Pini, G.A., Dilek, Y., Codegone, G., (2010) Mélanges and mélange-forming processes: a historical overview and new concepts. International Geology Review 52 (10–12), 1040–1105.

Flower, M.F.J., Dilek, Y., (2003) Arc-trench rollback and forearc accretion: 1. A collisioninduced mantle flow model for Tethyan ophiolites. Ophiolites in Earth History: Geological Society of London Special Publication, 218, pp. 21–42.

Frank, W.; Gansser, A.; Trommsdorff, V. (1977). "Geological observations in the Ladakh area (Himalayas); a preliminary report". Schweizerische Mineralogische und Petrographische Mitteilungen Bulletin 57 (1): 89–113.

Furnes, H., Dilek, Y., Pedersen, R.B., (2012) Structure, geochemistry, and tectonic evolution of trench-distal backarc oceanic crust in the western Norwegian Caledonides, Solund-Stavfjord ophiolite (Norway). Geological Society of America Bulletin 124, 1027–1047.

Gaetani, M., Garzanti, E., (1991) Multicyclic history of the northern India continental margin (northwestern Himalaya). American Association of Petroleum of Geologists Bulletin 75, 1427– 1446.

Gansser, A. (1964). The Geology of the Himalayas. Wiley Interscience, New York, pp 289

Gansser A (1974) The Ophiolitic Melange, a world-wide problem on Tethyan examples. Eclog Geol Helv 67(3):479-507

Gansser, A. (1977). The great suture zone between the Himalaya and Tibet - a preliminary account. Collo Int. CNRS Paris No.261. Ecologie et Geologie de L'Himalaya. 181-191.

Gao J, Klemd R (2001) Primary fluids entrapped at blueschist to eclogite transition: evidence from the Tianshan meta-subduction complex in northwest China. Contrib Mineral Petrol 142:1-14.

García-Casco, A., Torres-Roldán, R.L., Iturralde-Vinent, M.A., Millán, G., Núñez Cambra, K., Lázaro, C., and Rodríguez Vega, A., (2006) High pressure metamorphism of ophiolites in Cuba: Geologica Acta, v. 4, p. 63–88.

García-Casco, A., Lázaro, C., Torres-Roldán, R.L., Núñez Cambra, K., Rojas Agramonte, Y., Kröner, A., Neubauer, F., Millán, G., and Blanco-Quintero, I., (2008b) Partial melting and counterclockwise P-T path of subducted oceanic crust (Sierra del Convento mélange, Cuba): Journal of Petrology, v. 49, p. 129–161

Garzanti, E., Casnedi, R., Jadoul, F., (1986) Sedimentary evidence of a Cambro-Ordovician orogenic event in the northwestern Himalaya. Sedimentary Geology 48, 237– 265.

Garzanti, E., Baud, A., Mascle, G., (1987) Sedimentary record of the northward flight of India and its collision with Eurasia (Ladakh Himalaya India). Geodynamica Acta 1, 297– 312.

Garzanti, E., (1993) Sedimentary evolution and drowning of a passive margin shelf (Giumal Group; Zanskar Tethys Himalaya, India): palaeoenvironmental changes during final break-up of the Gondwanaland. In: Treloar, P.J., Searle, P.M. (Eds.), Himalayan Tectonics. The Geological Society Special Publication, vol. 74, pp. 277– 298.

Garzanti, E., (1999) Stratigraphy and sedimentary history of the Nepal Tethys Himalaya passive margin. Journal of Asian Earth Sciences 17, 805–827.

Gerya, T.V., Stöckhert, B., Perchuk, A.L., (2002) Exhumation of high-pressure metamorphic rocks in a subduction channel: a numerical simulation. Tectonics 21, 1056.

Gorman PJ, Kerrick DM, Connolly JAD (2006) Modeling open system metamorphic decarbonation of subducting slabs. Geochem Geophys Geosyst. doi: 10.1029/2005GC001125

Grujic, D., Hollister, L.S., Parrish, R.R., (2002) Himalayan metamorphic sequence as an orogenic channel: insight from Bhutan. Earth and Planetary Science Letters 198, 177–191.

Guiraud, M., (1982) Géothermobarométrie du faciès schiste vert à glaucophane. Modelisation et applications (Afghanistan, Pakistan, Corse, Bohème): Ph.D. thesis, Montpellier University.

Guillot, S., Peˆcher, A., Rochette, P., LeFort, P., (1993) The emplacement of the Manaslu granite of Central Nepal: field and magnetic susceptibity constraints. In: Treloar, P.J., Searle, P.M. (Eds.), Himalayan Tectonics. The Geological Society Special Publication, vol. 74, pp. 413–428.

Guillot, S., LeFort, P., Peˆcher, A., Barman, M.R., Aprahmaian, J., (1995) Contact-metamorphism and depth of emplacement of the Manaslu granite (Central Nepal)— implications for Himalayan orogenesis. Tectonophysics 241, 99– 119.

Guillot S, de Sigoyer J, Lardeaux JM, Mascle G (1997) Eclogitic metasediments from the Tso Morari area (Ladakh, Himalaya): evidence for continental subduction during India-Asia convergence. Contrib Mineral Petrol 128:197-212.

Guillot S, Hattori K, de Sigoyer J (2000) Mantle wedge serpentinization and exhumation of eclogites: insights from eastern Ladakh, northwest Himalaya. Geology 28:199–202

Halama R, John T, Herms P, Hauff F, Schenk V (2011) A stable (Li, O) and radiogenic (Sr, Nd) isotope perspective on metasomatic processes in a subducting slab. Chem Geol 281:151-166

Hall, R. (1976). Ophiolite emplacement and the evolution of the Taurus suture zone, southeastern Turkey. Geol Soc Am Bull 87:1078–1088.

Hall, R. (1980). Unmixing a Mélange: the petrology and history of a disrupted and metamorphosed ophiolite, southeastern Turkey. J Geol Soc 137:195-206

Hallam, A., (2005). Catastrophes and Lesser Calamities. Oxford University Press, Oxford, 240 pp.

Hallet, B., Molnar, P., (2001). Distorted drainage basins as markers of crustal strain east of the Himalaya. Journal of Geophysical Research 106, 13697–13709.

Hamilton, W., (1969) Tectonics of the Indonesian region: United States Geological Survey Professional Paper, v. 1078, 345 p.

Hara, H., Kimura, K., (2008) Metamorphic and cooling history of the Shimanto accretionary complex, Kyushu, Southwest Japan: implications for the timing of out-of-sequence thrusting. Island Arc 17, 546–559.

Harris, R.A., Sawyer, R.K., Audley-Charles, M.G., (1998) Collisional mélange development: geologic association of active mélange-forming processes with exhumed mélange facies in the western Banda orogen, Indonesia. Tectonics 17 (3), 458–479.

Hawkins, J.W., Melchior, J.T., (1985) Petrology of Mariana Trough and Lau Basin basalts. J. Geophys. Res. 90, 11431– 11468.

Hawkins, J.W., Allan, J.F., (1994) Petrologic evolution of Lau Basin sites 834 through 839. In: Hawkins, J.W., Parson, L.M., Allan, J.F., et al. (Eds.), Proc. Ocean Drill. Prog., Sci. Results, vol. 135, pp. 427–470. College Station, TX.

Hébert, R., Varfalvy, V., Huot, F., Wang, C.S., Liu, Z.F., (2000) Yarlung Zangbo ophiolites, southern Tibet revisited. 15th Himalaya-Karakorum-Tibet workshop. Earth Sci. Front. 7, 124– 126.

Hébert, R., Wang, C.S., Varfalvy, V., Huot, F., Beaudoin, G., Dostal, J., (2001) Yarlung Zangbo Suture Ophiolites and their suprasubduction zone setting. 16th Himalaya-Karakorum-Tibet workshop. J. Asian Earth Sci. 19, 27– 28.

Hébert, R., Huot, F., Wang, C.S., Liu, Z.F., (2003) Yarlung Zangbo ophiolites, southern Tibet revisited: geodynamic implications from the mineral record. In: Dilek, Y. (Ed.), Ophiolites in Earth History, Spec. Publ.-Geol. Soc. Lond. 218, pp. 165– 190.

Hermann, J., Muuntener, O., Scambelluri, M., (2000). The importance of serpentinite mylonites for subduction and exhumation of oceanic crust. Tectonophysics 327, 225– 238.

Hitz, B., Wakabayashi, J., (2012). Unmetamorphosed sedimentary mélange with high-pressure metamorphic blocks in a nascent forearc basin setting. Tectonophysics, 568–569, pp. 124–134

Hodges, K.V., (2000) Tectonics of the Himalaya and southern Tibet from two perspectives. Geological Society of America Bulletin 112, 324-350.

Hoefs, J. (1980). Stable isotope geochemistry. Springer.

Honegger, K., Dietrich, V., Frank, W., Gansser, A., Thoni, M. & Trommsdorff, V., (1982). Magmatism and metamorphism in the Ladakh Himalayas (the Indus-Tsangpo suture zone). Earth and Planetary Science Letters, 60, 253–292.

Honegger, K., Le Fort, P., Mascle, G., and Zimmermann, J-L., (1989). The blueschists along the Indus Suture Zone in Ladakh, NW Himalaya: Journal of Metamorphic Geology, v. 7, pp. 57-72.

Horton Jr., J.W., Rast, N. (Eds.), (1989). Mélanges and olistostromes of the Appalachians: Geological Society of America Special Papers, 228, p. 276.

Hough, M.L., Shields, G.A., Evins, L.Z., Strauss, H., Henderson, R.A., Mackenzie, S. (2006). A major sulphur isotope event at c 510 Ma: a possible anoxia-extinction. Volcanism connection during the Early-Middle Cambrian transition? Terra Nova, 18, pp. 257–263.

Hsü KJ (1968) Principles of melanges and their bearing on the Franciscan-Knoxville paradox. Geol Soc Am Bull 79:1063-1074

Hubbard, M.S., (1989) Thermobarometric constraints on the thermal history of the Main Central thrust zone and Tibetan slab, eastern Himalaya. Journal of Metamorphic Geology 7, 19– 30.

Jacobi, R.D., (1984). Modern submarine slides and their implications for mélange and the Dunnage Formation in north-centralNewfoundland. In: Raymond, L.A. (Ed.),Mélanges: their nature, origin, and significance: Geol. Soc. Am. Spec. Pap., 198, pp. 81–102.

Jan, M.Q., (1987) Phase chemistry of blueschists from eastern Ladakh, Himalaya. Neues Jahrbuch fuer Geologie und Palaeontologie 10, 613–635.

Jefferson, T. H. (1982). The preservation of fossil leaves in Cretaceous volcaniclastic rocks from Alexander Island, Antarctica. Geological magazine, 119, 291-300.

Kazmi, A. H., Lawrence, R. D., Dawood, H., Snee, L. W. and Hussain, S. S. (1984) Geology of the Indus suture zone in the Mingora-Shangla area of Swat. Geol. Bull. Univ. Peshawar 17, 127–144.

Kerrick, D.M., Connolly, J.A.D. (2001). Metamorphic devolatilization of subducted marine sediments and the transport of volatiles into the Earth's mantle. Nature 411:293-296.

Kessel, R., Schmidt, M., Ulmer, P., Pettke, T. (2005). Trace element signature of subduction-zone fluids, melts and supercritical liquids at 120–180 km depth. Nature 437:724–727.

King, R.L., Kohn, M.J., Eiler, J.M. (2003). Constraints on the petrologic structure of the subduction zone slab–mantle interface from Franciscan Complex exotic ultramafic blocks. Geol Soc Am Bull 115:1097–1109.

Kojima, S., Ahmad, T., Tanaka, T., Bagati, T.N., Mishra, M., Kumar, R., Islam, R., Khanna, P., (2001) Early Cretaceous radiolarians from the Indus suture zone, Ladakh, northern India. News of Osaka Micropaleontologists 12, 257–270.

Krieger, M.H., (1977). Large landslides, composed of megabreccia, interbedded in miocne basin deposits, southeastern Arizona. U.S. Geological Survey Professional Paper 1008 25p.

Lázaro, C., García-Casco, A., Neubaurer, F., Rojas-Agramonte, Y., Kröner, A., and Iturralde-Vinent, M.A., (2009) Fifty-fi ve-million-year history of oceanic subduction and exhumation at the northern edge of the Caribbean plate (Sierra del Convento mélange, Cuba): Journal of Metamorphic Geology, v. 27, p. 19–40

Le Bas, M.J., Lemaitre, R.W., Streckeisen, A. and Zanettin, B. (1986). A Chemical Classification of Volcanic-Rocks Based on the Total Alkali Silica Diagram. Journal of Petrology 27(3): 745-750.

LeFort, P., (1975) Himalayas—collided range—present knowledge of continental arc. American Journal of Science A275, 1 –44.

Lefort, P., (1996) Evolution of the Himalaya. In: Yin, A., Harrison, T.M. (Eds.), The Tectonics of Asia. Cambridge University Press, New York, pp. 95– 106.

Le Pichon, X., Fournier,, Jolivet, L., (1992) Kinematics, topography, shortening, and extrusion in the India–Eurasia collision. Tectonics. 11, 1085– 1098.

Li, G.B., Wan, X.Q., Liu, W.C., Bucher, H., Li, H.S., Goudemand, N. (2009). A new Cretaceous age for the Saiqu "mélange", southern Tibet, evidence from Radiolaria. Cretaceous Res., 30, 35–40

Liu, G., Einsele, G. (1994). Sedimentary history of the Tethyan basin in the Tibetan Himalayas. Geologische Rundschau 82, 32– 61.

Liu, G., Einsele, G. (1999). Jurassic sedimentary facies and paleogeography of the former Indian passive margin in southern Tibet. In: Macfarlane, A., Sorkhabi, R.B., Quade, J. (Eds.), Himalaya and Tibet: Mountain Roots to Mountain Tops. Geological Society of America Special Papers, vol. 328, pp. 75–108.

Lyon-Caen, H., Molnar, P. (1985). Gravity anomalies, flexure of the Indian plate, and the structure, support and evolution of the Himalaya and the Ganga Basin. Tectonics 4, 513– 538.

Mahéo, G., Bertrand, H., Guillot, S., Mascle, G., Pêcher, A., Picard, C., De Sigoyer, J. (2000). Témoin d'un arc immature téthysien dans les ophiolites du Sud Ladakh (NW Himalaya, Inde). Earth and Planetary Science Letters 330, 289–295.

Mahéo, G., Bertrand, H., Guillot, S., Villa, I.M., Keller, F., and Capiez, P. (2004). The south Ladakh ophiolites (NW Himalaya, India): An intra-oceanic tholeiitic origin with implication for the closure of the Neo-Tethys: Chemical Geology, v. 203, p. 273–303.

Mahéo G, Fayoux X, Guillot S, Garzanti E, Capiez P, Mascle G (2006) Relicts of an intra-oceanic arc in the Sapi-Shergol mélange zone (Ladakh, NW Himalaya, India): implications for the closure of the Neo-Tethys Ocean. J Asian Earth Sci 26:695–707.

Malatesta, C., Crispini, L., Federico, L., Capponi, G., Scambelluri, M., (2012). The exhumation of high-pressure ophiolites (Voltri–Massif, Wester–Alps): insights from structural and petrologic data on metagabbro bodies. Tectonophysics, 568, pp. 102–123.

Maluski, H., and Matte, P., (1984) Ages of Alpine tectonometamorphic events in the northwestern Himalaya (Northern Pakistan) by 39Ar/40Ar: Tectonics, v. 3, pp. 1–18.

Manning, C.E. (1997). Coupled reaction and flow in subduction zones: Silica metasomatism in the mantle wedge. In: Jamtveit B, Yardley BWD (ed) Fluid flow and transport in rocks. Chapman and Hall, London, pp 139–148.

Matsuoka, A., Kobayashi, K., Takei, M., Nagahashi, Yang, Q.T., Wang, Y., et al., (2001) Early middle jurassic (Aalenian) radiolarian fauna from the Xialu chert in the Yarlung Zangbo suture zone, southern Tibet. In: Metcalfe, I., Smith, J.M.B., Morwood, M., Davidson, I. (Eds.), Faunal and Floral Migrations and Evolution in SE AsiaAustralia. Balkema, Rotterdam, pp. 105– 110.

Matsuoka, A., Yang, Q., Kobayashi, K., Takei, M., Nagahashi, T., Zeng, Q.G., et al., (2002) Jurassic-Cretaceous radiolarian biostratigraphy and sedimentary environments of the Ceno-Tethys: records from the Xialu Chert in the Yarlung- Zangbo Suture Zone, southern Tibet. J. Asian Earth Sci. 20, 277 – 287. (17th International Himalaya–Karakoram–Tibet Workshop).

McCulloch, M. T. & Gamble, J. A. (1991).Geochemical and geodynamical constraints on subduction zone magmatism. Earth and Planetary Science Letters 102, 358–74.

McKenzie, D., Sclater, J.G. (1971). The evolution of the Indian Ocean since the Late Cretaceous. Geophysical Journal International 24, 437–528.

Meigs, A.J., Burbank, D.W., Beck, R.A., (1995) Middle–late Miocene (N10 Ma) formation of the Main Boundary Thrust in the western Himalaya. Geology 23, 423–426.

Mercier, J.L., Li, T.D., et al., (1984). La collision Inde-Asie coˆte´ Tibet. In: Mercier, J.L., Li, G.C. et al. (Eds.), Mission franco-chinoise au Tibet 1980: E ´ tude ge´ologique et e´ophysique de la crouˆte terrestre et du manteau supe´rieur du Tibet et de l'Himalaya. E ´ ditions du Centre National de la Recherche Scientifique, Paris, pp. 341–350.

Meschede, M. (1986) A method of discriminating between different types of midocean ridge basalts and continental tholeiites with the Nb-Zr-Y diagram. Chemical Geology, v. 56, p. 207-218.

Molnar, P., Tapponnier, P., (1975) Cenozoic tectonics of Asia: effects of a continental collision. Science 189, 419–426.

Molnar, P., and Tapponnier, P., (1977) The collision between India and Eurasia. Scientific American 236, 30–42.

Morrison, M. A. (1978). The use of 'immobile' trace elements to distinguish the palaeotectonic affinities of metabasites: Applications to the Palaeocene basalts of Mull and Skye, northwest Scotland. Earth and Planetary Science Letters 39, 407–16.

Mukherjee, B.K., Sachan, H.K. (2001). Discovery of coesite from Indian Himalaya: A record of ultra-high pressure metamorphism in Indian continental crust. Curr Sci 81:1358–1361.

Mukherjee, B.K., Sachan H.K. (2009). Fluids in coesite-bearing rocks of the Tso Morari Complex, NW Himalaya: evidence for entrapment during peak metamorphism and subsequent uplift. Geol Mag 156(6):876-889.

Mukherjee, S., Mulchrone, K. (2012). Estimating the Viscosity of the Tso Morari Crystallines Gneiss Dome, Indian Western Himalaya. Int J Earth Sci 101:1929–1947.

Murphy, M.A., Harrison, T.M. (1999). Relationship between leucogranites and the Qomolangma detachment in the Rongbuk Valley, south Tibet. Geology 27, 831– 834.

Najman, Y., Clift, P., Johnson, M.R.W., Roberson, A.H.F. (1993). Early stages of foreland basin evolution in the Lesser Himalaya, N India. In: Treloar, P.J., Searle, M.P. (Eds.), Himalayan Tectonics. The Geological Society Special Publication, vol. 74, pp. 541– 558.

Nakamura, N. (1974). Determination of REE, Ba, Fe, Mg, Na and K in carbonaceous and ordinary chondrites, Geochim. Cosmochim. Acta, 38, 757–775.

Nakata, T. (1972). Geomorphic history and crustal movements of the foothills of the Himalayas. The science report of the Tohoku University 22, 39–177.

Nakata, T., (1989). Active faults of the Himalaya of India and Nepal. Special Paper-Geological Society of America 232, 243– 264.

References

Nicolas, A., Girardeau, J., Marcoux, J., Dupre, B., Xibin, W., Yougong, C., Zheng, H., Xuchang, X. (1981). The Xigaze ophiolite (Tibet): a peculiar oceanic lithosphere. Nature 294:414–417.

Norman, T. (1975). Flow features of Ankara mélange. 9th Int Cong Sediment 4:261-269.

Pa´lfy, J., Deme´ny, A., Haas, J., Hete´nyi, M., Orchard, M.J., Veto, I. (2001). Carbon isotope anomaly and other geochemical changes at the Triassic-Jurassic boundary from a marine section in Hungary. Geology 29:1047–1050.

Parrish, R.R., Hodges, K.V. (1996). Isotopic constraints on the age and provenance of the Lesser and Greater Himalayan Sequences, Nepalese Himalaya. Geological Society of America Bulletin 108, 904– 911.

Patriat, P., Achache, J. (1984). India-Eurasia collision chronology has implications for crustal shortening and driving mechanism of plates. Nature 311, 615–621.

Pearce, J.A., Cann, J.R., (1973) Tectonic setting of basic volcanic rocks determined using trace element analyses. Earth Planet. Sci. Lett. 19 (2), 290–300.

Pearce, J.A., Norry, M.J. (1979) Petrogenetic implications of Ti, Zr, Y, and Nb variations in volcanic rocks. Contributions to Mineralogy and Petrology 69, 33-47.

Pearce J. A., Barker P. F., Edwards S. J., Parkinson I. J. & Leat P. T. (2000) Geochemistry and tectonic significance of peridotites from the South Sandwich arc-basin system, South Atlantic. Contributions to Mineralogy and Petrology 139, 36–53.

Phipps, S.P., (1984) Ophiolitic olistostromes in the basal Great Valley sequence, Napa County, northern California Coast Ranges. Geological Society of America Special Papers 198, 103–125.

Plank, T. (2005). Constraints from thorium/lanthanum on sediment recycling at subduction zones and the evolution of the continents. J Petrol 46:921–944

Ravikant, V. (2003) Metamorphic conditions from the Taglang La Formation, Tso Morari complex, SE Ladakh: general inferences for the tectonics of the NW Indian continental margin. In: Anand Mohan (Ed.) Milestones in Petrology, Memoir of the Geological Society of India, Paper No.19, pp. 409

Ravikant V., Pal T., Das D., (2004) Chromite from the Nidar ophiolite and Karzok Complex, Transhimalaya, eastern Ladakh: their magmatic evolution (with T. Pal, D. Das). Journal of Asian Earth Sciences, 24:177.

Rast, N., and Horton, J.W., Jr. (1989). Melanges and olistostromes in the Appalachians of the United States and mainland Canada; An assessment, *in* Horton, J.W., Jr., and Rast, N., eds., Mélanges and olistostromes of the Appalachians: Geological Society of America Special Paper 228, p. 1–16.

References

Raymond, L.A. (1984). Classification of mélanges: Spec Pap Geol Soc Am 198:7-20

Reuber, I., Colchen, M., Mevel, C. (1987). The geodynamic evolution of the south-Tethyan margin in Zanskar, NW Himalaya, as revealed by the Spontang ophiolitic me´lange. Geodinamica Acta 1, 283–296.

Robertson, A.H F. (2000). Formation of mélanges in the Indus Suture Zone, Ladakh Himalaya by successive subduction-related, collisional and post-collisional processes during Late Mesozoic-Late Tertiary time. Geological Society, London, Special Publications, v. 170, p. 333-374.

Robertson, A.H.F., Parlak, O., Ustaömer, T., (2009) Mélange genesis and ophiolite emplacement related to subduction of the northernmargin of the Tauride Anatolide continent, central and western Turkey. Geological Society, London, Special Publications 311, 9–66.

Rojay, B. (2013). Tectonic evolution of the Cretaceous Ankara Ophiolitic Mélange during the Late Cretaceous to pre-Miocene interval in Central Anatolia, Turkey. J. Geodyn., 65, pp. 66–81.

Saleeby, J., (1984) Tectonic significance of serpentinite mobility and ophiolitic melange. In: Raymond, L.A. (Ed.), Their Nature, Origin, and Significance: Geological Society of America Special Papers, 198, pp. 153–168.

Scaillet, B., France-Lanord, C., LeFort, P. (1990). Badrinath–Gangotri plutons (Garhwal, India)—petrological and geochemical evidence for fractionation processes in a High Himalayan leucogranite. Journal of Volcanology and Geothermal Research 44, 163– 188.

Scambelluri, M., Piccardo, G.B., Philippot, P., Robbiano, A., Negretti, L. (1997). High salinity fluid inclusions formed from recycled seawater in deeply subducted alpine serpentinite. Earth Planet Sci Lett 148:485–500.

Scambelluri, M., Philippot, P. (2001). Deep fluids in subduction zones. Lithos 55:213–227.

Schmid, S.M., Paterson, M.S., Boland, J.N. (1980). High temperature flow and dynamic recrystallization in Carrara Marble. Tectonophysics 65:245-280.

Schmidt, M. W., Poli, S. (2003). Generation of mobile components during subduction of oceanic crust. In: Rudnick RL (ed); Holland HD, Turekian KK (eed) Treatise on Geochemistry 3:567-590.

Searle, M.P.,Windley, B.F., Coward, M.P., Cooper, D.J.W., Rex, D.C., Tingdong, L., Xuchang, X., Jan, M.Q., Thakur, V.C., Kumar, S., (1987) The closing of Tethys and the tectonics of Himalaya. Geological Society of America Bulletin 98, 678–701.

Searle, M., Corfield, R.I., Stephenson, B., McCarron, J., (1997) Structure of the North India continental margin in the Ladakh-Zanskar Himalayas: implications for the

timing of obduction of the Spontang ophiolite, India–Asia collision and deformation events in the Himalaya. Geological Magazine 134 (3), 297–316.

Sengör, A.M.C., (1979) Mid-Mesozoic closure of Permo-Triassic Tethys and its implications. Nature 279, 590–593.

Sharma, K. K. (1998). Geologic and tectonic evolution of the Himalaya before and after the India-Asia collision. Proceedings of Indian Academy of Science 107(4), 265-282.

Sheraton, J. W. (1984). Chemical changes associated with high-grademetamorphism of mafic rocks in the East Antarctic Shield. Chemical Geology 14, 135–57.

Shervais, J. W. (1982). Ti-V plots and the petrogenesis of modern and ophiolitic lavas. Earth Planet. Sci. Lett. 59, 101–118.

Shervais, W.J., Choi, S.H., Sharp, W.D., Ross, J., Zoglman-Schuman, M., Mukasa, S.B. (2011) Serpentinite matrix mélange: implications of mixed provenance for mélange formation. In: Wakabayashi, J., Dilek, Y. (Eds.), Geological Society of America Special Papers, 480, pp. 1–30.

Silver, E.A., and Beutner, E.C., (1980) Melanges: Geology, v. 8, p. 32–34.

Spear, F.S. (1993). Metamorphic Phase Equilibria and Pressure-Temperature-Time Paths, 799 p. Mineralogical Society of America, Washington, D. C.

Steck, A., Spring, L., Vannay, J-C., Masson, H., Bucher, H., Stutz, E., Marchant, R., Tieche, J.-C. (1993). The tectonic evolution of the Northwestern Himalaya in eastern Ladakh and Lahul, India. In: Treloar, P.J., Searle, M.P. (Eds.), Himalayan Tectonics. Geological Society Special Publication, vol. 74, pp. 265– 276.

Steck, A., Epard, J.-L., Vannay, J.-C., Hunziker, J., Girard,M.,Morard, A., Robyr, M. (1998). Geological transect across the Tso Morari and Spiti areas: the nappe structures of the Tethys Himalaya. Eclogae Geologicae Helveticae 91, 103–121.

Sun, S. S. & Mcdonough W. F. (1989) Chemical and isotopic systematics of oceanic basalts: Implications for mantle composition and processes. In Saunders A. D. and Norry M. J. (eds.) Magmatism in Ocean Basins. Geological Society of London, Special Publications 42, pp. 313–46.

Sutre, E. (1990). Les formations de la marge nord-neotethysienne et les me´langes ophiolitiques de la zone de suture de l'Indus en Himalaya du ladakhInde. PhD Thesis, Poitier University, France, p. 662.

Tahirkheli, R. A. K., Mattauer, M., Proust F. & Tapponnier, P. (1979). The India-Eurasia suture zone in Northern Pakistan: Synthesis and interpretation of new data at plate scale. In: Farah, A. & De Jong, K. A. (Ed.): Geodynamics of Pakistan. - Geol. Surv. Pak., 125-130, Quetta 1979.

References

Thakur VC, Virdi NS (1979) Lithostratigraphy, structural framework, deformation and metamorphism of the southeastern region of Ladakh, Kashmir Himalaya, India. Him Geol 9:63-78

Thakur, V. C., Misra, D. K. (1984) Tectonic framework of the Indus and Shyok suture. Tectonophysics 101, 207-220.

Thakur V C, (1990) Indus tsangpo suture zone in ladakh—its tectonostratigraphy and tectonics. Proceedings of the Indian Academy of Sciences - Earth and Planetary Sciences June 1990, Volume 99, Issue 2, pp 169-185

Thakur, V.C., (1992) Geology of Western Himalaya. Pergamon Press, New York, 363 pp.

Thompson, G. (1973). A geochemical study of the low temperature interaction of sea-water and oceanic igneous rocks. Transactions of the American Geophysical Union 54, 1015–19.

Tribuzio, R., Messiga, B., Vannucci, R. & Botazzi, P. (1996). Rare-earth element redistribution during high-pressure low-temperature metamorphism in ophiolitic Fe-gabbros (Liguria,Northwestern Italy): Implications for light REE mobility in subduction zones. *Geology* 24, 711–14.

Valdiya, K.S. (1980). Geology of the Kumaon Lesser Himalaya. The Himachal Press, Wadia Institute of Himalayan Geology, Dehra Dun.

Valley, J. (1986). Stable isotope geochemistry of metamophic rocks, *in* Valley, J. W., Taylor, H. P., and O'Neil, J. R., editors, Stable isotopes in high temperature geological processes: Mineralogical Society of America Reviews in Mineralogy, v. 26, p. 445-489.

Van Westrenen W., Blundy J. D. & Wood B. J. (2001) High field strength element/rare earth element fractionation during partial melting in the presence of garnet: Implications for identification of mantle heterogeneities. Geochemistry, Geophysics, Geosystems 2, 2000GC000133.

Vannay, J.C., Grasemann, B., (1998) Inverted metamorphism in the High Himalaya of Himachal Pradesh (NW India): phase equilibria versus thermobarometry. Schweizerische Mineralogissche und Petrographische Mitteilungen 78, 107– 132.

Veizer, J., Ala, D., Azmy, K. et al .(1999). 87Sr/86Sr, d13C and d18O evolution of Phanerozoic seawater. Chem Geol 161:59–88.

Vermeesch, P. (2006). Tectonic classification of basalt with classification trees. Geochimica et Cosmochimica Acta 70, 1839–48.

Virdi, N.S., Thakur, V.C., Kumar, S. (1977). Blueschist facies metamorphism from the Indus suture zone of Ladakh and its significance. Him Geol 7:479–482.

Wadia, D.N. (1931). The syntaxis of the northwest Himalaya: its rocks, tectonics and orogeny. Records of Geological Survey of India 65, 189– 220.

Wallmann, K. (2001). The geological water cycle and the evolution of marine d18O values. Geochim Cosmochim Acta 65:2469–2485.

Wang, X.B., Bao, P.S., Xiao, X.C. (1987). Ophiolites of the Yarlung Zangbo (Tsangbo) River, Xizang (Tibet). Publishing House of Surveying and Mapping, Beijing.

Wang, C. S., Liu, Z. F. and Hébert, R. (2000). The Yarlung-Zangbo paleo-ophiolite, southern Tibet: Implications for the dynamic evolution of the Yarlung-Zangbo suture zone. Journal of Asian Earth Sciences, 18: 651–661.

White, W. M. (2007). Geochemistry: An-online Text Book. Johns Hopkins University Press, Baltimore.

Wickham, S.M., Taylor, H.P. (1987). Stable isotope constraints on the origin and depth of penetration of hydrothermal fluids associated with Hercynian regional metamorphism and crustal anatexis in the Pyrenees. Contrib Mineral Petrol 95:255–268.

Winchester, J. A. & Floyd, P. A. (1976). Geochemical magma type discrimination: Application to altered and metamorphosed basic igneous rocks. Earth and Planetary Science Letters 28, 459–69.

Winchester, J. A., and Floyd, P. A. (1977). Geochemical discrimination of different magma series and their differentiation products using immobile elements, Chemical Geology, vol.20, pp.325-343.

Wood, D. A., J. Tarney, J. Varet, A. D. Saunders, Y. Bougault, J. L. Joron, M. Treuil, and J. R. Cann. (1979). Geochemistry of basalts drilled in the North Atlantic by IPOD Leg 49: Implications for mantle heterogeneity, Earth Planet. Sci. Lett., 42, 77–97.

Wood, D.A. (1980). The application of a Th-Hf-Ta diagram to problems of tectonomagmatic classification and to establishing the nature of crustal contamination of basaltic lavas of the British Tertiary volcanic province. Earth and Planetary Science Letters, 50, pp. 11– 30.

Wu, H.R. (1993). Upper Jurassic and Lower Cretaceous radiolarians of Xialu chert, Yarlung Zangbo ophiolite belt, southern Tibet. In: Blueford, J.R., Murchey, B.L. (Eds.), Radiolaria of Giant and Subgiant Fields of Asia, Nazarov Memorial Volume, Micropaleontol. Spec. Pap., vol. 6, pp. 115– 136.

Yeats, R. S., Nakata, T., Farah, A., Fort, M., Mirza, M. A., Pandey, M. R., Stein, R. S. (1992). The Himalayan Frontal Fault System: Annales Tectonicae 6, 85–98.

Yin, A., Harrison, T.M. (2000). Geologic evolution of the Himalayan–Tibetan orogen. Annual Reviews of Earth and Planetary Science 28, 211–280.

References

Yin, A. (2006). Cenozoic tectonic evolution of the Himalayan orogen as constrained by along-strike variation of structural geometry, exhumation history, and foreland sedimentation Earth Sci. Rev, 76, pp. 1–131

Zack, T., John, T. (2007). An evaluation of reactive fluid flow an trace element mobility in subducting slabs. Chem Geol 239:199-216.

Ziabrev, S.V., Aitchison, J.C., Badengzhu, Davis, A.M., Luo, H., Liu, J.B. (2001). More about the missing Tethys: Bainang terrane Tibet. 16th Himalaya-Karakorum-Tibet workshop. J. Asian Earth Sci. 19, 82–83.

Zhao, W., Nelson, K.D., and the Project INDEPTH Team. (1993). Deep seismic reflection evidence for continental underthrusting beneath southern Tibet. Nature 366, 557– 559.

Zhao, Z. F., Zheng, F. Y., Chen, X. R., Xia, X. Q. & Wu, B. Y. (2007). Element mobility in mafic and felsic ultrahigh-pressure metamorphic rocks during continental collision. Geochimica et Cosmochimica Acta 71, 5244–66.

Curriculum Vitae & List of Publications

KOUSHICK SEN (Research Scholar)
WADIA INSTITUTE OF HIMALAYAN GEOLOGY
33, GMS ROAD DEHRADUN-248001
Mob: 9557626798, Email: koushick.geol@gmail.com

Research Topic (Ph.D): "Formation and tectonic evolution of Zildat Ophiolitic Mélange, Indus Suture Zone, NW Himalaya, India"

Educational Qualification

B.Sc. : **Geology** from **J.K. College** Purulia, Burdwan University, India (2005)
M.Sc. : **Applied Geology** from **Presidency College**, Kolkata, University of Calcutta, India (2007)
M.Tech : **Petroleum Exploration** from **Indian School of Mines**, Dhanbad, India (2009)
Ph.D (Submitted 2014): **University of Petroleum & Energy Studies**, Dehradun.

M.Sc. Dissertation: (Under Prof. Gautam Ghosh, Presidency University)

"Structural analysis of Iron Ore Group of rocks in between Joda-Khondbandh. (Western Iron Ore Basin), SINGBHUM",
During this I worked with field meso-scopic structures to validate the superposed structural deformation (fold morphology) focusing their regional heterogeneity in terms of classify them under superposed nomenclature.

M.Tech. Dissertation: (Under Prof. Shalivahan, ISM Dhanbad)

"Real Time Monitoring of drill site operations & geological data & their formation evaluation",
Real-Time Monitoring is an eye on well operations and facilitates quick decisions in the base those can't be taken at the well site. I have learned PERFORM View 1.5 software, which provides digital display of different drilling (e.g. ROP, RPM, WOB, Hook load, etc.) and geological parameters (e.g. Gas shows). Based on these data, drill site operations monitoring and quick-look formation evaluation is done. Formation evaluation has been done with a special emphasis on Shaly-sand analysis for the calculation of matrix volume, clay volume; bound water, free water and hydrocarbon occupied porosities.

Field of Interest

Subduction Zone processes, Structure & Tectonics, Petrology & Geochemistry, Stable Isotope, Petroleum Geology and exploration prospective.

Scholarships/Awards/Honours

Qualified Graduate Aptitude Test for Engineering in 2007 (**GATE** 2007)

Qualified National Eligibility Test in 2011 (**UGC-CSIR NET** JRF+Lecturureship)

Scholarship from **MHRD** (Ministry of Human Resource, India) during M.Tech (2007-2009)

Wadia National Fellowship Pursuing research (PhD) in Himalayan Geology, 2009-present

Travel grant from International Association of Sedimentologists (**IAS**) to present paper in 14th Bathurst Meeting of Carbonate Sedimentologists 2011, held at **Bristol University, United Kingdom**.

Sponsorship from leading E&P companies like Chevron, Conoco-Phillips, Shell, Petrobras and ExxonMobil, to attend the 14th Bathurst Meeting of Carbonate Sedimentologists 2011, held at Bristol University, United Kingdom.

First prize for best **scientific photography** in 2010, awarded by WIHG.

Second prize for **scientific slogan** competition on National Science Day 2011, awarded by WIHG.

First Prize in Poster Presentation on Himalayan Day Celebration in 2013 at WIHG.

Elected as **Assistant General Secretary** of Student Union at J.K.College Purulia(W.B.) for the academic session 2004-2005.

School captain at S.E.Rly.Boys.H.S.School, Adra (W.B) for the academic session 1998-99

Selected for JBNSTS (Jagadish Bose National Science Talent Search) in school time.

Instrumentation & Technical Skills

Structural and lithological mapping
Transmitted and reflected light microscopy
Isotope Ratio Mass Spectrometry (IRMS) for Oxygen and Carbon Stable Isotope analysis also the Oxygen Isotope for Silicates.
Scanning electron microscopy
Energy dispersive X – ray spectroscopy
Raman spectroscopy
EPMA (for semi quantitative analysis of major elements)
Well Logging & Formation Evaluation

Training & Courses

Training in **OIL INDIA LIMITED**, DHULIAJAN, ASSAM. During M.Tech. in 2008.

Training at K.D.M.I.P.E., **O.N.G.C**., DehraDun on oil and gas exploration for period of five weeks

M.Tech Dissertation project done in **GSPC** (Gujarat State Petroleum corporation), Gandhinagar, Gujarat.

Training in **UCIL** (Uranium Corporation of India Ltd), Jadugora, Jamshedpur.

Training in **Geological Survey of India** on Structural Mapping at Kuju camp, Ranchi.

Membership & Affiliation

Student member of American Geophysical Union (**AGU**)
Student member of International Association of Sedimentologists (**IAS**)
Student Member of **SwissSed**, Switzerland
Life member of **Himalayan Geology**
Life member of **SGTSGINDIA**

International Research Paper (*peer reviewed*)

1. **Sen Koushick**, Das Souvik, Mukherjee Barun K, Sen Koushik., 2013,Bimodal stable isotope signatures of Zildat Ophiolitic Mélange, Indus Suture Zone, Himalaya: implications for emplacement of an ophiolitic mélange in a convergent set-up, International Journal of Earth Sciences. Vol 102 (7) 2033-2042 (Impact Factor- 2.34)

2. Das Souvik, Mukherjee Barun, Basu Asish and **Sen Koushick (Jr).,** 2015, Peridotitic minerals of the Nidar ophiolite in NW Himalaya, sourced from the mantle transition zone and above, Geological Society of London (accepted)

3. Das Souvik, **Sen Koushick**, Mukherjee Barun K, Mukherjee Soumyajit., Natural CO2 sequestration of altered ultramafic from Himalayan Ophiolite, Ladakh India. International Journal of Earth Sciences (under review)

Conferences presented in National & International forum:

1. **Sen Koushick**, Mukherjee Barun K, Ghosh Sumit K., 2010, "Heterogeneous behavior … NW Himalaya", In Rock Deformation and Structure conference by SGTSG INDIA, held in Jadavpur University, India

2. **Sen Koushick**, Das Souvik, Mukherjee Barun K., 2011, "Significance.. final emplacement" In 14th Bathurst Meeting of Carbonate Sedimentologist, Bristol University, United Kingdom (Received International Travel Grant)

3. **Sen Koushick**, Mukherjee Barun K, Sen Koushik., 2011, "Multiphase deformation of …. NW Himalaya", In Geodynamics & Metallogenesis of Indian Lithosphere,Banaras Hindu University, India

4. **Sen Koushick**, 2011, "Deformation heterogeneity….. microstructure", In Indian Monsoon and Himalayan Geodynamics, Wadia Institute of Himalayan Geology, Dehradun, India

5. **Sen Koushick**, Mukherjee Barun K, Sen Koushik., 2013, "Evidences of euxinic .... ophiolitic mélange, In WIHG-IGU workshop 2013: Modern Prospective in Himalayan Geosciences, Dehradun, India

6. **Sen Koushick**, "The Dynamics of Subduction Zone Melange in Convergent Set-up..", In WIHG on Himalayan Day Celebration (Received First Prize)

Popular articles:

Sen Koushick, "Pseudo-Nodules in Chakrata Formation: A syndepositional record of paleo-seismicity", Cover Photo published in Journal of Himalayan Geology, Vol.31,No.2,2010.